Republic of Iraq
Ministry of Higher Education
and Scientific Research
University of Babylon
College of Engineering
Mechanical Engineering Department

CFD Analysis of Thermoelastohydrodynamic Performance of Plain Journal Bearing Lubricated with Nanolubricates

A Thesis Submitted to the
College of Engineering / University of Babylon in
Partial Fulfillment of the Requirements for the Degree of
Master of Science in/ Engineering/ Mechanical Engineering
/Applied Mechanic

By

Zainab Hafiz Kadhim Kebash

Supervised by

Prof. Dr. Basim A. Abass **Prof. Dr. Saba Y. Ahmed**

2021 A.D. **1442 A.H.**

بسم الله الرحمن الرحيم

قَالَ كَذَٰلِكِ قَالَ رَبُّكِ هُوَ عَلَيَّ هَيِّنٌ
ۖ وَلِنَجْعَلَهُ آيَةً لِلنَّاسِ وَرَحْمَةً مِنَّا ۚ
وَكَانَ أَمْرًا مَقْضِيًّا

صدق الله العلي العظيم

سورة مريم آية ﴿21﴾

Certification

We certify that this thesis entitled "**CFD ANALYSIS OF THERMOELASTOHYDRODYNAMIC PERFORMANCE OF PLAIN JOURNAL BEARING LUBRICATED WITH NANOLUBRICATES**" was prepared by **Zainab Hafiz Kadhim ….** under our supervision at the University of Babylon in a partial fulfillment of the requirements for the degree of Master of Science in Mechanical Engineering (Applied Mechanics).

We recommend that this thesis be forwarded for examination in accordance with the regulation of the University of Babylon.

Signature

Prof. Dr. Basim A. Abass

(First Supervisor)

Signature

Prof. Dr. Saba Y. Ahmed

(Second Supervisor)

Dedication

This thesis is dedicated to those who have provided me with encouragement, inspiration, courage, and strength, particularly to my parents, my brothers, and my sisters who have been nicely my supporter until my research was fully finished.

Zainab 2021

Acknowledgments

This dissertation would not have been possible without expressing my gratitude and thanks to ALLAH (be glorious) for all the blessings bestowed upon me.

I would like to express my heartfelt thanks and gratitude to my supervisors, ***Prof. Dr. Saba Y. Ahmed*** *and* ***Prof. Dr. Basim A. Abass*** *for their guidance, invaluable instructions, help, and unwavering encouragement throughout the preparation of my study. I'd like to express my gratitude to the head of the mechanical engineering department at the University of Babylon, for their guidance and support. I'd also like to express my appreciation to my family and friends especially (Toma) and zalid for their assistance throughout this process.*

Zainab 2021

Table of Contents

List of Figures

List of Tables

Nomenclature

Symbol	Definition
a_{nue}	The volume fraction of the nucleation site which can be taken as 5×10^{-4}.
c	Radial clearance, m.
c_p	Specific heat of base oil, $J/kg\ °C$.
D	Journal or Shaft diameter, m.
e	Eccentricity between shaft and bearing, m.
f	Coefficient of friction.
F_{evap} F_{cond}	The coefficient of condensation which can be taken as 0.01. The coefficient of evaporation which can be taken as 50 .
F_{fr}	Friction force, N.
H	The power loss, kW.
h Δh	Film thickness, m. Relative rigid displacement of the two bearing surfaces.
k	Thermal conductivity, $W/m.°C$.
L	Length of the bearing, m.
L/D	Aspect ratio.
N	Speed of Rotation, RPM.
Ne, Nc	Mass transfer source terms connected to the growth and collapse of the vapor bubbles respectively.
O'	Bearing center.
O	Shaft center.
p	This pressure in the local fluid film, N/m^2.
p_b	Bubble surface pressure, .

$\boldsymbol{PV}$	Pressure of Vaporization, Pa.
$\boldsymbol{p_v}$	Saturation pressure of the fluid, Pa.
$\boldsymbol{Q_s}$	End leakage, m^3/s.
$\boldsymbol{R_b}$	Outer radius of bearing, m.
$\boldsymbol{R_{bc}}$	The radius of a bubble which can be taken as 10^{-6}, m.
$\boldsymbol{R_j}$	Radius of shaft, m.
$\boldsymbol{r_i}$	Inner radius of bearing, m.
$\boldsymbol{t}$	Time, sec.
$\boldsymbol{U_j}$	The journal speed, m/s.
$\boldsymbol{W}$	Load Carrying Capacity, N.
$\boldsymbol{x}$	Co-ordinates in direction of motion.
$\boldsymbol{y}$	Co-ordinates perpendicular in direction of motion.
$\boldsymbol{z}$	Co-ordinates through the film.
Greek Symbols	
$\boldsymbol{\beta}$	The viscosity–temperature index.
$\boldsymbol{\varepsilon}$	Eccentricity ratio.
$\boldsymbol{\sigma}$	Liquid tension coefficient, mN/m.
$\boldsymbol{\Delta}$	Total elastic deformation of the shaft and bearing system, m.
$\boldsymbol{\delta_E}$ $\boldsymbol{\delta_T}$	Elastic deformation, m. Thermal deformation, m.
$\boldsymbol{\Delta_T}$	Thermal deformation at nodal point due to thermal expansion of bearing shell, m.
$\boldsymbol{\Delta_P}$	Elastic deformation at nodal point due to hydrodynamic pressure, m.

$\boldsymbol{\theta}$	Angular coordinate, $degree$.
$\boldsymbol{\phi}$	Attitude angle, $degree$.
$\boldsymbol{\mu_0}$	Base fluid viscosity, $Pa.sec$.
$\boldsymbol{\mu_{nf}}$	Nano-lubricant of oil viscosity, $Pa.sec$.
$\boldsymbol{v}$	The Poisson ratio.
$\boldsymbol{\rho}$	Base fluid density, kg/m^3.
$\boldsymbol{\rho_v}$	Vapor density, kg/m^3.
$\boldsymbol{\tau}$	Shear Stress, N/m^2.
$\boldsymbol{\Phi}$	Volume fraction.
$\boldsymbol{\omega}$	The journal speed, rad/s.
Matrices	
$\boldsymbol{C_P}$	Elastic deformation matrix.
$\boldsymbol{C_T}$	Thermal expansion matrix.
Subscript	
$\boldsymbol{B}$	Bearing
$\boldsymbol{I}$	inner.
$\boldsymbol{J}$	Journal
$\boldsymbol{l}$	liquid.
$\boldsymbol{O}$	outer.
$\boldsymbol{V}$	vapor.
abbreviation	
$\boldsymbol{CFD}$	Computational Fluid Dynamics.
$\boldsymbol{CSD}$	Computational Structure Dynamics.
$\boldsymbol{DOE}$	Design of Experiments.
$\boldsymbol{EHD}$	Elastohydrodynamic
$\boldsymbol{FDM}$	Finite difference Method.
$\boldsymbol{FEM}$	Finite Element Method.

$\boldsymbol{FSI}$	Fluid-Structure Interaction.
$\boldsymbol{MOGA}$	Multi-Objective Genetic Algorithm.
$\boldsymbol{PRESTO}$	Pressure Implicit with Splitting of Operators.
$\boldsymbol{RSA}$	Response Surface Analysis.
$\boldsymbol{THD}$	Thermohydrodynamic.
$\boldsymbol{TEHD}$	Thermoelastohydrodynamic.
$\boldsymbol{UDF}$	User-Defined Function.
$\boldsymbol{MOFT}$	Minimum oil film thickness.
$\boldsymbol{API-SF}$	American Petroleum Institute.
$\boldsymbol{ISO\ VG68}$	The International Standards Organization.
$\boldsymbol{SAE}$	Society of Automotive Engineers.
$\boldsymbol{PTPA}$	Parabolic temperature profile technique.
$\boldsymbol{AWS}$	Anti-wear hydraulic oil.

ABSTRACT

This work deals with a study of a three-dimensional CFD analysis and multi-phase flow phenomena for hydrodynamic journal bearing with integrated cavitation. The simulations are carried out considering the realistic bearing deformations by two-way fluid-structure interactions (FSI) along with cavitation using ANSYS Workbench software. The design optimization module is used to generate the optimized solution of the attitude angle and eccentricity for the combination of operating speed and load. Bearings with and without cavitation are investigated. The load carried by this type of bearings drops substantially with the increase of the oil film temperature resulting due to the thermal effect as a result of viscous shearing of the oil film and the elastic deformation of the bearing material. It was found that the performance of the base oil can be improved by blending with different Nano-particles with different volume fractions. It was inspected that the load carried by the bearing enhanced when using such type of lubricants. Different types of nanoparticles such as TiO_2, Al_2O_3, CuO, Nano-particles are used as dispersed materials with the base oil to enhance its physical properties and hence the static performance of the bearing. The data of the operating characteristics of such bearing are very important for the bearing designer and employers to eliminate the higher oil film temperature which causes the bearing failure. In the current work, the plain journal bearing lubricated with different Nano lubricants was numerically modeled considering the effects of oil film temperature and elastic deformation of the bearing material. Moreover, cavitation can occur at the divergent zone of the bearing leading to the damage and failure of components and limiting the maximum applied load. Hence, the effect of cavitation on the performance of the bearing must be considered for reliable design. The modified Krieger-Dougherty equation has been implemented with the

thermal viscosity model to consider the variation of the Nano-lubricant viscosity with the oil film temperature and to evaluate its effective viscosity. Computational Fluid Dynamic (CFD) was used to model the fluid film of the bearing while the Fluid-Structure Interaction (FSI) was used to model the elastic deformation in the bearing material. The elastic deformation was transferred to the fluid film and vice versa using the two-way FSI technique in ANSYS FLUENT program. The equilibrium position of the shaft center due to the convenient operating conditions was determined using a suitable optimization technique. A validation study has been implemented to ensure the correctness of the numerical model by comparing the results of different cases (THD, TEHD, THD with Nano-lubrication) obtained in the present work with that obtained by different workers numerically and experimentally. The validation results ensure the implementation of the numerical model confidently. The bearing performance has been examined at different particle volume fractions of the Nano-particles, journal speeds, and different eccentricity ratios. The bearing performance has been examined at different particle volume fractions of the Nano-particles, journal speeds, and different eccentricity ratios. The results obtained in the present work demonstrate that the maximum oil film pressure increases by 6% to about 20% when lubricated with different Nano-lubricants in comparison with that of pure oil at with depicted the load carried by the bearing becomes about 14.3% and the attitude angle of the bearing decreases by 11% to 37% with the expense of increasing the friction force by 16% and the increase in bearing deformation when lubricated with such Nano lubricant increases about 18% when the bearing is lubricated with TiO_2 when the volume fraction of such nanoparticles increases to 0.03 in comparison with that lubricated with pure oil.

Chapter One

INTRODUCTION

CHAPTER ONE

INTRODUCTION

Different configurations of plain hydrodynamic journal bearings are enormously engaged to engineering applications because of their higher performance, higher damping, and ease in manufacture. They can be used to support the crankshaft of a tractor's, the turbine/generator unit in hydro-power stations, and many revolving machines which have at least one rotating section that must be separated from the machine's stationary portion. The lubricant is used to keep the two surfaces from rubbing on each other by generating thin film which can be sheared without causing harmful effects on the surfaces**[60]**. The bearings consist of a rotating shaft (journal) which rotates freely in a supporting metal sleeve as can be shown in the **figure(1.1)**. Although, their design and construction may be relatively simple, but the theory of these bearings is complex. Mineral oil is commonly used as a lubricant. However, these bearings become unstable at higher speeds. The lubricant is cavitated at the divergent zone of the bearing when the pressure drops below its saturation pressure resulting in a release of the dissolved air in the form of air bubbles which makes the flow of the lubricant in this zone behaves as a two-phase flow**[47]**.

The heat generated in the oil film due to viscous shearing results in a higher oil film and surface temperatures which leads to a considerable

decrease in oil viscosity and deterioration of the oil film. This becomes more considerable when the bearing works at high journal speeds and applied loads. Moreover, the oil flow field is modified which influences the performance of the bearing. Although, when the bearing is subjected to higher loads the elastic deformation of the bearing material becomes significant resulting in oil film thickness alteration which negatively affects the performance of the bearing. However, the bearing surface deformation becomes higher when it works at higher oil film temperature due to the effect of the thermal deformation which is superimposed with the mechanical deformation and the softening of the bearing material**[60]**. Because of that, a realistic estimation of the bearing performance is required considering the combined effect of the above-mentioned parameters.

Nanoparticles are increasingly being utilized to create solutions to modern engineering difficulties. They are used to prepare different types of Nano-lubricants that can be used with the journal bearings. These fluids include the dispersion of Nano-materials into the base engine oil to meet specific requirements such as high thermal conductivity and favorable tribological properties. Moreover, using such type of lubricant minimizes the friction between mating surfaces since the Nano-materials work as third-body lubricants, transforming into small microscopic ball bearings that minimize friction between two touching surfaces**[61]**.

In the present work, the static characteristics of plain journal bearing lubricated with different Nano-lubricants have been deliberate considering thermal and elastic deformation effects. The cavitation effect on the performance parameters of such bearings was also considered. Titanium oxide (TiO_2), aluminum oxide (Al_2O_3), and copper oxide (CuO)

nanoparticles are commonly used in preparing Nano-lubricants due to their good mechanical characteristics with reducing friction and wear. The static characteristics of the journal bearing lubricated with Nano-lubricant are discussed using CFD technique with the fluid flow field to calculate the oil film pressure and temperature distributions while two-way fluid-structure interaction (FSI) is used with the bearing structure to calculate the elastic deformation of the bearing material. The elastic deformation was then used with the fluid film and vice-versa. Such analysis was implemented using ANSYS-FLUENT 19.R2 computer program. For this purpose, the fluid field is discretized to the suitable number of finite volume cells while the bearing structure is discretized to a suitable finite element according to a suitable convergence test.

The modified Krieger Dougherty equation is implemented with the viscosity-temperature equation to consider the effects of the nanoparticle volume fraction, aggregate ratio, and the oil film temperature on the Nano-lubricant viscosity**[48]**. Such equation is implemented to the ANSYS-FLUENT 19.R2 programs by using a suitable user define function written in C^{++} language.

The flow in the cavitation zone is assumed a two-phase flow. The Zwart–Gerber–Balamri cavitation model is used to include the effect of the oil cavitation on the performance of the journal bearing**[47]**. The fluid-structure interaction is implemented by transferring the data was from the fluent program to the structural analysis by ANSYS and vice-versa using a built-in interface. The equilibrium position of the journal center is obtained by using the surface optimization technique. A validation study is implemented to demonstrate the CFD model of the present work by comparing the oil film pressure and temperature data obtained by the solution of the numerical model of the current work with that obtained by

different workers. The results show a good agreement which allows using of the suggested numerical model with high confidence.

The obtained results displayed that using different Nano-lubricants to lubricate the journal bearing enhances the maximum oil film pressure, the load carried by the bearing, and the side leakage of the oil from both sides of the bearing. Also, it is observed that elastic and thermal deformations, as well as the cavitation effects, are significantly affecting the bearing performance. The peak pressure of the oil film drops significantly when considering the combined effect of oil film temperature, elastic deformation, and cavitation.

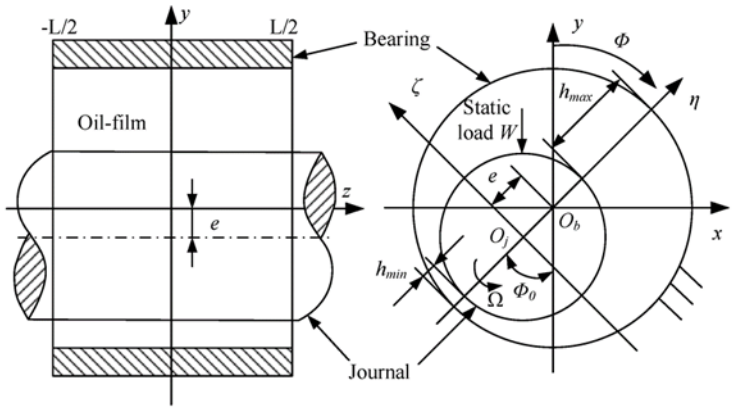

Figure(1.1) The geometry of the Hydrodynamic journal bearing system**[60].**

1.1. Main Objectives of the Present Work

The main goals of the present work are:

1. Investigate the effect of dispersing different nanoparticles of TiO_2, Al_2O_3, and CuO on the Thermo-elasto-hydrodynamic steady-state performance of plain journal bearings.

2. Investigate the effect of different affecting parameters such as journal speed, nanoparticles volume fraction, and the eccentricity

ratio on the Thermo-elasto-hydrodynamic steady-state performance of such bearings.

3. Define the equilibrium position of the journal center and the optimum values of the attitude angle and the vertical component of the load by using suitable optimization techniques.

4. Using CFD Technology in Ansys Fluent 2019 R2 with C++ program language.

Chapter Two

LITERATURE REVIEW

CHAPTER TWO

LITERATURE REVIEW

Hydrodynamic journal bearings are a special type of fluid-lubricated bearings that completely separates the shaft and bearing by a thin layer of fluid film during normal operation. Fundamentally, journal bearing consists of the rotating shaft, the bearing itself, and the fluid lubricant, usually oil. Hydrodynamic bearings are characterized by simplicity and higher damping. Hence, they are found in hundreds of different industrial applications and are known for long life and high load-carrying capacity such as marine propellers, electric generators, hard disk drives, gas turbines, turbo generators, hydro-turbines, and IC Engines[60]. This chapter provides a critical review of the available literature related to the thermoelastohydrodynamic performance of circular journal bearings. The survey of literature will be discussed as follows:

- Effect of thermal and elastic deformation on the performance of journal bearings.
- Effect of Nano lubrication on the performance of journal bearings.
- Numerical methods for the analysis of hydrodynamic journal bearing.

2.1. Effect of thermal and elastic deformation on the performance of journal bearings

The effect of bearing elastic deformation on the performance characteristics of the cylindrical journal bearing with hydrodynamic lubrication (HD) and elastohydrodynamic lubrication (EHD) methods is studied by **Hill et al. (2010)[1]**. It was observed that the fluid film thickness increases with the eccentricity ratio for the elastic bearing more than the rigid one while the attitude angle and the load-carrying capacity decrease.

Thermohydrodynamic lubrication analysis is implemented by **Sun et al. (2010)[2]** for misaligned plain journal bearing considering surface roughness. Reynolds, energy, and heat conduction equations are solved numerically using the finite difference method. It has been observed that the maximum oil film pressure, load carrying capacity, maximum oil film temperature, frictional coefficient, misalignment moment, and the end leakage flow rate increased as surface roughness increased.

In another work, the effect of misalignment created through an asymmetric journal deflection on the thermohydrodynamic journal bearing analysis is studied by **He et al. (2012)[3]** Energy and the Reynolds' equations are solved numerically by direct iterative with successive over-relaxation using five-point central difference method. The effect of misalignment on the temperature, pressure, and viscosity was discussed. The obtained results show that the temperature, oil film pressure, and oil viscosity were affected by the misalignment angle which was increased with the increase of the applied load. It was also observed that the oil leakage increases as the velocity and the bearing width increase otherwise the minimum oil film thickness (MOFT) increase with considering asymmetry of journal deflection. However, in experimental investigation

for the thermal performance of journal bearing with either single or twin axial grooves.

Brito et al. (2012)[4] found that under heavy loads the twin axial groove arrangement deteriorates the bearing performance in comparison with single groove arrangement. It was also concluded that the knowledge of the feed flow rate through each groove can be used to improve the bearing performance.

The effects of thermal boundary conditions on thermohydrodynamic lubrication of plain journal bearings with a single axial groove have been studied by **Zhang et al. (2013)[5]**. The Reynolds, Energy, and Heat conduction equations were solved numerically using the finite difference method. It was observed that the appropriate selection of the thermal boundary conditions(TBCs) was important to obtain reasonable results.

Thermohydrodynamic performance of grooved journal bearing with the role of lubricant feeding conditions has been analyzed. The effects of one and two feeding grooves on the thermal performance of the journal bearing have been discussed by **Brito et al. (2014)[6]**. Reynolds, the Energy and Heat conduction equations were solved numerically using a suitable FORTRAN program. It has been observed that the bearing of twin grooves offered superior results more than that of a single groove.

Akbarzadeh et al. (2018)[7] conducted a multi-objective optimization for thermohydrodynamic lubrication of partial journal bearing. The central difference technique with successive over-relaxation was used to calculate the performance parameters of such bearing. The viscosity was assumed to be changed with the temperature. Further, the effect of bearing speed, load, and inlet oil temperature on the objective functions is illustrated. In this problem, the bearing power loss, the

minimum oil film thickness, and the maximum oil temperature are selected as three objective functions and the radial clearance and length-to-diameter ratio are considered as two important design variables.

Lambha et al. (2019)[8] suggested elastohydrodynamic analyses of rotor system supported by cylindrical journal bearing lubricated with couple stress fluid. Modified Reynold's equation and three-dimensional elasticity equations were solved by using an iterative procedure. It was concluded that employing a couple stress fluids (non-Newtonian fluid) rather than a Newtonian fluid enhances the load-carrying capacity, efficiency, and performance of the system.

Li et al. (2019)[9] provided a comprehensive analysis of the performance of thermohydrodynamic misaligned journal bearing by solving the generalized Reynolds, Heat conduction, and Energy equations. Numerical findings reveal that the journal axial movement (caused by the pressure gradient) on the bearing performance is maximal when the thermal effect is considered.

Chetti et al. (2019) [10] presented the effect of the elastic deformation on the static characteristics of journal bearing lubricated with non-Newtonian fluid. The analysis was achieved by solving the modified Reynolds' equation to consider the effect of non-Newtonian fluid behavior numerically using a suitable viscosity pressure model. It was observed that the elastic deformation decreases the bearing load-carrying capacity, pressure, side leakage, and attitude angle.

Sekhar et al. (2019)[11] studied the Newtonian and non-Newtonian behavior of hydrodynamic journal bearing including thermal effect. Pressure, and temperature profiles were studied. A semi-analytical solution was obtained by solving continuity and momentum equations along with

the energy equation under isothermal boundaries to obtain the oil film pressure and temperature distributions. A significant increase in pressure was obtained when the bearing was lubricated with the non-Newtonian lubricant that has a higher power-law index. It was also evident that temperature increases when the bearing works at a higher eccentricity ratio.

Liu et al. (2019)[12] analyzed the effects of double conical, plain, and double parabolic profiles on the elastohydrodynamic lubrication of the journal bearing considering surface roughness effect under the steady operating situation. The finite element method was used for calculating the elastic deformation of the bushing surface, while finite-difference with direct iterative and successive over-relaxation was used to calculate the oil film temperature. It was observed that the bearing with a double parabolic profile has been enhanced the minimum film thickness, and low asperity contact pressure and friction, which leads to reduced edge wear.

The combined effects of the oil film temperature, elastic deformation of the bearing material, and the roughness of journal surface on the performance of heavily loaded misaligned journal bearing working at high speeds were studied by **Zhang and Lin (2019)[13]**. Thermoelastohydrodynamic lubrication model including the effect of shaft misalignment and journal surface texture were used to analyze the performance of such bearing. The effects of cavitation and viscosity variation were also considered. The obtained results show an increase in maximum oil film pressure and load-carrying capacity with a sharp increase in oil film temperature due to journal misalignment.

2.2. Effect of Nano lubrication on the performance of journal bearings

The most important related works that deal with the effect of different nanoparticles dispersed in lubricant on the performance of journal bearings are presented in this section.

The static features of an externally adjustable fluid film bearing lubricated with API-SF lubricant blended with CuO, TiO_2, and Diamond nanoparticles have been studied by **Shenoy et al. (2012) [14]**. The Reynolds equation was solved numerically for various operating conditions such as the eccentricity ratio (0.1-1.2) and the volume fraction of nanoparticles. It was observed that at a volume fraction of nanoparticles dispersed in the base lubricant leads to an increase in the pressure distribution, load-carrying capacity, friction force, while decreasing lubricant end leakage flow. It was also observed that the titanium dioxide nanoparticles result in significantly higher-pressure values in comparison with that obtained by the CuO and Dimond nanoparticles.

Binu et al. (2014) [15] studied the effect of the variable viscosity on journal bearing performance lubricated with TiO_2 Nano lubricant. The modified Krieger-Dougherty viscosity model with a measured particle packing fraction of 7.77 was used to calculate lubricant viscosity. The finite difference method was used to solve Reynold's equation. The effect of Nano lubricant viscosity on the friction force, load-carrying capacity, and pressure distribution were discussed. A 35% increase in load-carrying capacity was obtained when the bearing was lubricated with oil blended by 0.015 volume fraction of TiO2 nanoparticle in comparison with that lubricated with pure oil.

In another work, **Binu et al. (2014)[16]** studied the steady-state performance of journal bearing lubricated with a couple stress lubricants blended with TiO_2 nanoparticles. Krieger Dougherty's viscosity model was also used to calculate the Nano lubricant effective viscosity. It has been found that the load-carrying capacity of the bearing increases by 45% while the friction force increases by 40% when lubricated with oil containing

TiO_2 nanoparticle with 0.01 volume fraction and 0.03108 couple stress parameter as compared to that lubricated with pure oil.

Nicoletti (2014)[17] investigated the effects of using Nano lubricants on thermohydrodynamic performance of journal bearings considering variable Nano lubricants viscosity-temperature variation. The effects of adding Si, SiO_2, Al, Al_2O_3, Cu, and CuO nanoparticles to the ISO VG68 oil have been discussed. An increase in load-carrying capacity by 10% was obtained due to the higher volumetric heat capacity of the oil which decreases the oil film temperature and higher viscosity distribution. It was observed that the best results were achieved by adding CuO nanoparticles to the oil.

Aluminum and zinc oxides nanoparticles were used by **Babu et al. (2014)[18]** to improve the performance of the journal bearing lubricated with engine oil 15W40. A model was developed to relate the viscosity and temperature of the lubricant. The Reynolds and the Energy equations were solved using MATLAB code and the powerful finite element technique. The effects of both thermo and isoviscous lubrication on the bearing friction force, attitude angle, load capacity, and end leakage flow were discussed. It has been observed that the load-carrying capacity and friction force increase while the end leakage and the attitude angle decrease when the bearing works at a higher eccentricity ratio for both thermo and isoviscous cases.

Gunnuang et al. (2015)[19] studied the characteristics performance of a journal bearing lubricated with oil containing Al_2O_3 additive. Non-Newtonian fluid on the Carrera viscosity model was represented for oil SAE10W50. The finite difference method and multilevel multigrain technique were used to solve the Reynolds and Energy equations. Based on

the results obtained the load-carrying capacity improves by adding Al_2O_3 nanoparticles with no change in oil film temperature.

The Aluminum oxide nanoparticles were also used by **Solghar (2015)[20]** as an additive to improve the performance of journal bearings. Thermohydrodynamic (THD) performance of journal bearings lubricated with pure oil and oil dispersed with (Al_2O_3) nanoparticles was analyzed considering cavitation effect. Energy, Continuity, and Momentum equations were solved numerically using finite volume and SIMPLER algorithm. The effects of pure and Nano lubricant on the load-carrying capacity, friction coefficient, pressure profile, and the temperature field were discussed. An enhancement in pressure profile and decrease in oil film temperature has been observed for the bearing lubricated with oil dispersed with Al_2O_3 nanoparticles in comparison with that lubricated with pure oil. The loading capacity and the friction coefficient increase with the addition of the nanoparticles.

Suryawanshi et al. (2018)[21] analyzed the performance of plain and elliptical journal bearings working with different industrial lubricants. A four-ball Tribo-tester with operating conditions specified by ASTM standards was used to specify the rheological properties of the oils blended with 0.5% wt Titanium dioxide (TiO_2) nanoparticles. It has been observed that the addition of TiO_2 nanoparticles to the lubricant increases oil viscosity, frictional force, pressure distribution, load carrying capacity, and attitude angle whilst reducing the oil flow rate. An elliptical bearing working with Nano lubricant shows excellent performance over the plain journal bearing.

Another thermohydrodynamic analysis was implemented by **Jamalabadi et al. (2019)[22]** for a plain journal bearing lubricated with TiO_2 Nano lubricant. The Reynolds equation model is used to calculate the

oil-film pressure developed in hydrodynamic journal bearings by applying the Nano-based lubricants. The effects of nanoparticles volume fraction, types of lubricant, and rotational speed were studied. The obtained results show that the temperature rise, average shear stress and dissipation power were increased with the rotational speed and increasing of the dispersed TiO_2 nanoparticles.

Recently, the performance of rigid and flexible journal bearing lubricated with Nano lubricant was investigated by **Khan et al. (2020)[23]**. The effective viscosity of Nano lubricant was calculated using the Krieger-Dougherty implemented with the non-Newtonian model. The modified Reynolds equation was solved with appropriate boundary conditions using the finite difference method to evaluate the static performance parameters at different values of power-law index and eccentricity ratios. The obtained results show an increase in friction force, fluid film pressure, and load-carrying capacity with the increase of nanoparticle concentration for both rigid and elastic bearings while an insignificant effect of the elastic deformation was observed on the static performance parameters.

The finite element method was used by **Ramaganesh et al. (2020)[24]** to analyze the performance of Nano lubricated journal bearing using the COMSOL program. The effect of different Nano lubricant additives such as CuO, WS_2 and TiO_2 blended into SAE20W40 on the performance of journal bearing loaded by 10kN at 3000 r.p.m journal speed. It was observed that the minimum oil film pressures obtained when the bearing is lubricated with oil-containing nanoparticles of CuO while it became higher when the bearing is lubricated with SAE20W40 dispersed with TiO_2 nanoparticles. However, the viscosity increased, and hence the oil film thickness when the oil dispersed with a higher percentage of

nanoparticles which minimized the contact between the bearing and the journal.

The heating effect of non-Newtonian bio-lubricant, obeying power-law model, dispersed with TiO_2 nanoparticles on the performance of journal bearing with different aspect ratios (0.5-2) was studied by Dhanola **and Garg (2020)[25]**. The effects of power-law index ranging from 0.9 to 1.1, journal rotational speed (500-2500), eccentricity ratio ranges from 0.1 to 0.8, the oil inlet temperature of 40^{o}C, and volume fraction of TiO_2 ranges from 0.01 to 0.04 on the performance of such bearing were studied. The results obtained demonstrated a substantial improvement in bearing load capacity, friction force, maximum pressure, and marginal variation of the side leakage and attitude angle when using the bio based nano lubricant.

The Performance Properties of steady-state for elliptical bearing lubricated with mineral oils based on nanoparticles are studied by **Dang et al. (2020)[26]**. Energy and the Reynolds' equations are solved numerically by the Finite difference method with successive over-relaxation using MATLABVR R2020a software with the Krieger Dougherty method to calculate viscosity. Two types of nanoparticles have been used to design the parameters: namely, CuO and TiO_2 with 0.5, 1.0, and 2.0 wt.% concentrations have been separated with three different viscosity grades of oil at an eccentricity ratio range (0.5-0.9). It is observed that the pressure distribution and load capacity increase with an increase in the concentration of nanoparticles. The temperature distribution is determined by the PTPA technique, and power losses increase slightly with the nanoparticles' concentration.

The hydrodynamic pressure profile of the journal bearing lubricated with Al_2O_3 Nano-lubricant was studied by **Bui et al. (2020)[27]**. The hydrodynamic pressure is calculated by solving two-dimensional Reynolds'

equations. The effects of the applied load (300,500 and 800N) and angular velocities of 94,141 and 214 rad/s on the performance of a journal bearing lubricated with BP Vistra 300-4T oil dispersed with Al_2O_3 nanoparticles with a concentration of 1 gram per liter at temperatures ranging from 50 to 65 degrees Celsius have been studied. It has been shown that the pressure profile of a hydrodynamic bearing changes with the addition of Al_2O_3 Nano powder, load, and speed. It has been also obtained that there is no direct proportionality between the hydrodynamic pressure profile and the viscosity of Lubricated Oil with Al_2O_3 Nano powder.

An experimental investigation of the performance of TiO_2 Nano lubricated journal bearing was performed by **Singh et al. (2020)[28]**. The impact of using lubricant with different TiO_2 volume fractions on the bearing with journal speed of 1400rpm loaded with 600 and 1000 N has been investigated. The experimental observations confirm the great enhancement of the oil film pressure, the load-carrying capacity, friction coefficient, and the maximum oil film temperature of the bearing when lubricated with TiO_2 Nano lubricant.

The most study on the effect of Nano lubrication on the journal bearing performance was implemented by **Tushar et al. (2021)[29]**. The effects of adding Al_2O_3, TiO_2, and CuO nanoparticles to the Veedol Avalon ISO Viscosity grade 46 oil with different volume fractions (0.25%, 0.5%, 1%and 2%) on the performance of plain journal bearing have been studied. The modified Krieger-Dougherty viscosity model was used to include the effects of nanoparticles aggregation size and the nanoparticles volume fractions on the oil viscosity. Base oil, as well as prepared Nano lubricants, are experimentally tested at load conditions of 300N and 450 N for two different speeds 250 and 500 rpm. The obtained results reveal an increase in maximum pressure as well as load-carrying capacity when the bearing

was lubricated with Nano lubricant compared to the base oil. Also, the experiment verification shows an improvement of 3 to 21% in maximum pressure and 5 to 23% in load capacity for different nanoparticle volume fractions ranging from 0.5 to 2 vol % compared to the base oil.

In another work, **Dang et al. (2021)[30]** studied the effect of TiO_2 and CuO based Nano lubricants on the static thermal performance of circular journal bearing. The performance of such bearing was compared when lubricated with both types of Nano lubricants. The viscosity variation with volume fraction of nanoparticles and their aggregate size has been considered by using the modified Krieger Dougherty model. The oil film pressure and temperature are calculated using a prepared computer program written in MATLABR2020a software considering the effect of variation in the thermo physical properties of Nano lubricants. The obtained result demonstrated an increase in load-carrying capacity by 14.23% at journal speed of 2000rpm, eccentricity ratio of 0.6, and 2%wt addition of TiO_2 while it becomes 9.23% in the case of CuO under the same circumstances.

2.3. Computational fluid dynamics (CFD) Analysis of journal bearing

An extensive literature review for the implanted works to analyze the journal bearings performance using a computational fluid dynamic approach is presented in this section. Computational fluid dynamics (CFD) is a branch of fluid mechanics that uses numerical analysis and data structures to analyze and solve problems that involve fluid flows. Computers are used to perform the calculations required to simulate the free-stream flow of the fluid, and the interaction of the fluid (liquids and gases) with surfaces defined by boundary conditions. With high-speed supercomputers, better solutions can be achieved, and are often required to solve the largest and most complex problems. Ongoing research yields software that improves the accuracy and speed of complex simulation.

Liu et al. (2010)[31] suggested elastohydrodynamic analyses of a rotor-bearing system using the CFD-FSI method. It was observed that the CFD-FSI Approach gives more accurate results for elastohydrodynamic and hydrodynamic analyses of the rotor bearing. The study was implemented for a bearing with radial clearance (30 μm), bearing diameter (0.03 m), insert thickness (0.0015 m), backing thickness (0.0085 m), and length (0.015 m) using three types of solid materials (Steel, Babbitt, Nylon). The results reveal that elastic deformation had a considerable effect on the rotor-bearing system.

A comprehensive analysis for journal bearings transient flow field with the application of CFD-FSI techniques was implemented by **Li et al. (2012)[32]**. Continuity and Momentum equations are solved numerically by coupling the MATLAB code and FLUENT. The results assure that computational fluid dynamics is an appropriate tool for the simulation of the rotor-bearing system. It has been observed that the pressure is created in the converging zone of the bearing while the cavitation did not happen in the diverging zone.

The elastohydrodynamic behavior of a plain cylindrical journal bearing subjected to radial loads has been studied by **Bendaoud et al. (2012)[33]**. Journal bearing with bearing clearance (0.09 mm), rotational speed (1000–9000 r/min), oil supply pressure (0.08 MPa), oil supply temperature 40 ^{o}C, and ambient temperature (37–39 ^{o}C) was studied. The Reynolds and the elastic deformation equations were solved numerically using an appropriate finite element method, employing ANSYS CFX code. It was noted that the frictional torque and the axial flow rate were influenced by the high load application. It was observed that the maximum pressure, frictional torque, and minimum oil film thickness increased by 28%, 15%, and 18% respectively the applied that the pressure.

Chasalevris and Sfyris (2013)[34] analyzed the performance of journal bearing with different aspect ratios (L/D=0.25,0.5,1 and 4) and linearly varying fluid film using FDM and CFD methods. The results demonstrated that the eccentricity ratio, the pressure, and the attitude angle decrease with the Somerfield number.

Lin et al. (2013)[35] demonstrated a transient analysis for a journal bearing including thermal and cavitation effects using the CFD-FSI approach based on a suitable physical model. This method was found to be a very useful tool for studying bearing lubrication problems. Multi grooves stainless steel bearing with numbers of grooves (2-6) and journal rotational speed range (10,000-50,000 rpm) was studied. It was observed that the load, temperature, eccentricity ratio, and pressure increased while the minimum film thickness decreased with increasing the externally applied load. The temperature rise became higher as the rotational speed increased and the cavitation problem became more severe.

A Computational Fluid Dynamics approach using ANSYS FLUENT software was used to perform a thermohydrodynamic analysis for a circular journal bearing by **Singla et al. (2014)[36]**. The analysis was carried out for a bearing with journal rotational speed of (2000) rpm, inlet lubricant temperature (30 °C), and the bearing radial clearance (0.1 mm) at constant viscosity. It was found that when the viscosity is maintained constant, a greater lubricant temperature rises and maximum pressure is obtained which affects the load-carrying capacity of the bearing.

An investigation of the distribution of hydrodynamic pressure in journal bearing with clearance (0.004 mm) and length/diameter of 0.5 lubricated with non-Newtonian lubricant using the CFD method was implemented by **Czaban (2015)[37]**. The effect of heat due to the lubricant shear was neglected while the effect of the oil type was extensively studied.

Based on the results obtained the pressure and lift capacity of the bearing lubricated with Newtonian lubricant was lower than that lubricated with non-Newtonian lubricant.

Dhande and Pande (2016,2017 and 2018)[38-40] investigated the performance circular (one lobe) hydrodynamic bearing with CFD-FSI techniques. A comparison between results with and without cavitation for the pressure distribution and the oil vapor distribution has been implemented. A circular bearing with a wide range of journal speed from 1000 to 5000 rpm, eccentricity ratio range (0.2-0.6), shaft diameter (50 mm), clearance (5×10^{-5} m), and length of (0.25 m) has been studied. It was found that the pressure increases with the increase in both speeds and eccentricity ratios while lower pressure distribution is obtained when considering the cavitation effect. The same behavior was found for the vapor distribution. The peak pressure value drops when the effects of elastohydrodynamic and cavitation were considered.

In later work, **Dhande et al. (2019)[41]** suggested a CFD model analyze three-Lobe journal bearing using two-way fluid-structure interaction to consider the effect of the bearing elastic deformation. It has been observed that the distribution of pressure in the three-lobe bearing is significantly influenced by the eccentricity ratio as compared to the rotational speed. The obtained results also show that three-Lobe bearings should be used at lower eccentricity ratios and higher speeds.

Chen et al. (2019)[42] analyzed the performance of grooved journal bearing considering the deformation of the bearing liner and cavitation using the fluid-structure interaction (FSI) technique. Journal bearing with (1 to 3) 120^{o} grooves, journal rotational speed of 100 rpm working at eccentricity ratio of 0.6 has been studied. Numerical results obtained proposed that groove shapes and operating conditions play critical roles in

changing the elastohydrodynamic characteristic of journal bearing. The results also show that the fluid-structure interaction technique is an effective method to analyze elastohydrodynamic lubrication of the journal bearing.

In another work, **Chen et al.(2019)[43]** studied the effect of groove shapes on the hydrodynamic characteristics of a journal bearing with a varied number of grooves. The Reynolds, Energy, and Heat conduction equations are solved numerically using the (CFD) method, considering actual characteristics such as cavitation and thermal effects. Bearing a diameter of 200 mm, journal rotational speed range (400-1000 rpm), eccentricity ratios range (0.3-0.9) was studied in a laminar flow regime. The results showed that the influence of the groove form cannot be overlooked on the hydrodynamic performance of a journal bearing. It is also observed that the number of grooves, eccentricity ratio, and rotational speed affect the cavitation volume fraction.

CFD technique was used by **Kyrkou and Nikolakopoulos (2020)[44]** to analyze the thermo-hydrodynamic performance of finite length journal bearings and analytical solutions for infinitely long and narrow bearings. The numerical and analytical solutions were implemented for a bearing with applied load range (2-10 kN), eccentricity ratio (0.1-0.9), and journal rotational speed range (1000-4000 rpm). The simulation assumes variable oil viscosity and the bearing examined with both industrial and environmentally adapted lubricants (AWS-100, ISO VG 32). It has been found that using lubricant type AWS-100 results in a higher temperature in all cases while using lubricant ISO-VG32 leads to more uniform temperature distribution.

A comprehensive analysis for the journal bearing performance with and without cavitation is provided by **Rasep et al. (2021)[45]**. Reynolds,

Energy, and Heat conduction equations are solved numerically via ANSYS FLUENT. Journal bearings lubricated with engine oil (SAE20W40), palm oil, and water were considered. The design parameters studied are the journal rotational speed 1500 rpm, attitude angle $49^{o,}$ and eccentricity ratio 0.8. It is observed that the cavitation model provides a more accurate prediction of hydrodynamic pressures and corresponding load-carrying capacity with engine oil (SAE20W40). However, When comparing the palm oil to engine oil, The overall film pressure of the journal bearing is reduced by 63.6%, when the bearing is lubricated with palm oil in comparison with SAE20W40 allowing for a drop in the load support and friction strength. In another view, because palm oil is environmentally friendly, this type of lubricant has a great potential to replace motor oil in the future.

2.4. Closing Remarks

The effect of Nano lubrication on the performance of journal bearings has a greater attention last few year. Referring to the aforementioned survey of literature the most recent work that has been implemented in this field is the work done by **Tushar et al. (2021)[29]**. In his doctoral thesis, Tusher studied the effect of three types of nanoparticles Al_2O_3, $TiO_{2,}$ and CuO on the performance of cylindrical journal bearings under isothermal conditions. Two-dimensional solution using a prepared computer program. The bearing elastic deformation and the cavitation effects are not considered. However, the presented work extended Tushar's work to include thermal, bearing elastic deformation, and cavitation effects on the performance of circular journal bearings using three-dimensional CFD with fluid-structure interaction (FSI). Two-way fluid-structure interaction was used to analyze the effect of elastic deformation while the optimization technique was used to precisely locate the journal center following

Dhande's approach(2019)[41]. From all of the above notes, the main concluding remark is: The point studied in the current work is up to date and not studied before in this manner.

Chapter Three

MATHEMATICAL MODEL

CHAPTER THREE

MATHEMATICAL MODEL

The current study examines the thermoelastohydrodynamic (TEHD) performance of journal bearing lubricated with Nano-lubricant. For this purpose, a mathematical model was put forward to analyze the performance of the journal bearings under such circumstances. Equations required to analyze the bearing fluid and solid domains in addition to the required rheological equations used to describe the dependence of different physical and thermal properties on the fluid film temperature will be presented in this chapter. Hence, the main fluid dynamic conservation laws, such as Momentum, Energy, and Continuity equations considering cavitation and lubricant recirculation as well as the propagation of deformation in the bearing material will be presented. The main outputs of the present analysis, due to the appropriate inputs such as load, speed, rheological properties of the nano-lubricant, and bearing dimensions, are stresses, oil temperatures, pressure distribution, vapor volume fraction, frictional force, bearing deformation, and load-carrying capacity.

3.1. Assumptions

The following are the main assumptions adopted to simplify the present TEHD analysis of journal bearing lubricated with Nano-lubricant:

- Navier Stokes equation with variable viscosity in three- dimensions.
- Only steady-state analysis was considered.
- Smooth bearing surfaces (neglecting roughness effect).
- The lubricant was assumed to be Newtonian.
- Laminar flow of lubricant was considered.
- The oil viscosity was assumed to be a function of temperature only.
- Incompressible flow.

3.2. Governing Equations

The performance analysis for the journal bearing with the geometry shown in **figure (3.1)** was implemented by modeling such bearing using suitable governing equations.

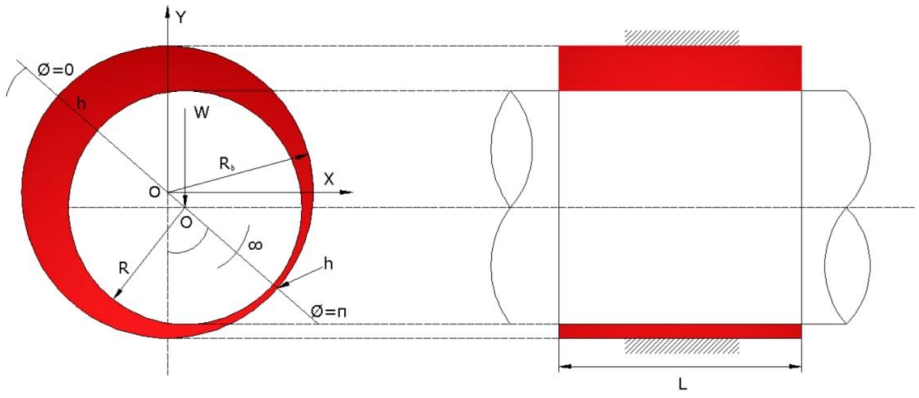

Figure(3.1) The geometry of the Hydrodynamic journal bearing system.

The following are the main equations used for this purpose.

3.2.1 Conservation equations

Pressure distribution in the fluid domain of the hydrodynamic journal bearings is controlled by solving the continuity and momentum equations. The following continuity equation is adopted in the present work.[46]

$$\frac{\partial u}{\partial x}+\frac{\partial v}{\partial y}+\frac{\partial w}{\partial z}=0 \qquad \ldots(3.1)$$

The flow of the bearing lubricant in three dimensions (X, Y, and Z)can be defined by solving the three-dimensional Navier-Stokes equations. They are commonly used in mathematical modeling of the hydrodynamic journal bearings. The following Navier Stokes equations were used in the present study [46].

Momentum Equation in x-direction:

$$\rho\frac{Du}{Dt}=-\frac{\partial p}{\partial x}+\frac{\partial}{\partial x}\left[2\mu\frac{\partial u}{\partial x}+\lambda\text{div u}\right]+\frac{\partial}{\partial y}\left[\mu\left(\frac{\partial u}{\partial y}+\frac{\partial v}{\partial x}\right)\right]+\frac{\partial}{\partial z}\left[\mu\left(\frac{\partial u}{\partial z}+\frac{\partial w}{\partial x}\right)\right]+S_{Mx} \qquad \ldots(3.2)$$

Momentum Equation in y-direction:

$$\rho\frac{Dv}{Dt}=-\frac{\partial p}{\partial y}+\frac{\partial}{\partial x}\left[\mu\left(\frac{\partial u}{\partial y}+\frac{\partial v}{\partial x}\right)\right]+\frac{\partial}{\partial y}\left[2\mu\frac{\partial v}{\partial y}+\lambda\text{div u}\right]+\frac{\partial}{\partial z}\left[\mu\left(\frac{\partial v}{\partial z}+\frac{\partial w}{\partial y}\right)\right]+S_{My} \qquad \ldots(3.3)$$

Momentum Equation in z-direction:

$$\rho\frac{Dw}{Dt}=-\frac{\partial p}{\partial z}+\frac{\partial}{\partial x}\left[\mu\left(\frac{\partial u}{\partial z}+\frac{\partial w}{\partial x}\right)\right]+\frac{\partial}{\partial y}\left[\mu\left(\frac{\partial v}{\partial z}+\frac{\partial w}{\partial y}\right)\right]+\frac{\partial}{\partial z}\left[2\mu\frac{\partial w}{\partial z}+\lambda\text{div u}\right]+S_{Mz} \qquad \ldots(3.4)$$

Where ' u ', ' v ', and ' w ' are the surface velocity components in the x, y, and z directions, respectively.

3.2.2 Energy Equation

The oil film temperature of the journal bearing lubricated with Nano-lubricant can be determined by solving the following three-dimensional energy equation[46]:

$$\rho C_p \left(u \cdot \frac{\partial T}{\partial x} + w \cdot \frac{\partial T}{\partial z} \right) = \frac{\partial}{\partial y} \left(k \frac{\partial T}{\partial y} \right) + \mu \left[\left(\frac{\partial u}{\partial y} \right)^2 + \left(\frac{\partial w}{\partial y} \right)^2 \right] \quad \ldots(3.5)$$

The term on the left side represents the heat transfer by convection, while that on the right side represents the conduction and the viscous dissipation.

3.2.3 Cavitation Model

Cavitation in journal bearing is a process that involves the release of dissolved gas in the divergent zone of the bearing at pressures below saturation pressure as cab be shown in **figure(3.2)**.

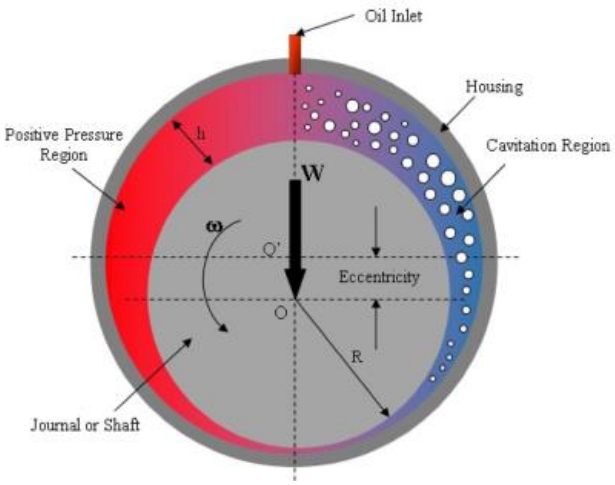

Figure(3.2) Cavitation process and release of the dissolved gas in the liquid[39].

A new release of dissolved gas was obtained when the flow advances further in the divergent region. However, as the bubbles inter the

convergent region again a pressure recovery takes place and the bubbles are dissolved again in the oil in a process that is slower than the release of such bubbles in the divergent zone. The oil-vapor mass transfer in the cavitation zone was governed by the following equation [47]:

$$\frac{\partial}{\partial t}(a_v, \rho_v) + \nabla(a_v \cdot \rho_v \cdot v_v) = N_e - N_C \quad \ldots (3.6)$$

where $N_e$and N_C account for the mass transfer between the liquid and vapor phases in cavitation. In the current work the Zwart–Gerber–Balamri cavitation model is used to include the effect of the oil cavitation on the performance of the journal bearing. Assuming that all the bubbles in a system have the same size, Zwart-Gerber-Belamri [47] proposed that the total interphase mass transfer rate per unit volume (R) is calculated using the bubble density numbers (n), and the mass change rate of a single bubble. Such a model is adopted due to its reliable predictive efficiency and strong convergence behavior. It can be presented as follows [47]:

$$\text{If } p < p_v$$

$$N_e = F_{evap} \cdot \frac{3 \cdot a_{nue}(1 - a_v) \cdot \rho_v}{R_{bc}} \cdot \sqrt{\frac{2}{3} \cdot \frac{p_v - p}{\rho_l}} \quad \ldots (3.7)$$

$$\text{If } p \geqslant p_v$$

$$N_C = F_{cond} \frac{3 \cdot a_v \cdot \rho_v}{R_{bc}} \cdot \sqrt{\frac{2}{3} \cdot \frac{p - p_v}{\rho_l}} \quad \ldots (3.8)$$

R_{bc} is the radius of the bubble which can be described by the following the generalized Rayleigh-Plesset equation[47]:

$$R_{bc}\frac{d^2R_{bc}}{dt^2}+\frac{3}{2}\left(\frac{dR_{bc}}{dt}\right)^2=\frac{p_b-p}{\rho_l}-\frac{2\sigma}{\rho_l\cdot R_{bc}}-4\cdot\frac{\mu_l}{\rho_l\cdot R_{bc}}\cdot\frac{dR_{bc}}{dt} \quad \dots(3.9)$$

The second-order terms and the surface tension forces are ignored. Hence, equation (3.9) is reduced to:

$$\frac{dR_{bc}}{dt}=\sqrt{\frac{2}{3}\cdot\frac{p_b-p}{\rho_l}} \quad \dots(3.10)$$

3.2.4 Rheological and physical properties of Nano lubricant

The most important rheological property of Nano-lubricant is the oil viscosity which can be modeled by using the following Krieger-Dougherty equation**[48]:**

$$\mu_{nf}=\mu\left[1-\frac{\varphi}{\varphi_m}\right]^{-[\eta]\varphi_m} \quad \dots(3.11)$$

Where

μ is the base fluid dynamic viscosity, $\mathrm{N.s/m^2}$.

η is the intrinsic viscosity with the standard value of 2.5 for monodisperse, as defined by Kole and Dey**[49]**.

φ_m denotes the maximum particle packing fraction, which ranges from 0.495 to 0.54 and is around 0.605 at high shear rates**[50]**.

φ is the solid nanoparticles' volume fraction.

Applying the above values of η and φ_m to the equation (3.11) the modified Krieger-Dougherty equation can be expressed as**[51]**:

$$\mu_{nf}=\mu\left(1-\frac{\varphi_a}{\varphi_m}\right)^{-2.5\varphi_m} \quad \dots(3.12)$$

Where

$$\varphi_a = \varphi \left(\frac{a_a}{a}\right)^{3-D} \quad \text{... (3.13)}$$

Where D represents the fractal index for Nano fluids with a standard value of 1.8[50]. $\frac{a_a}{a}$ represents the radii of aggregate to primary particle size ratio. Experimental values for aggregate ratio obtained in reference [29] are adopted in the present work. Hence, aggregate ratios of 4,3.33 and 3.5 are adopted for TiO_2, Al_2O_3, and CuO respectively.

To introduce the effect of oil film temperature on the oil viscosity, the following base lubricant viscosity-temperature relationship can be used:

$$\mu = \mu_0 \exp[-\beta(T - T_{in})] \quad \text{... (3.14)}$$

β the oil viscosity coefficient. For most lubricants, it can be taken as 0.032[52].

Substitute the expression of base oil viscosity into the Krieger-Dougherty equation (3.14) to get:

$$\mu_{nf} = \mu_0 \exp\left[-\beta(T - T_{in})\right]\left(1 - \frac{\varphi_a}{\varphi_m}\right)^{-2.5\varphi_m} \quad \text{... (3.15)}$$

The density of the Nano-lubricant (ρ_{nf}) can be evaluated as[20]:

$$\rho_{nf} = (1 - \varphi)\rho_f + \varphi\rho_p \quad \text{... (3.16)}$$

By defining $C_{p,nf}$ as the thermal power of the Nano fluid, then[20]:

$$\rho_{nf} C_{p,nf} = (1 - \varphi)\left(\rho C_p\right)_f + \varphi\left(\rho C_p\right)_p \quad \text{... (3.17)}$$

Subscripts p, f, and nf refer to particle, the base fluid, and Nano fluid, respectively.

The Nanofluid thermal conductivity can be determined by using the following Maxwell-Garnett's model[20]:

$$k_{nf} = k_f \left[\frac{(k_p + 2k_f) - 2\varphi(k_f - k_p)}{(k_p + 2k_f) + \varphi(k_f - k_p)} \right] \quad \ldots (3.18)$$

3.2.5 Elasticity Equation

The bearing fluid flow domain was greatly affected by the deformation of the bearing shell which must be calculated carefully to obtain reliable results for the bearing performance characteristics. The elastic deformation and the stresses induced in the body of the bearing shell can be obtained by solving the following three-dimensional finite element elasticity equation[53]:

$$[k][d] = [f] \quad \ldots (3.19)$$

Where: $[d]$ is the displacement vector, $[f]$ is the nodal force vector and $[k]$ is the stiffness matrix.

The generated strain can be calculated as:

$$[\epsilon] = [B]\{d\} \quad \ldots (3.20)$$

where $[B]$ represents the matrix that connects the strains to the nodal displacements.

Finally, using three-dimensional Hooks law to calculate the mechanical stress in the bearing material as follows:

$$[\sigma] = [D][\epsilon] \quad \ldots (3.21)$$

Where $[D]$ refers to the constitutive matrix, which can be calculated as:

$$[D] = \begin{bmatrix} A & B & B & 0 & 0 & 0 \\ B & A & B & 0 & 0 & 0 \\ B & B & A & 0 & 0 & 0 \\ 0 & 0 & 0 & C & 0 & 0 \\ 0 & 0 & 0 & 0 & C & 0 \\ 0 & 0 & 0 & 0 & 0 & C \end{bmatrix} \quad \text{... (3.22)}$$

A, B, C are constants that can be calculated as:

$$A = \frac{E(1-v)}{(1+v)(1-2v)} \quad \text{... (3.23)}$$

$$B = \frac{Ev}{(1+v)(1-2v)}$$

$$C = \frac{E}{2(1+v)}$$

3.2.6 Oil Film Thickness

The fluid film thickness h is calculated in terms of the bearing radial clearance and attitude angle using the following formula[54]:

$$h = C \cdot (1 - X \cdot \cos\theta - Y \cdot \sin\theta) \quad \text{... (3.24)}$$

The effect of thermal and mechanical deformations on the oil film thickness can be expressed as:

$$h = C.(1 - X \cdot \cos\ \theta - Y \cdot \sin\ \theta + \delta_E + \delta_T) \quad \text{... (3.25)}$$

3.2.7 Bearing Performance Parameters

The following are the main bearing performance parameters:

3.2.7. 1 Load-Carrying Capacity

The load-carrying capacity is determined by integrating the oil film pressure (p_j) over the shaft surface area. Load components in both directions x and y can be calculated as follows[54]:

$$F_y = \iint_{A_i} P_j \cdot \cos\theta \cdot (dA_j) \quad \text{... (3.26)}$$

$$F_x = \iint_{A_j} P_j \cdot \sin\theta \,.(dA_j) \quad \text{... (3.27)}$$

The load capacity by the bearing can be calculated as:

$$W = \sqrt{(F_y)^2 + (F_x)^2} \quad \text{... (3.28)}$$

The equilibrium point of the journal center can be achieved when the vertical component of the bearing load capacity (F_y) is equal to the external load (W) $(F_x \approx 0)$. The bearing attitude angle can be evaluated as:

$$\phi = \tan^{-1}\left(\frac{F_y}{F_x}\right) \quad \text{... (3.29)}$$

3.2.7. 2 Friction Force

The friction force at the bearing and the journal surfaces can be evaluated as[54]:

$$F_{fr} = \iint \tau \cdot (dA) \quad \text{... (3.30)}$$

Hence, the friction coefficient can be calculated as:

$$f = \frac{F_{fr}}{W} \quad \text{... (3.31)}$$

3.2.7. 3 Power Loss

The frictional force causes power loss, which can be calculated by the equation[54]:

$$H = f\ WU_j \quad \text{... (3.32)}$$

3.2.7. 4 Side Leakage of the Flow

The oil side leakage flow can be expressed as[54] :

$$Q_s = \int_{\theta_1}^{\theta_2} \frac{h^3}{12\mu}\left(\frac{\partial P}{\partial z}\right)_{z=0 and\ L} d\theta \quad \text{... (3.33)}$$

Chapter Four

COMPUTATIONAL PROCEDURE

COMPUTATIONAL PROCEDURE

CHAPTER FOUR

Thermoelastohydrodynamic analysis of journal bearing can be attained by using two commercially available approaches. The first one is the finite difference method based on solving Reynolds, Energy, and elasticity equations simultaneously. However, it is incapable of analyzing complex geometries and flow. The second is the Computational Fluid Dynamics (CFD) approach, which consists of complete solutions of Momentum, Continuity, Energy, and elasticity equations. It offers solutions for complex flow problems. ANSYS FLUENT is a powerful solver that allows solving CFD problems of extremely complex computations at a low cost. Hence, this code is adopted in the present work to implement the numerical analysis of the Thermoelastohydrodynamic (TEHL) lubrication of the journal bearings lubricated with Nano-lubricant. The following sections highlighted the details of the numerical analysis performed.

4.1. Numerical Analysis

The numerical analysis of the plain journal bearing consists of evaluating the temperature and hydrodynamic forces of lubricant using finite volume method via FLUENT 2019 R2 software and then using these forces for the structural analysis of the bearing shell using the finite

element method (FEM) via ANSYS 2019R2 software using simultaneous Fluid-Structure Interaction (FSI) to include the effect of modifying fluid film thickness on the TEHL of such bearings. An optimization technique was used to determine the optimum location of the shaft for a given load and speed, as well as to understand the necessary bearing design parameters. The following are the main steps of the numerical analysis used to attain the solution:

4.1.1 Bearing geometry

The aligned cylindrical bearing with the system of geometry and coordinates system shown in **figure(4.1)** with the geometrical and physical properties shown in **table (4.1) and (4.2)** respectively is used for the analysis of the current study. It consists of a rotating journal with radius R_j and fixed bearing with radius r_b with oil-filled the gap between them. The flow was assumed to be laminar with smooth bearing surfaces. The bearing supported a constant vertical applied load 'W' acting extremely in the direction of the Y-axis. The applied load is balanced by the load-induced due to the oil film pressure generated in this bearing's converging zone.

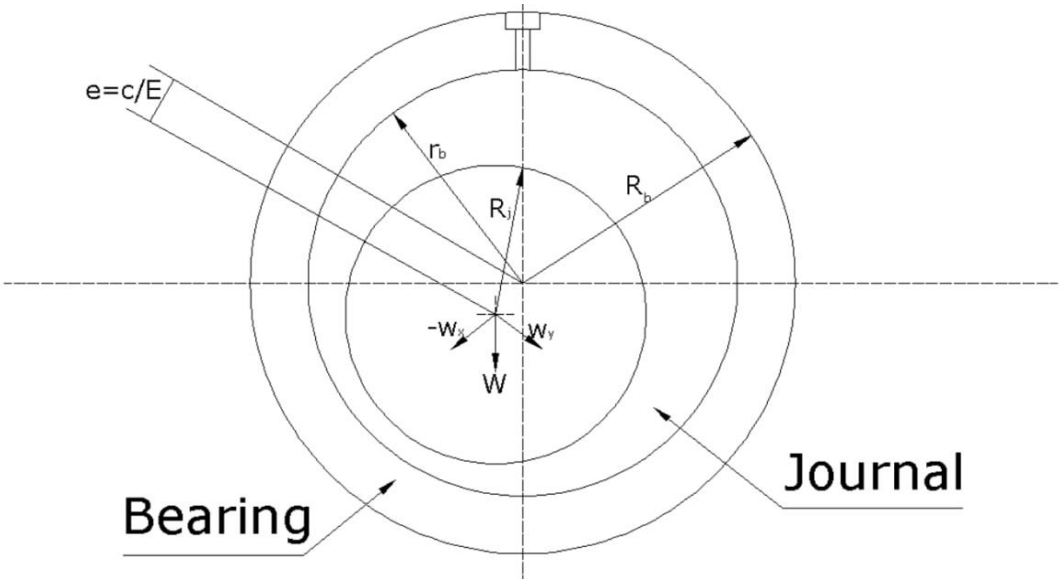

Figure(4.1) The geometry of the Hydrodynamic journal bearing system.

Table(4.1) Geometrical and operating parameters**[54]**.		
Parameter	**Units**	**Value**
L/D		0.5
$\mathbf{r_s}$	mm	24.95
$\boldsymbol{r_i}$	mm	25
$\boldsymbol{r_o}$	mm	30
$\boldsymbol{\varepsilon}$		0.1-0.9
$\boldsymbol{\theta}$	$Degree$	49
$\boldsymbol{N}$	r/min	2000-3000-4000
$\boldsymbol{T_i}$	$°C$	40
$\boldsymbol{c}$	mm	0.05
$\boldsymbol{\mu_i}$ **at Ti °C**	$N\ s/m^2$	0.0788
$\boldsymbol{\beta}$	$°C^{-1}$	0.032
$\boldsymbol{\rho_{oil}}$	Kg/m^3	875
$\boldsymbol{C_{Poil}}$	$J/kg\ °C$	2000
$\boldsymbol{k_{oil}}$	$W/m.°C$	0.13
$\boldsymbol{P_V}$	Pa	29185
$\boldsymbol{\Phi}$		(0-3) %

Table(4.2) The nanoparticle materials' physical characteristics**[17]**.			
	ρ (kg/m^3)	C_P (J/(kg/K))	K (W/(m/K))
Titanium dioxide ($\boldsymbol{TiO_2}$)	4230	710	8.4
Alumina ($\boldsymbol{Al_2O_3}$)	3970	765	36
Copper oxide (CuO)	6310	565	18

4.1.2 Finite Volume Method Computing Procedures (FVM)

As shown in chapter 3 the transport equations **((3.1), (3.2), (3.3), (3.4) and (3.5))** are all similar and contain diffusion and convection terms which allows them to be put in the common form as shown below[46]:

$$\frac{\partial(\rho\Phi)}{\partial t} + \text{div}(\rho\Phi u) = \text{div}(\Gamma \,\text{grad}\,\Phi) + S_\Phi \quad \ldots(\mathbf{4.1})$$

For φ=1 (i.e. continuity equation), u, v, w (three velocity component), S_Φ (represents the source term) and Γ (diffusion coefficient).

Since all the transport equations are assumed in steady-state so, the equations are deduced to the following form:

$$\frac{\partial}{\partial x}(\rho v_i \Phi) = \frac{\partial}{\partial x_i}\left(\frac{\Gamma\Phi\,\partial\Phi}{\partial \mathrm{x_i}}\right) + S_\Phi \quad \ldots(\mathbf{4.2})$$

The form of the diffusion coefficient and source term in the general equation for φ are shown in **table (4.3)**.

Table(4.3) Coefficients of Diffusion plus Source term in the general equation for φ [46].

Equation	φ	Γ_φ	S_φ
continuity	1	0	0
***x*-Momentum**	u	μ	$\left[\frac{\partial}{\partial x}\left(\mu\frac{\partial u}{\partial x}\right)+\frac{\partial}{\partial y}\left(\mu\frac{\partial v}{\partial x}\right)+\frac{\partial}{\partial z}\left(\mu\frac{\partial w}{\partial x}\right)\right]$
***y*-Momentum**	v	μ	$\left[\frac{\partial}{\partial x}\left(\mu\frac{\partial u}{\partial y}\right)+\frac{\partial}{\partial y}\left(\mu\frac{\partial v}{\partial y}\right)+\frac{\partial}{\partial z}\left(\mu\frac{\partial w}{\partial y}\right)\right]$
z-Momentum	w	μ	$\left[\frac{\partial}{\partial x}\left(\mu\frac{\partial u}{\partial z}\right)+\frac{\partial}{\partial y}\left(\mu\frac{\partial v}{\partial z}\right)+\frac{\partial}{\partial z}\left(\mu\frac{\partial w}{\partial z}\right)\right]$
Energy	T	$\lambda f / cp_f$	0

The control volume equations for each of φ are obtained by integrating equation (4.1) over the appropriate control volume that centered about the location of φ, as shown below[46]:

$$\int_A \boldsymbol{n} \cdot (\rho \Phi \mathrm{u}) \boldsymbol{dA} = \int_A \boldsymbol{n} \cdot (\Gamma \mathrm{grad}\ \Phi) \boldsymbol{dA} + \int_{CV} \boldsymbol{S_\Phi dV} \quad \ldots (\mathbf{4.3})$$

After linearized resulting in[46]:

$$a_p \Phi_p = a_E \Phi_E + a_W \Phi_W + a_N \Phi_N + a_S \Phi_S + a_T \Phi_T + a_B \Phi_B + S_u \quad \ldots (\mathbf{4.4})$$

And:

$$a_p = a_E + a_w + a_N + a_S + a_T + a_B - S_p \quad \ldots (\mathbf{4.5})$$

In each discrete equation, S_u and S_p indicated both the source terms. A typical control volume in which P (central node) is added to the six nearby nodes [E, W, N, S, T, B] to identify respectability as East, West, North, South, Top, and Bottom as shown in **figure (4.2)**.

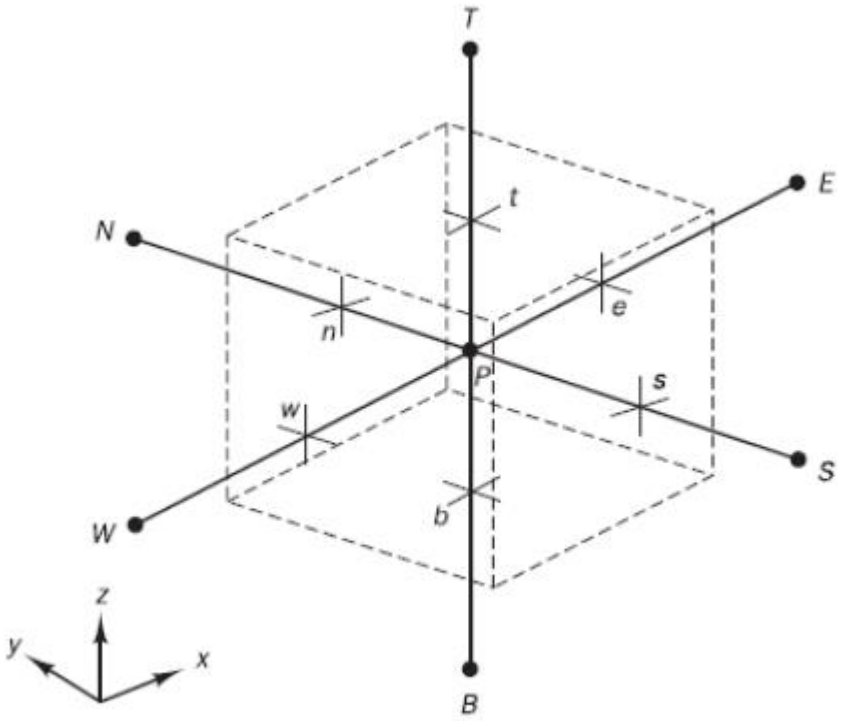

Figure(4.2) Discretization using a control volume and neighboring nodes**[46].**

In both momentum equations and energy equations, pressure and velocity compounds have a relationship that introduces restrictions to the flow field solution. Where limitations are related to a nonlinearity in the set of equations in which the pressure-velocity coupling is solved iteratively, for example using the SIMPLEC (SIMPLE-Consistent algorithm)**[46]**.

The SIMPLEC algorithm follows the same steps as the SIMPLE algorithm, with the exception that the momentum equations are altered in such a way that the SIMPLEC velocity correction equations exclude terms that are less significant than those omitted in SIMPLE.

Pseudo-velocities are now defined as[46]:

$$\hat{u}_{i,J,K} = \frac{\Sigma a_{mdz} u^*_{mdz} + s_{i,J,K}}{a_{i,J}}$$
$$\hat{v}_{l,j,K} = \frac{\sum a_{mdz} v^*_{mdz} + s_{l,j,K}}{a_{I,j}} \quad \ldots (\mathbf{4.6})$$
$$\hat{w}_{l,J,k} = \frac{\sum a_{mdz} w^*_{mdz} + s_{I,J,k}}{a_{I,J,k}}$$

$$u_{i,J,K} = \hat{u}_{i,J,K} + d_{i,J,K}\left(p_{I-1,J,K} - p_{I,J,K}\right)$$
$$v_{l,j,K} = \hat{v}_{l,j,K} + d_{l,j,K}\left(p_{I,J-1,K} - p_{I,J,K}\right) \text{ where; } \left(d_{i,J,K} = \frac{A_{i,J,K}}{a_{i,J,K} - \Sigma a_{mdz}} \quad d_{l,j,K} = \frac{A_{l,j,K}}{a_{I,J,K} - \Sigma a_{mdz}} \quad d_{kIJ,k} = \frac{A_{k,J}}{a_{I,J,k} - \Sigma a_{mdz}} \right) \quad \ldots (\mathbf{4.7})$$
$$w_{I,J,k} = \hat{w}_{I,J,k} + d_{I,J,k}\left(p_{I,J,K-1} - p_{I,J,K}\right)$$

$$a_{I,J} p_{I,J} = a_{I+1,J} p_{I+1,J} + a_{I-1,J} p_{I-1,J} + a_{I,J+1} p_{I,J+1} + a_{I,J-1} p_{I,J-1} + b_{I,J} \quad \ldots (\mathbf{4.8})$$

For determining the equations of momentum, the pressure components must be used[46]:

$$a_{i,J,K} u^*_{t,J,K} = \sum a_{mdz} u^*_{mdz} + \left(p^*_{I-1,J,K} - p^*_{I,J,K}\right) A_{i,J,K}$$
$$a_{I,j,K} v^*_{I,j,K} = \sum a_{mdz} v^*_{mdz} + \left(p^*_{t,l-1,K} - p^*_{I_1 J,K}\right) A_{I,j,K} \quad \ldots (\mathbf{4.9})$$
$$a_{I,J,k} w^*_{I,J,k} = \sum a_{mdz} w^*_{mdz} + \left(p^*_{r,l-1,K} - p^*_{I_k J,K}\right) A_{I,J,k}$$

Then, a pressure correction equation derived from the equation of continuity is solved to calculate the pressure component adjustment[46]:

$$p = p^* + p' \quad \ldots (\mathbf{4.10})$$

$$u = u^* + u'$$
$$v = v^* + v' \quad \ldots (\mathbf{4.11})$$
$$w = w^* + w'$$

$$\begin{aligned} a_{i,J,K}(u_{i,J,K} - u^*_{i,J,K}) &= \sum a_{mdz}(u_{mdz} - u^*_{mdz}) \\ &+[(p_{I-1,J,K} - p^*_{I-1,J,K}) - (p_{I,J,K} - p^*_{I,J,K})]A_{i,J,K} \\ a_{I,j,K}(v_{I,j,K} - v^*_{I,j,K}) &= \sum a_{mdz}(v_{mdz} - v^*_{mdz}) \\ &+[(p_{I,J-1,K} - p^*_{I,J-1,K}) - (p_{I,J,K} - p^*_{I,J,K})]A_{I,j,K} \\ a_{I,J,k}(w_{I,J,k} - w^*_{I,J,k}) &= \sum a_{mdz}(w_{mdz} - w^*_{mdz}) \\ &+[(p_{I,J,K-1} - p^*_{I,J,K-1}) - (p_{I,J,K} - p^*_{I,J,K})]A_{I,J,k} \end{aligned} \quad \ldots (\mathbf{4.12})$$

As a result, the velocity correction components (u', v', w') can be calculated using the pressure correction field in the following fashion[46]:

$$\begin{aligned} a_{„J,K}u'_{t,J,K} &= \sum a_{mdz}u'_{mdz} + (p'_{I-1,J,K} - p'_{I,J,K})A_{i,J,K} \\ a_{I,j,K}v'_{I,j,K} &= \sum a_{mdz}v'_{mdz} + (p'_{t,d-1,K} - p'_{I,j,K})A_{I,j,K} \\ a_{I,J,k}w'_{I,J,k} &= \sum a_{mdz}w'_{mdz} + (p'_{I,J,l-1} - p'_{I_kJ,k})A_{I,J,k} \end{aligned} \quad \ldots (\mathbf{4.13})$$

SIMPLEC's (u)velocity correction equation can be written as follows:

$$\begin{aligned} u'_{t,J} &= d_{i,J}(p_{I-1,J} - p_{I,J}) \\ v'_{I,j} &= d_{l,j}(p_{I,J-1} - p_{I,J}) \\ w'_{k,j} &= d_{k,j}(p_{k,J-1} - p_{k,J}) \end{aligned} \quad \text{where;} \quad \left(\begin{aligned} d_{i,J} &= \frac{A_{i,J}}{a_{i,J} - \sum a_{nb}} \\ d_{I,J} &= \frac{A_{I,J}}{a_{I,J} - \sum a_{nb}} \\ d_{k,J} &= \frac{A_{k,J}}{a_{k,J} - \sum a_{nb}} \end{aligned} \right) \quad \ldots (\mathbf{4.14})$$

As a result, the adjusted velocity field can be calculated as follows using equation (4.11):

$$u'_{t,J,K} = d_{i,J,K}\left(p_{I-1,J,K} - p_{I,J,K}\right)$$
$$v'_{I,j,K} = d_{l,j,K}\left(p_{I,J-1,K} - p_{I,J,K}\right) \text{ where; } \begin{pmatrix} d_{i,J,K} = \dfrac{A_{i,J,K}}{a_{i,J,K} - \sum a_{mdz}} \\ d_{I,j,K} = \dfrac{A_{I,j,K}}{a_{I,j,K} - \sum a_{mdz}} \\ d_{I,J,k} = \dfrac{A_{I,J,k}}{a_{I,J,k} - \sum a_{mdz}} \end{pmatrix} \quad \ldots (\mathbf{4.15})$$
$$w'_{I,J,k} = d_{I,J,k}\left(p_{I,J,K-1} - p_{I,J,k}\right)$$

depicted **figure(4.3)** a flowchart of how this algorithm progresses towards optimizing these guessed fields, and repeating the procedure until the velocity/pressure fields are converging.

The PRESTO (PREssure STaggering Option) scheme computes the "staggered" (that is, face) pressure using the discrete continuity balancing for a "staggered" control volume about the face. Notably, equivalent accuracy is reached using a similar technique for triangular, tetrahedral, hybrid, and polyhedral models. All meshes are compatible with the PRESTO! scheme**[54]**.

When first-order accuracy is required, quantities at cell faces are calculated by assuming that the cell center values of any field variable indicate a cell-average value and are consistent over the whole cell; the face quantities are equal to the cell quantities. Consequently, when first-order upwinding is selected, the face value Φ_f in the upstream cell is made equal to the cell-center value of the face value Φ in the downstream cell**[54]**.

On structured meshes aligned with the flow direction, the QUICK method is often more accurate. The QUICK scheme can be used for

unstructured or hybrid meshes as well; in these cases, the usual second-order upwind discretization scheme (described in Second-Order Upwind Scheme) will be used at the faces of non-hexahedral (or not quadrilateral, in 2D) cells, as described in Second-Order Upwind Scheme. When the parallel solver is employed, the second-order upwind strategy will also be used at partition boundaries, in addition to being used at the partition boundaries**[54]**. **Table(4.4)** depicted the CFD simulation solution of methods.

Table(4.4) CFD simulation solution of methods[54].

Pressure-velocity coupling	Discretization Methods				
	Gradient	Pressure	Momentum	Energy	Volume fraction
SIMPLEC	Least squares cell-based	PRESTO	first-order Upwind	first-order Upwind	QUICK

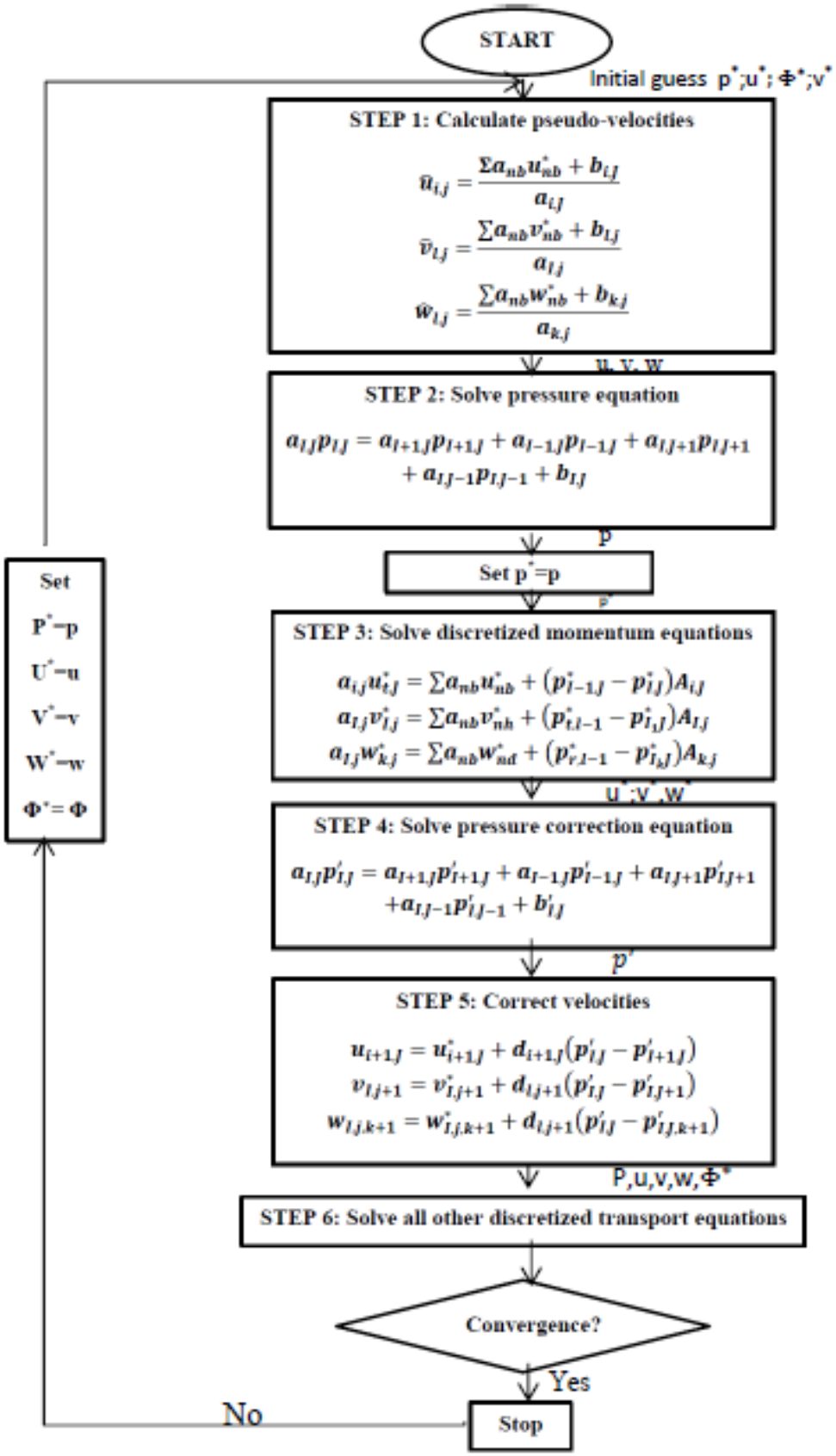

Figure(4.3) The SIMPLEC Algorithm Flowchart[46].

4.1.3Mesh generation

The oil film domain of the bearing under study is created using a CAD program as shown in **figure(4.4)**. It is discretized into three layers along the radial direction. A total of 133767 hexahedral finite volume cells with 0.3mm thickness are created in the circumferential direction. **Figure(4.5)** shows the geometry and mesh of the solid domain for the shaft and the bearing.

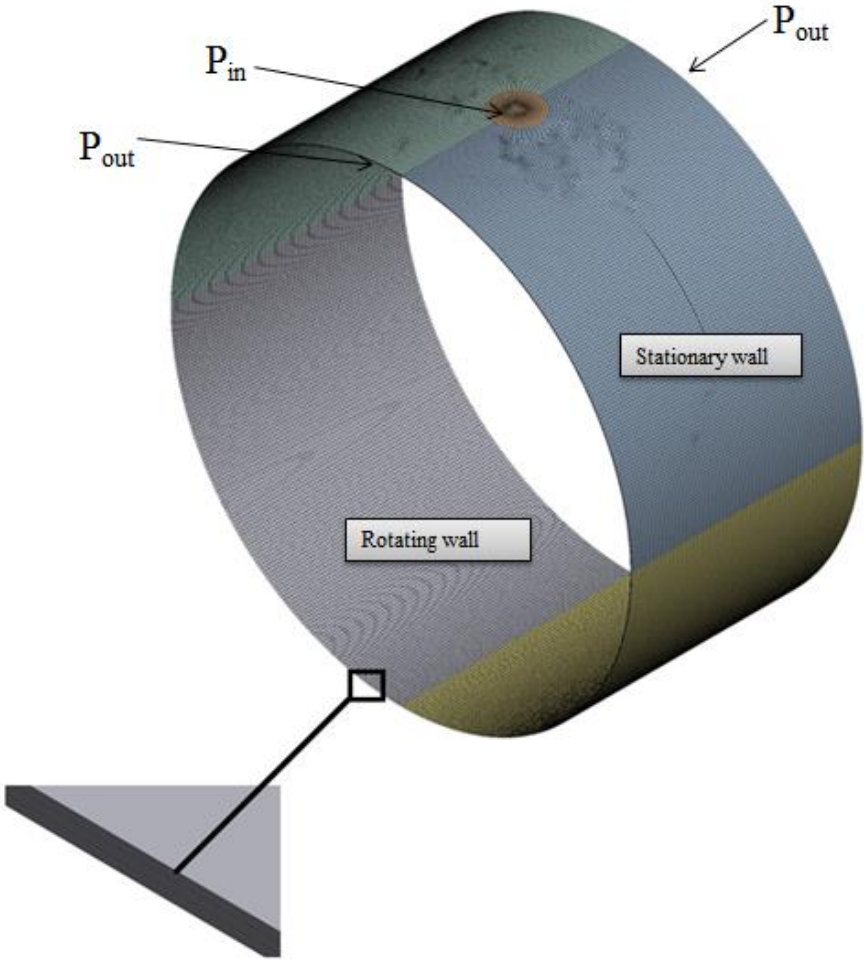

Figure(4.4) Geometry and mesh details of the fluid domain**.**

The solid domain was also discretized into 86871 tetrahedral finite elements along the circumferential direction to evaluate the material deformation and the stresses induced as can be shown in **Figure (4.5a-b)**.

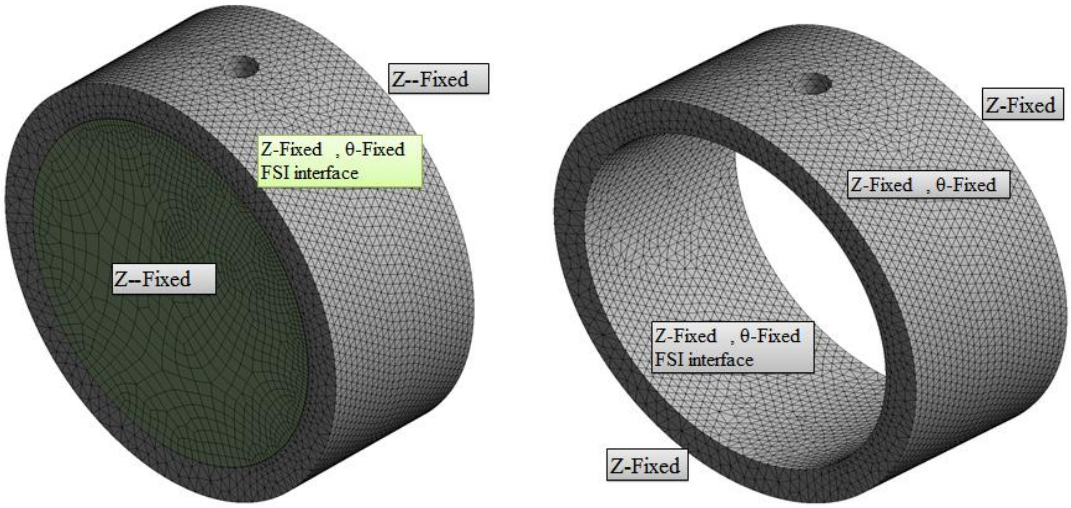

(a) (b)

Figure(4.5) Geometry and mesh of solid domain for the shaft and the bearing**.**

4.1.4Dynamic meshing

A dynamic meshing technique with a diffusion-based smoothing approach is used to model mesh movement. In this approach, the mesh deformation is controlled by the diffusion equation based on mesh displacement speed. The moving boundaries are generally used to determine the boundary conditions from this equation. The Laplace equation then defines the propagation of boundary displacements in the transformed mesh's internal nodes. The diffusion coefficient is used to manage the impact of moving boundaries on internal nodes. The diffusion-based smoothing has a higher computational cost than other smoothing methods, it has the advantage of maintaining the best mesh quality and allowing greater boundary deformation without mesh rupturing. Bad quality elements or mesh defects cannot be smoothed by this method, but

rather move together with the pre-computed (at the beginning of each mesh update) displacement velocity.

4.1.5 Study of Mesh Independence

To ensure the accuracy of the solution, a mesh independence study for the TEHD model is conducted for a journal bearing with an eccentricity ratio of 0.5 and a rotating speed of 1000 rpm. It is performed by observing the three predicted parameters including pressure, deformation, and load for various levels of grid refinement as shown in **table(4.5)** and **figure(4.6a-c)**. It can be observed from **table(4.5)** that using element thickness of 0.3mm with three layers in the radial direction and the total number of hexahedral cells of 133767 elements in circumferential direction leads to a good mesh quality with an aspect ratio of 35.966 and approximately the same values of the different parameters. Hence the number of elements of 133767 was adopted for the fluid domain.

Table(4.5) The fluid domain FSI analysis results at various mesh grid densities.

Body Size (mm)	Mesh Layers (r)	Aspect ratio	Element number	Pressure (Pa)	Deformation (μm)	Load (N)
0.9	3	107.13	15366	655794.6	0.030743	360.7267152
0.8	3	94.225	19509	655321.6	0.030753	360.1868488
0.7	3	83.326	25116	646503.7	0.030319	356.5371553
0.6	3	71.422	33996	657520.7	0.030898	360.8967868
0.5	3	59.995	48042	657881.6	0.030921	359.1397649
0.4	3	47.615	76185	657572.6	0.030925	351.7762836
0.3	3	35.966	133767	657762.3	0.030932	343.2067273
0.2	3	23.998	298956	657755.8	0.030938	338.8426399
0.9	4	142.84	20488	710979.3	0.033397	393.5231542
0.8	4	125.64	26012	712900.2	0.033374	395.2618143
0.7	4	111.1	33488	711759.7	0.033422	392.1056762
0.6	4	95.23	45328	708493.2	0.033171	389.3031501
0.5	4	79.993	64056	703716.2	0.032976	386.9049031
0.4	4	63.486	101580	714588.9	0.033599	387.796373
0.3	4	47.956	178356	714802.1	0.033611	377.8640294
0.2	4	31.997	398608	714781.5	0.033619	369.2931084

Although the grid dependence test is shown in **figure(4.6a-c)** shows that the minimum elements required are 133767 elements however the aspect ratio of such elements is used as the main criterion in selecting their suitable number. The total number of elements more than 710979 elements produces a higher aspect ratio which affects the values of the pressure, deformation, and load leading to produce a higher relative error.

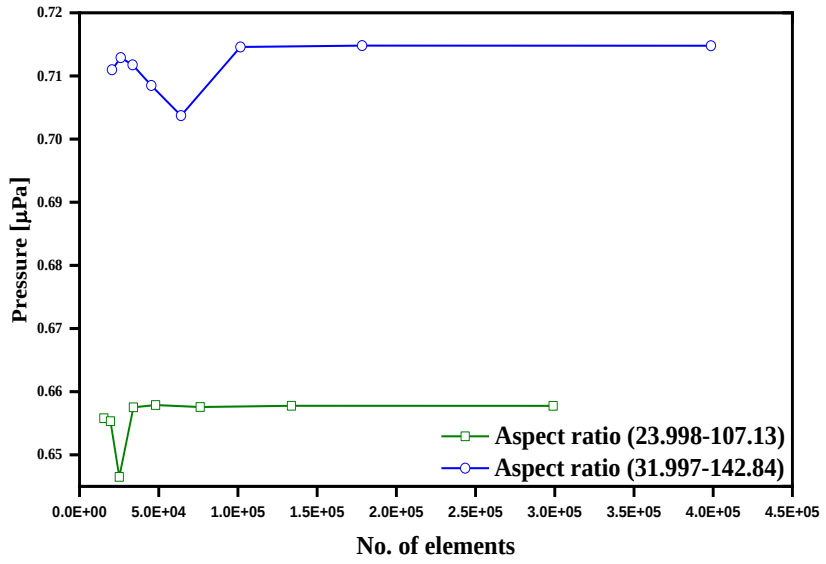

(a) Pressure parameter.

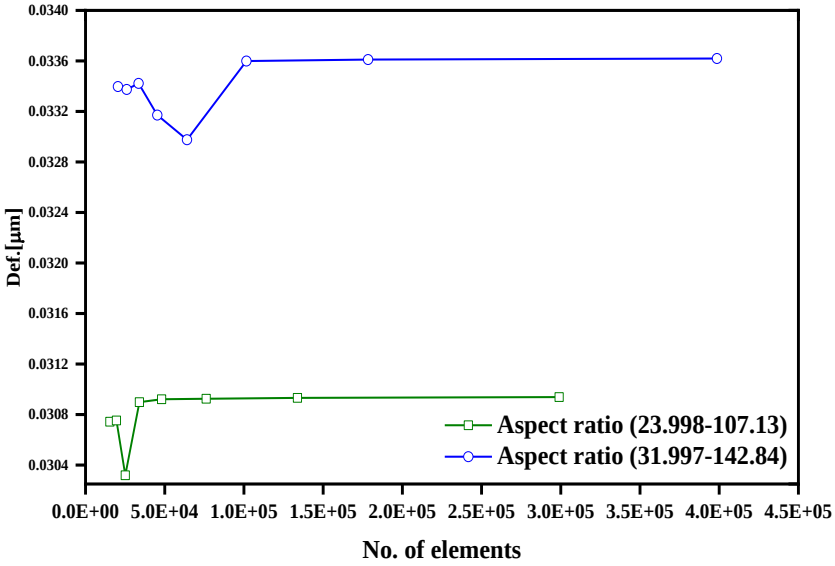

(b) Deformation parameter.

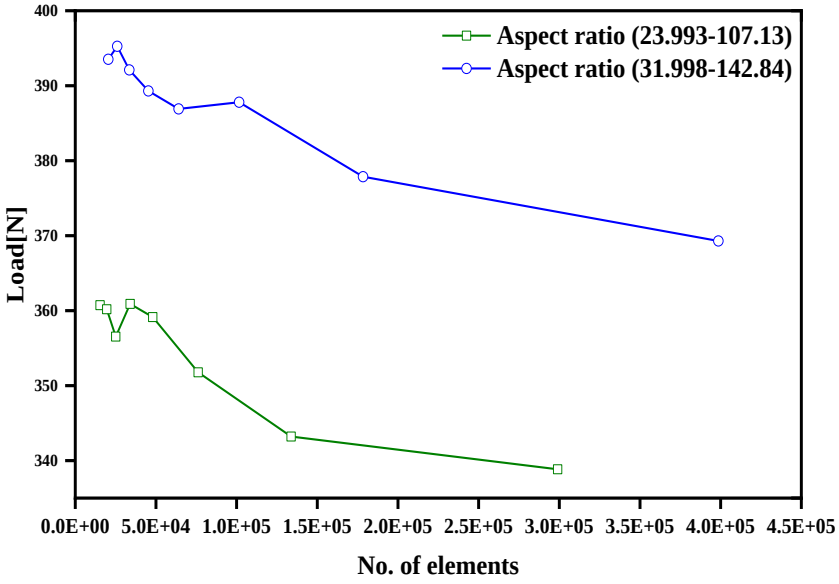

(c) Load parameter.

Figure(4.6) Convergence test.

4.1.6 Fluid-Structure Interaction (FSI)

The interaction of the fluid-structure (FSI) includes relating the fluid dynamics and structural mechanics of the bearing. The bearing is subjected to a hydrodynamic force exerted by the fluid flow that causes it to deform, thus altering the flow domain. FSI modelling can be implemented by using one-way or two-way FSI. One-way FSI is commonly used for smaller structural deformations with no need for flow updating and recalculation. The measured flow and thermal fields are transferred from CFD to FEA by ANSYS software R2 2019 with weak coupling in terms of the two domains in this case. However, in two way FSI technique the fluid flow is adjusted in response to structural deformations by iteratively transferring the data between FLUENT and the structural analysis as can be shown in the block diagram of **figure(4.7)**.

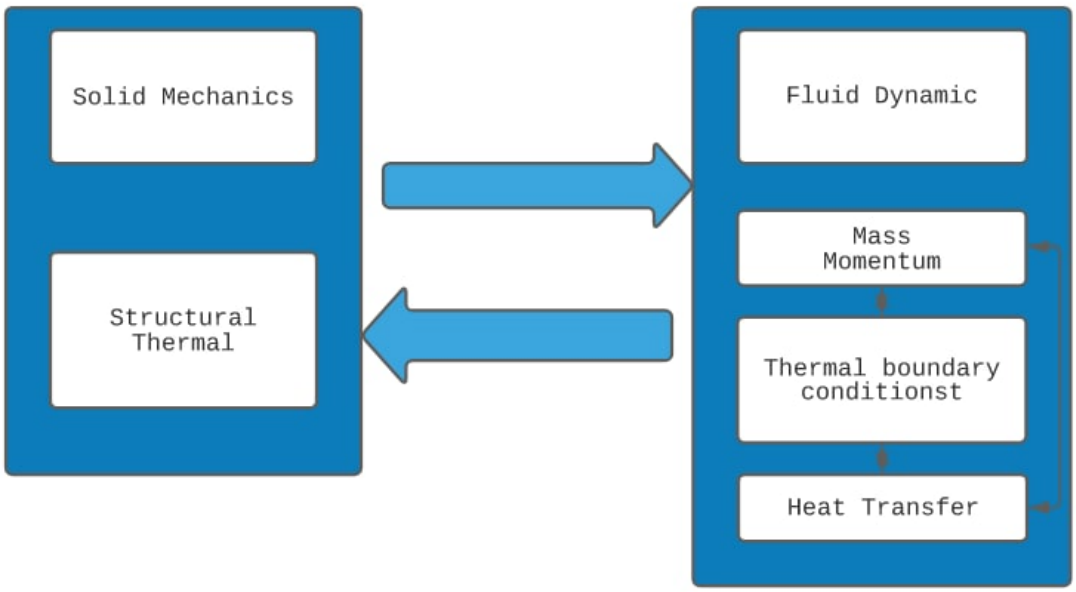

Figure(4.7) The general procedure of Two-Way Fluid-structure interaction.

Two-way FSI is used in this study to evaluate the bearing deformations and flow dynamic re-modelling. ANSYS' static structural capability is used to find bearing deformations, while CFD is used to quantify hydrodynamic pressure and forces. The methodology used to obtain the solution by FEM can be summarized here in[54].

Consider a node (k,l) on the inner surface of the bearing shell subjected to a unit force F_0. The displacement of an arbitrary point (i,j)on the surface corresponding to the applied force, F_0, is denoted by $(\Delta_E)_{i,j}^{k,l}$. Hence the flexibility matrix can be written as:

$$C_{P1}\big((k,l,i,j) = (\Delta_P)_{i,j}^{k.l} \qquad \ldots(4.16)$$

For a nodal force distribution normal to the inner surface, $P(k,l)$ the displacement at a node i,j is:

$$\delta_E(i,j) = \sum_k \sum_l F(k,l) C_{P1}(k,l,i,j) \quad \ldots(4.17)$$

Let ΔA then represent the surface of an element that acts under pressure, where:

$$F(k,l) = P(k,l).\Delta A \quad \ldots(4.18)$$

Where P(k,l) indicates the pressure that acts on the element. As a result, Eq. (4.17) becomes

$$\delta_E(i,j) = \sum_k \sum_l p(k,l) C_p(k,l,i,j) \quad \ldots(4.19)$$

Where

$$C_P((k,l,i,j) = C_{P1}((k,l,i,j) \cdot \Delta A \quad \ldots(4.20)$$

Again, for a unit temperature high above an element (m, n) $|T_0(k,l)| = 1$, the 'i' node of the bearing shell will experience an extension of $(\Delta_T)_i^{m,n}$ and

$$C_T(m,n,i) = (\Delta_T)_i^{m,n} \quad \ldots(4.21)$$

When the expansions are added together, we get

$$\delta_T(i,j) = \sum_m \sum_n \Delta T(m,n) C_T(m,n,i) \quad \ldots(4.22)$$

The static structure is used to obtain the matrices $C_P(k,l,i,j)$ and $C_T(m,n,i)$. Hence, The oil film thickness, h given in Eq.(3.24), can be calculated as soon as $\delta_T(i,j)$ and $\delta_E(i,j)$ are known. The oil film thickness equation can be written in discrete form as[54]

$$h(i,j) = C_p - X \cdot \cos(\theta) - Y \cdot \sin(\theta) - \left(C_p - C_b\right)\cos\left(\theta - \theta_p\right) + \delta_E(i.j) + \delta_T(i,j) \quad \ldots(4.23)$$

The circumferential and axial nodal points are denoted by i,j respectively. The displacement parameters $\delta_E(i,j)$ and $\delta_T(i,j)$ are calculated using Eqs. (4.19) and (4.22), respectively.

Figure (4.8) depicted the flow chart for the Two-way FSI solution technique:

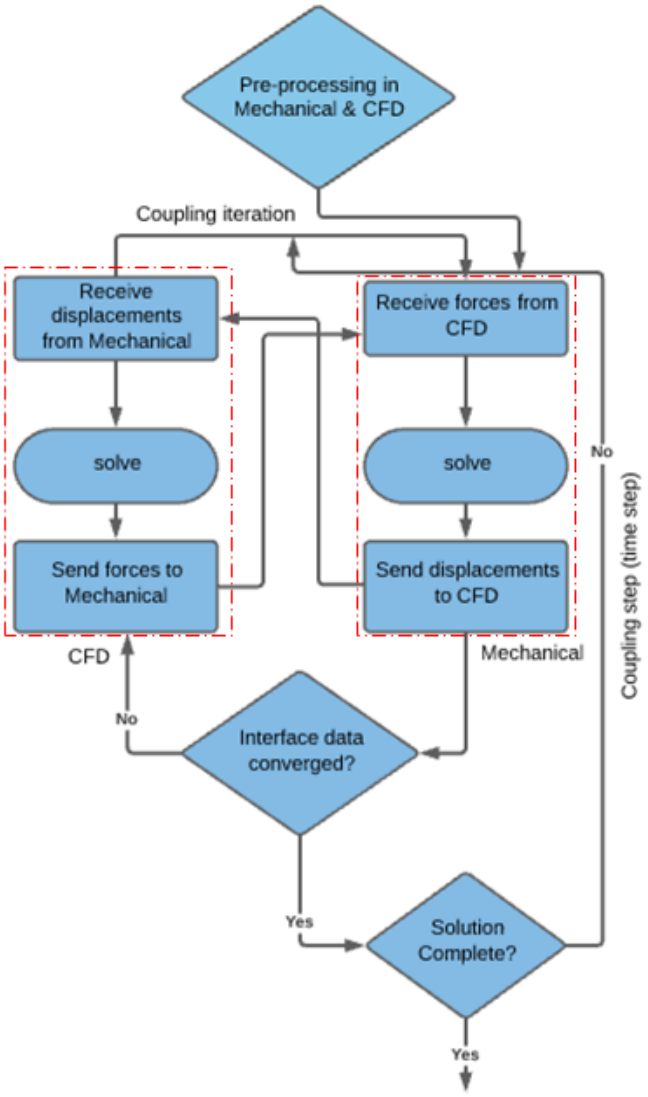

Figure(4.8) Flow Chart of Two Way structure.

4.1.7 Boundary Conditions and Assumptions

The lubricant supply hole is designated as a 'pressure inlet' while the lubricant's sides are designated as a 'pressure outlet' with ambient pressure. Most works in this field take the inlet pressure in the range of (0.2-0.6MPa) **[56]**. So, the inlet pressure of 0.2MPa is adopted in the present work.

The bearing is modeled as a stationary wall while the shaft was moving with absolute rotation speed. The shaft axis position is determined by assuming an arbitrary value of eccentricity with the attitude angle and these values are fed as input to the shaft rotation axis origin. The dynamic mesh technique is used to model the change in fluid domain thickness, for flow film analysis, the fluid film is meshed using ANSYS software. The SIMPLEC algorithm method is employed, with a convergence tolerance of 10^{-4} and 50 iterations used to complete the solution.

4.1.8 Methodology of the Solution

Thermoelastohydrodynamic analysis is implemented in the present work using computational fluid dynamics including the effect of cavitation zone. A two-phase fluid flow model is used to analyze the flow in the cavitation zone. The following are the main steps followed to get the CFD solution of the present work:

1. Input parameters are specified in the design modeler using parametric sets.
2. The journal bearing with suitable dimensions is modeled using a CAD program.
3. The bearing model is imported to the ANSYS FLUENT program. The fluid film of the bearing was discretized to finite volume cells using the FLUENT program while the bearing shell is discretized to finite elements using the ANSYS program.
4. The mixture model, in conjunction with the Zwart-Gerber-Belamari model, was used to simulate the cavitation zone of the bearing.
5. To improve the qualities of the pure oil, nano lubricants oils are added to increase the accuracy with which the task is carried out. When the Nano was added, the oil's viscosity changed with temperature, calculated by the modified Krieger-Dougherty equation.
6. The steady-state pressure solver is used with double precision.
7. The energy equation is turned on for thermohydrodynamic (THD) and thermo-elasto-hydrodynamic (TEHD) studies.
8. The temperature-dependent viscosity variations are included in the analysis using a user-defined function (UDF) written in C^{++} language

and using the DEFINE PROPERTY macro (For details refer to Appendix-A.)

9. The boundary conditions described in section 4.2.6 are used.
10. The velocity field and the preliminary user-preset pressure field were determined iteratively.
11. A pressure correction equation is used to boost the pressure and velocity field, yielding interim solutions for all conservation equations. The equations are iterated until they fulfill the convergence criterion.
12. SIMPLEC algorithm is used for pressure velocity coupling with a presto pressure environment. For the convection terms of each governing equation, the first-order upwind with discernment scheme equation is used, except that the pressure is solved utilizing the PRESTO (super-pressure option).
13. With the aid of custom field functions, the X-pressure force and Y-pressure force are established. The surface monitors are designed to measure the mass flow rate over the pressure inlet and outlet, as well as the X and Y forces on the shaft. For better precision, all residual terms were given a convergence tolerance of 10 E-4.
14. The deformations are estimated employing an ANSYS structural module based on the methodology of a finite element. A dynamic meshing technique with a diffusion-based smoothing approach is used to model mesh movement.
15. The fluid-solid interfaces are defined, as well as the structural boundary conditions. The displacements were transmitted to the built-in interface application.
16. Fluid forces are transferred from FLUENT to Static Structure and displacements from Static Structure to FLUENT using the built-in data transfer interface known as system coupling. The transfer of the data is seen in **Figure (4.9)**. The flow field is therefore altered until the shaft is optimally positioned.

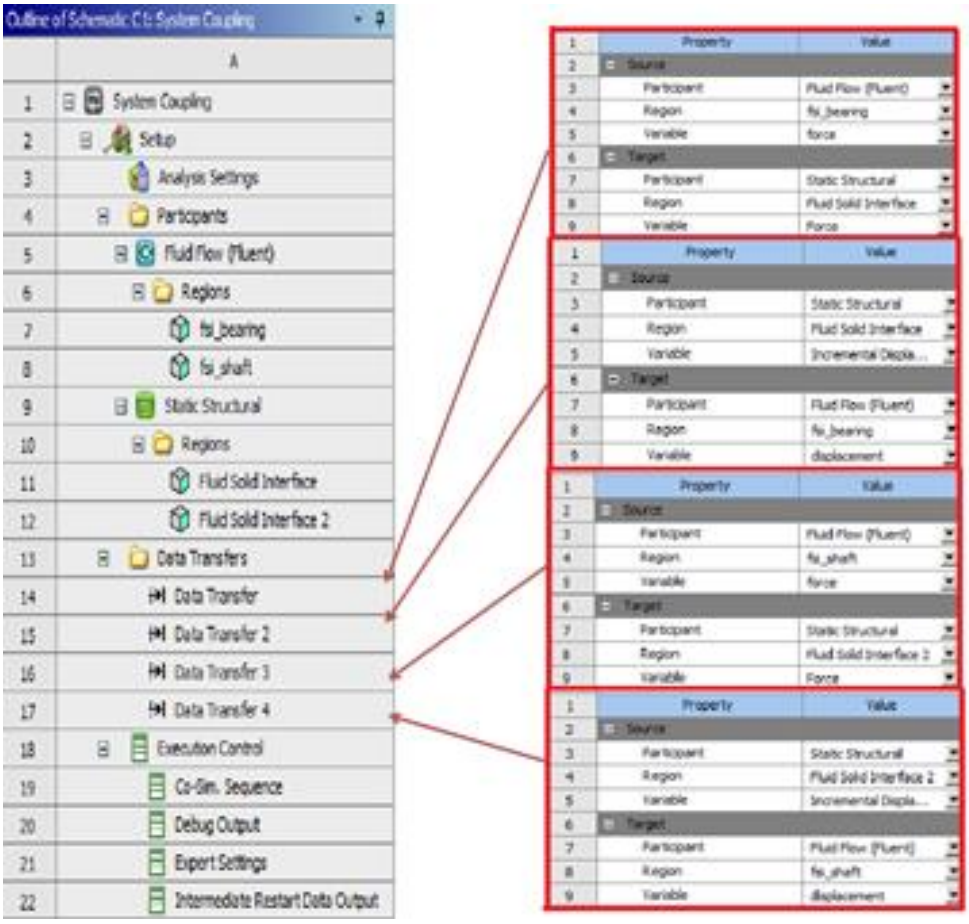

Figure(4.9) Data transfer using system Coupling.

4.1.9 Shaft equilibrium position

The shaft's equilibrium position can be found when the shaft load and fluid force component in the vertical direction are in balance at a constant journal speed. At the balance position, the forces of the fluid in the vertical direction (Y load) are equilibrated with the externally applied load on the shaft (W) with the fluid force in the horizontal direction (X imbalance) must be equal to zero. For this purpose, the shaft rotational axis is fixed at a predefined position concerning attitude angle and eccentricity in a parametric form. The computational fluid dynamics (CFD) domain is used to compute fluid forces, while the structural domain is used to compute structural deformations. Elastohydrodynamics is performed by transforming CFD fluid forces to the structural domain and vice versa. The shaft's equilibrium position is then determined through design optimization.

Initially, perfect balance in the X and Y directions is not attained because the shaft rotation axis is fixed, i.e., it is not permitted to float. As a result, design exploration cannot be used to obtain a response surface with various shaft and equilibrium positions. **Figure (4.10)** illustrates the shaft locations in terms of eccentricity vs. X-direction fluid reaction force, whereas **Figure (4.11)** displays the shaft position versus Y-direction fluid reaction force. The goal is to locate a position on this response surface where the X imbalance is zero and the shaft load is balanced by the fluid reaction force in the Y-direction. As a result, the problem is changed into an optimization problem, to find the X-imbalance zero and Y-load equal to shaft load, resulting in the shaft's correct equilibrium position.

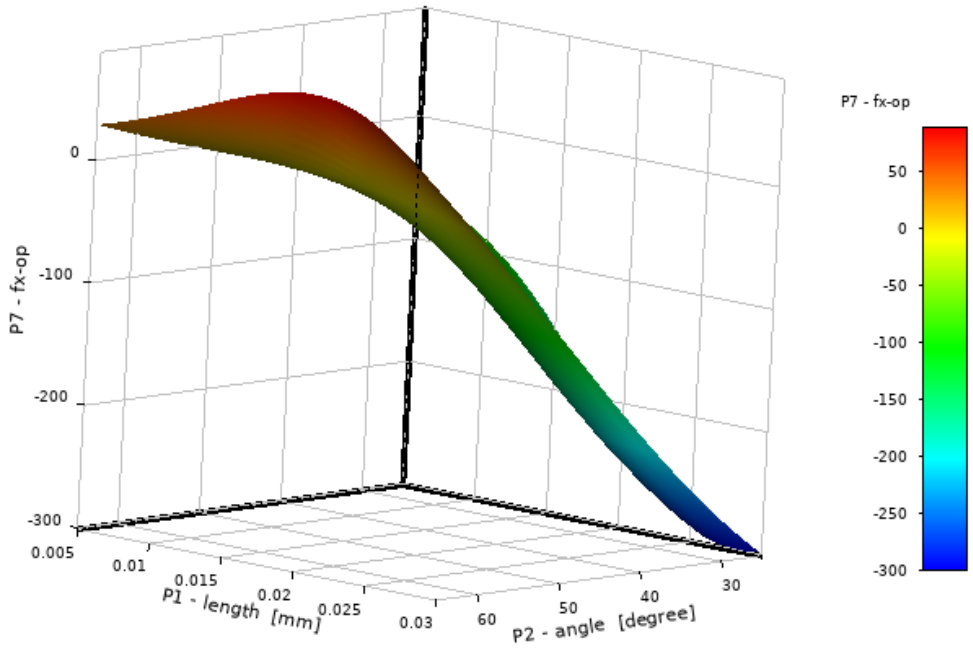

Figure (4.10) Response Surface of horizontal.

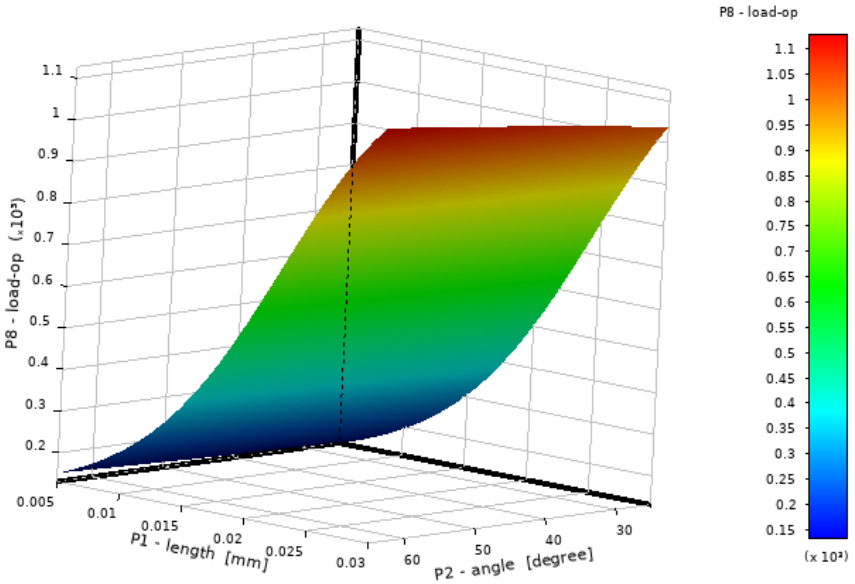

Figure (4.11) Response Surface for Vertical Load.

There are three stages to the design exploration, namely: the design of experiments **(DOE)**, Response Surface Analysis **(RSA)**, and Optimization. DOE is used to calculate a set of eccentricities and attitude angles that are then used to construct the response surface depicted in **Figure (4.12)**.

Table of Outline A2: Design Points of Design of Experiments

	A	B	C	D	E	F	G	H	I	J	K
1	Name	Update Order	P1 - length (mm)	P2 - angle (degree)	P3 - Mesh Max	P6 - fy-op	P7 - fx-op	P8 - load-op	P9 - Total Deformation Maximum (um)	P10 - X-origin (m)	P11 - Y-origin (m)
2	1 DP 7	1	0.023056	31.667	33.37	-640.74	-222.79	678.37	0.063599	-1.210*E-05	-1.9623E-05
3	2 DP 9	3	0.028611	40.556	42.038	-1233.9	-184.49	1247.7	0.12406	-1.8603E-05	-2.1738E-05
4	3 DP 3	4	0.011944	53.889	30.291	-196.22	17.608	197.01	0.015325	-9.6496E-06	-7.0395E-06
5	4 DP 6	5	0.020278	49.444	32.077	-514.48	-43.455	516.31	0.044656	-1.5407E-05	-1.3184E-05
6	5 DP 2	6	0.0091667	27.222	27.585	-154	-95.427	181.17	0.011238	-4.1932E-06	-8.1514E-06
7	6 DP 4	7	0.014722	36.111	28.389	-276.4	-90.873	290.96	0.023015	-8.6766E-06	-1.1894E-05
8	7 DP 5	8	0.0175	62.778	34.03	-348.3	70.242	355.31	0.029985	-1.5562E-05	-8.0052E-06
9	8 DP 8	2	0.025833	58.333	37.205	-847.09	130.01	857.01	0.080773	-2.1987E-05	-1.3562E-05
10	9 DP 1	9	0.0063889	45	29.357	-123.21	-71.712	142.56	0.0075373	-4.5176E-06	-4.5176E-06

Figure (4.12) Design Points as a result.

The eccentricity and attitude angle higher and lower bounds are stated, and the solution is expected to fall within these bounds. To obtain design points, an optimal space-filling design procedure is applied, and a matrix of

experiments is created. These design features serve to create an answer surface that analyzes the interaction between eccentricity, angle of attitude, and output parameters (fluid reaction forces).

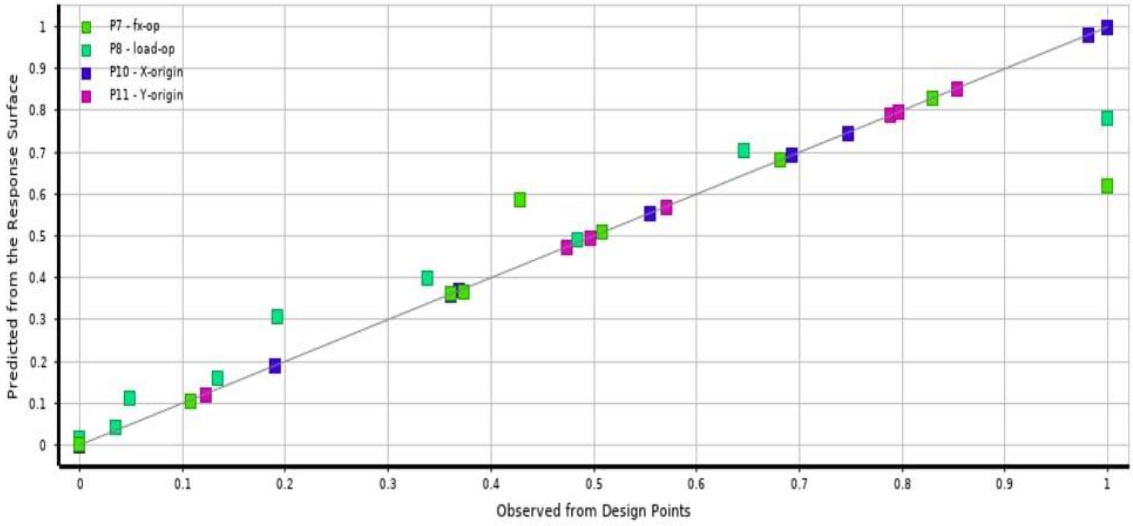

Figure (4.13) Goodness of Fit Curve.

Figure (4.13) shows the goodness of fit is used to determine how well the surface fits the data points. The response surfaces are analyzed to determine the values of potential solutions that meet the optimization requirements. The optimization is based on the evaluation of the response surface using the Multi-Objective Genetic Algorithm (MOGA) based on notions of elitism with non-parametric analytical regression. It allows for many objectives and restrictions to be met to discover the globally optimal solution. More refinement design points are added to the solution to acquire a closer solution, and the procedure is continued until the optimum equilibrium position of the shaft is attained.

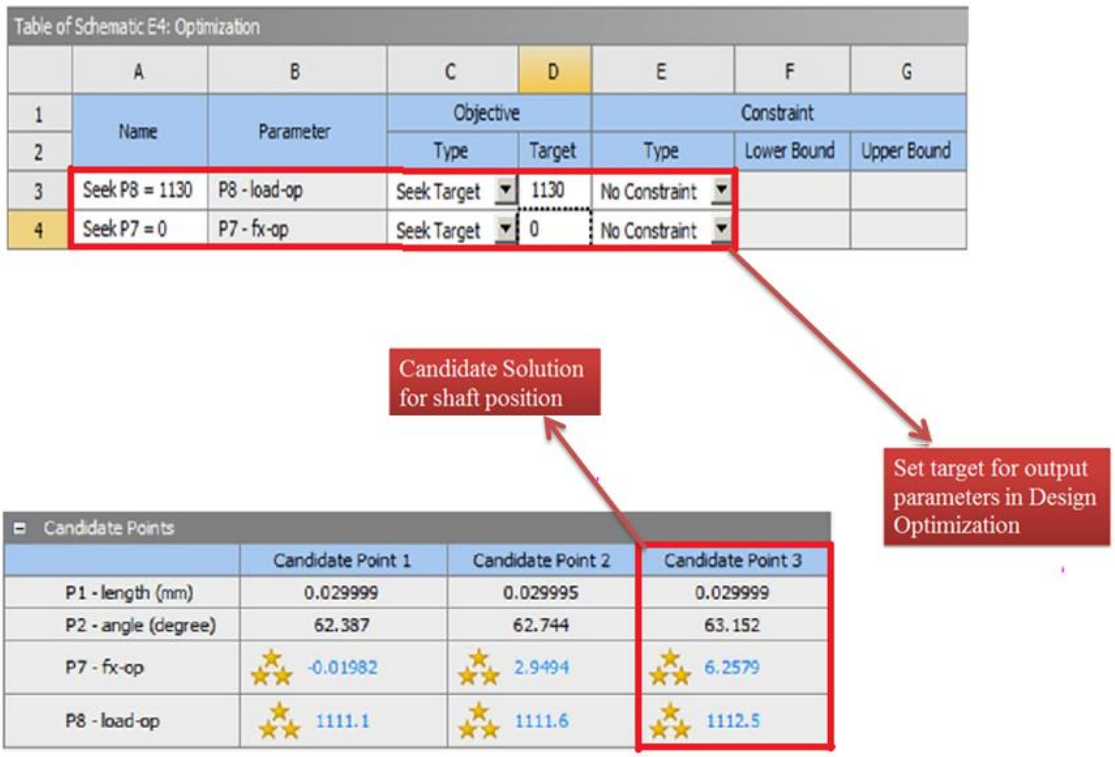

Figure (4.14) Constraints on optimization and possible solutions provided by the optimization module.

Based on the restrictions given, the module provides three optimal solutions, known as candidate points (shown in **Figure (4.14)**). If the solution remains unsatisfactory, a new refinement point from the response surface might be added to obtain the best feasible optimal solution. For the selected ideal design point, the whole cycle of solutions is repeated, to achieve the optimal solution for the performance of the bearing.

Figure (4.15) depicts the complete schematic diagram for numerical simulation.

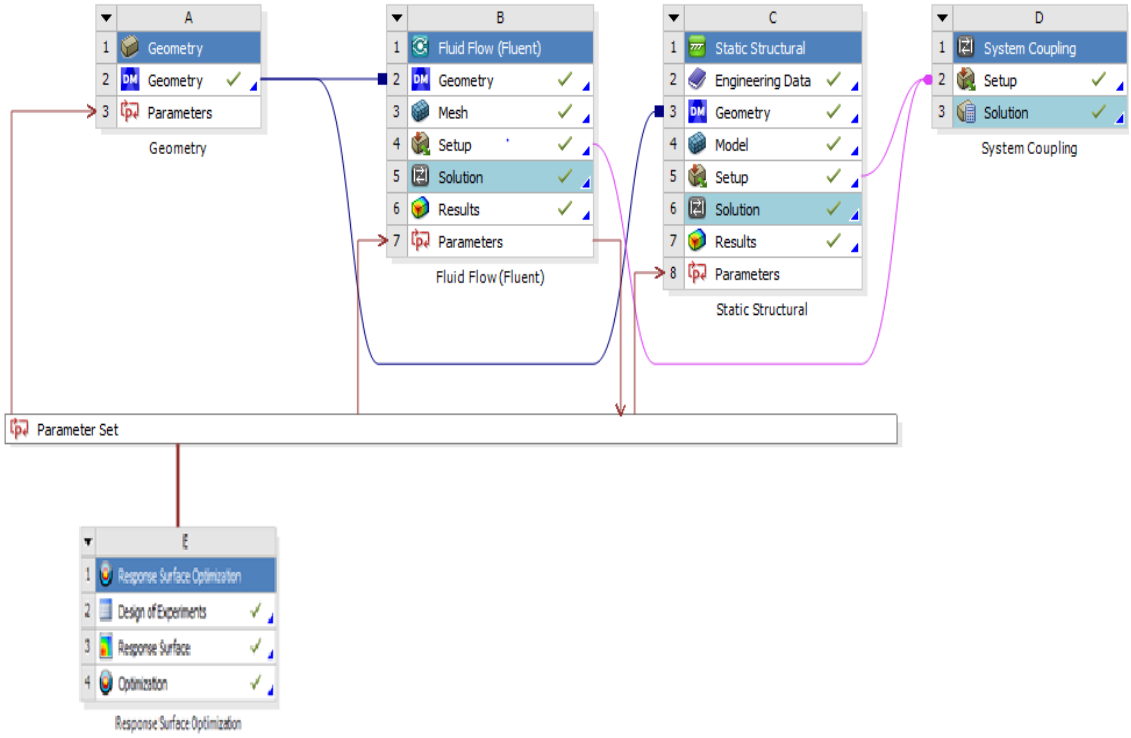

Figure(4.15) Numerical Simulation Schematic diagram.

4.1.10 Cavitation Model

Cavitation is a phenomenon that involves the release of dissolved gas at pressures below saturation pressure, the formation of gas bubbles, and the dissolution into a liquid at higher pressures. Due to cavitation, a portion of the lubricant oil turns to oil-vapor, resulting in a two-phase flow in the bearing flow. The mixture model is a simplified multiphase model that performs nearly as well as a full multiphase model but takes less time to calculate. As a result, the mixture model is employed in this study to simulate two-phase flow in a bearing. In the present work, the flow in the cavitation zone was treated by using the mixture model which solves the mixture's continuity and momentum equations, as well as the vapor phase's volume fraction equation. These equations involve mass transfer between

phases, which is solved using a suitable cavitation model. Zwart-Gerber-Belamari model was adopted to treat the cavitation flow region of the bearing.

4.1.11 Reynolds Number Calculation

The type of flow condition is significant in computational fluid dynamics (CFD) since it determines the type of viscous model to be utilized for the analysis. By calculating the Reynolds number, the flow condition is determined. If the Reynolds number is less than2000, the flow is called laminar; otherwise, it is turbulent. The Reynolds number is calculated as follows **[57]**:

$$Re = \frac{\rho . \omega . R . C}{\mu} \qquad \ldots(4.24)$$

For various working speeds of the current work, the estimate of the Reynolds number using Eq.4.24 is as follows:

The lubricant's characteristics are as follows: Kinematic viscosity, $\mu = 0.0788\ \text{Pa}\,.\,\text{Sec}$, density, $\rho = 875\ \text{kg/m}^3$ and the bearing's geometric details are Radial clearance $\text{C} = 0.05\ \text{mm}$ and Radius, $R = 24.95\ \text{mm}$.

The Reynolds number is less than 2000 and so flow is considered as 'Laminar' for analytic purposes, as shown in **Table (4.6)** below.

Table(4.6) Reynolds Number estimation for different speeds for operating.

N (RPM)	ω (rad/s)	Re
2000	209.3333333	2.899751481
3000	314	4.349627221
4000	418.6666667	5.799502961

Chapter Five

RESULTS AND DISCUSSION

CHAPTER FIVE

RESULTS AND DISCUSSION

The results of thermoelastohydrodynamic (TEHD) performance of journal bearings lubricated with Nano-lubricants are presented and discussed in this chapter. The main performance characteristics such as circumferential pressure distribution, temperature distribution, load-carrying capacity, friction coefficient, and lubricant side leakage have been investigated numerically using the CFD technique through ANSYS FLUENT (2019 R2) software. Effects of nanoparticles volume fraction, bearing elastic and thermal deformations in addition to the effect of cavitation and variable lubricant viscosity effects on the journal bearing performance are considered. The equilibrium position of the bearing was investigated using a suitable optimization technique. Validation of the present work mathematical model against existing results published in available literature has been implemented. The obtained data have been presented using different methods such as curves, contours, and bar charts.

5.1. Validation Study

The mathematical model adopted to analyze TEHD performance of journal lubricated with Nano lubricant as well as the 3D-CFD technique

followed are validated by comparing some of the results obtained in the present work with that obtained by **Ferron et al. (1983)[58]**, **Li et al. (2019)[56], Solghar(2015)[20], Tushare et al.(2021)[29] and Dhende and Pande (2017)[54]**. **Figure (5.1)** shows a comparison between the temperature distribution obtained in the present work with that obtained by **Ferron et al. (1983)[58]** for a bearing lubricated with pure oil in the simulation used the following assumptions were made: lubricant supply pressure of 101.325 kPa, rotating speed of 2000 RPM. It can be observed from this figure that the results are in good agreement with a maximum deviation of 1.26%. **Figure (5.2)** shows a comparison between the results obtained in the present work for the the bearing load when it works at different eccentricity ratios with that obtained by **Ferron et al. (1983)[58]** experimentally and theoretically. This figure shows that the results obtained in the present work are well agreed with that obtained by **Ferron et al. (1983)[58]** with a maximum deviation of 3.38% between the results. It can also be shown from this figure that the results obtained in the present work are well correlated to the experimental work carried out by **Ferron et al.(1983)[58]** for a bearing with a clearance of 0.145µm. The deviation between the experimental results of **Ferron et al.** and that obtained in the present work ranges from 17.7% at low loads to 4.4% at higher loads. Another comparison between the oil film temperature distribution obtained in the present work and that obtained experimentally by **Ferron et al.(1983)[58]** and numerically by **Li et al. (2019)[56]** is presented in **figure (5.3)**. It can be observed from this figure that the results obtained in the present work are fitted excellently to that obtained by **Li et al.** with a negligible maximum deviation of 0.41% while they are in good agreement with that obtained experimentally by **Ferron et al. (1983)[58]**. The results of thermohydrodynamic oil film pressure distribution obtained in the present work are validated with that obtained numerically by **Li et al.**

(2019)[56] and experimentally by **Dhande and Pande (2016)[39]** for a journal bearing works at speed range (1000-3000-5000rpm) as can be shown in **figure (5.4)**. The results presented in this figure depict that the results obtained in the present work are in good agreement with those obtained by **Li et al.(2019)[56]** and **Dhende and Pande (2016)[39]**. The geometry and boundary conditions described in the work of **Solghar(2015)[20]** for a bearing lubricated with oil containing Al_2O_3 nanoparticles were used to validate the three-dimensional CFD analysis implemented in the present work for a journal bearing working under the same circumstances as depicted in **figure (5.5a)**. The findings exhibit a high degree of agreement spatially at the effective zone of the bearing. A comparison of the pressure results obtained in the present work with that obtained by **Tushare et al. (2021)[29]** can be shown in **figure (5.5b, c, d)** for a bearing with a journal rotational speed of 250 RPM, the oil film thickness of 93.896 μm, bearing length of 40 mm and C/R of 0.0055. The bearing was lubricated with a base oil blended with different types of nanoparticles (TiO_2, Al_2O_3, and CuO). The results were found in good agreement with a maximum deviation of (6.8%). The deviation of the results came from the numerical approaches adopted in both studies. Tushar's results were obtained using a one-dimensional model solved numerically using a prepared MATLAB program while those obtained in the present work were obtained using a three-dimensional model solved by using ANSYS-FLUENT which is expected to give more reliable results. In all cases, the load carried by the bearing was calculated and found to be 300N which is exactly the value obtained by **Tushare et al.(2021)[29]**. The contours obtained for the oil film pressure distribution and the deformation of the bearing surface obtained by the 3D-CFD with FSI analysis implemented in the present work were validated with that obtained by **Dhende and Pande (2017)[54]** as presented in **figures (5.6)** and **(5.7)**.

These figures show that the findings demonstrate a high degree of agreement. The above validation analysis allows high confidence for using the present work mathematical model to analyze the performance of a journal bearing lubricated with different types of Nano-lubricants.

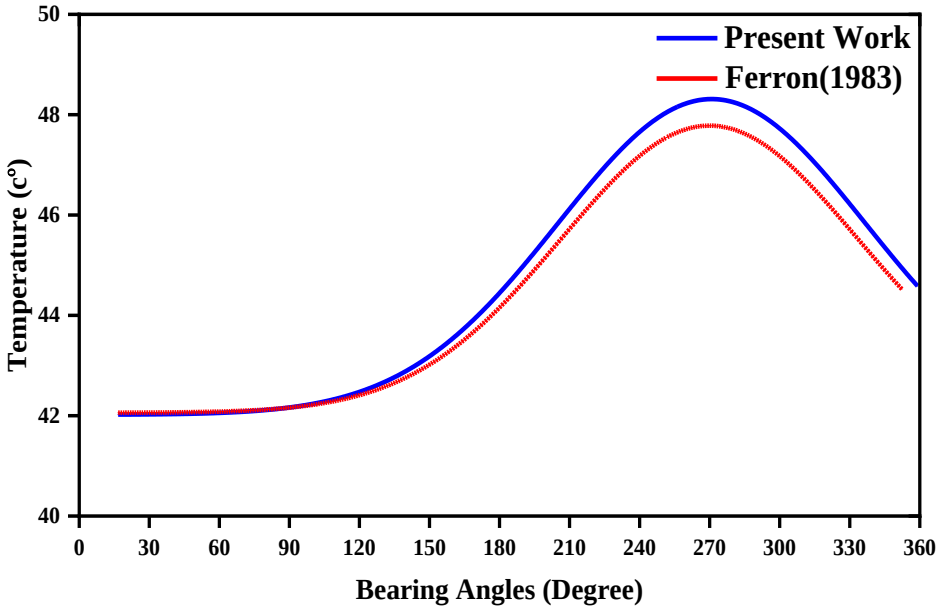

Figure(5.1) Bearing Temperature distribution.

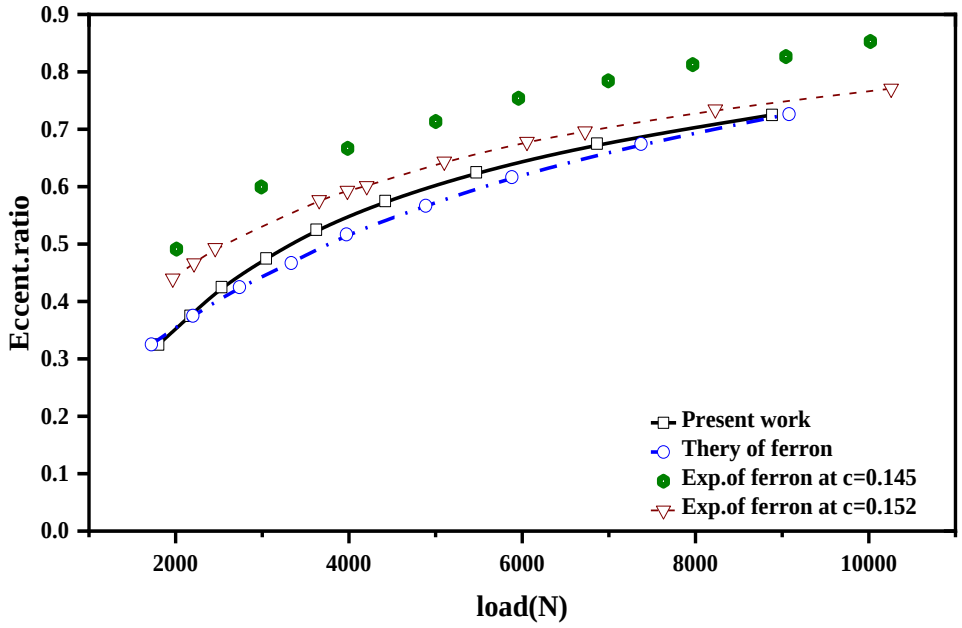

Figure(5.2) Eccentricity ratio vs. the load carried by the bearing Journal speed 2000RPM.

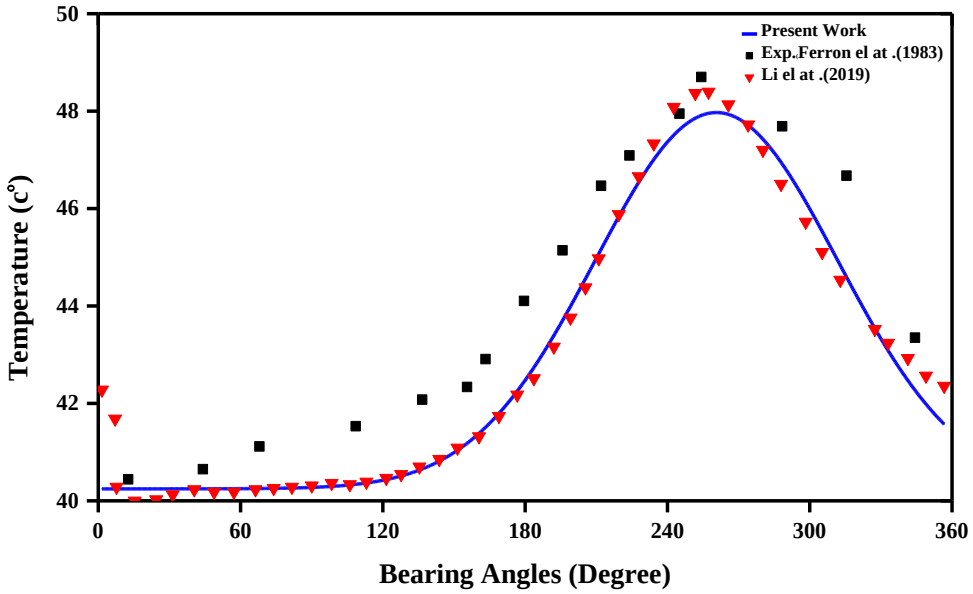

Figure(5.3) Comparison between the results of the temperature distribution obtained in the present work with that obtained by **Li et al. (2019)[56]** and **Ferron et al.(1983)[58].**

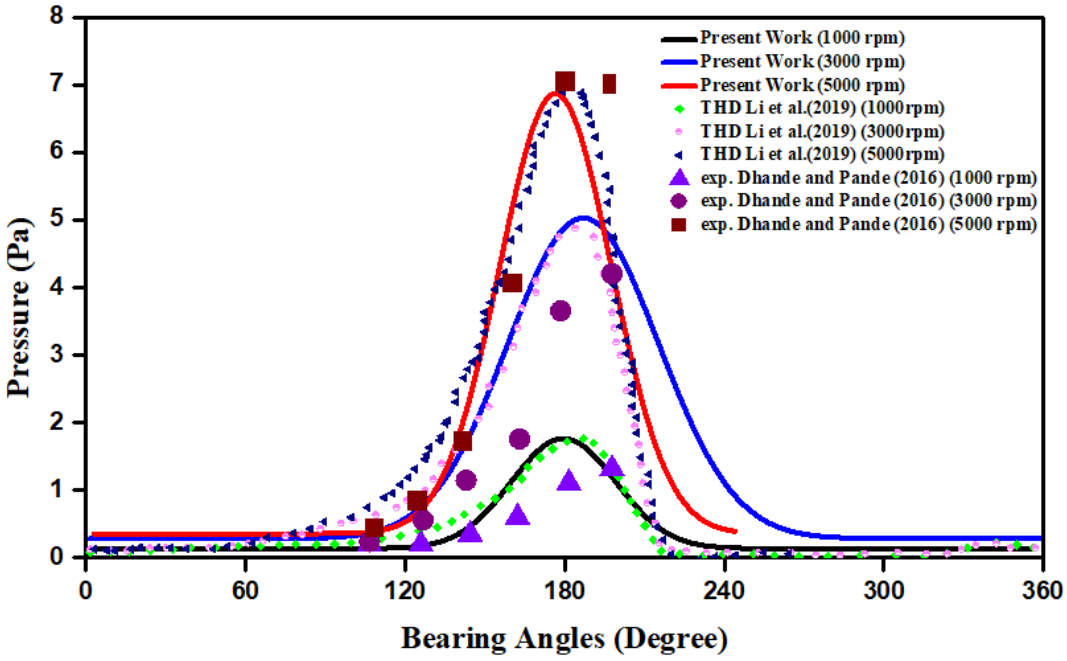

Figure(5.4) Circumferential pressure distribution validation.

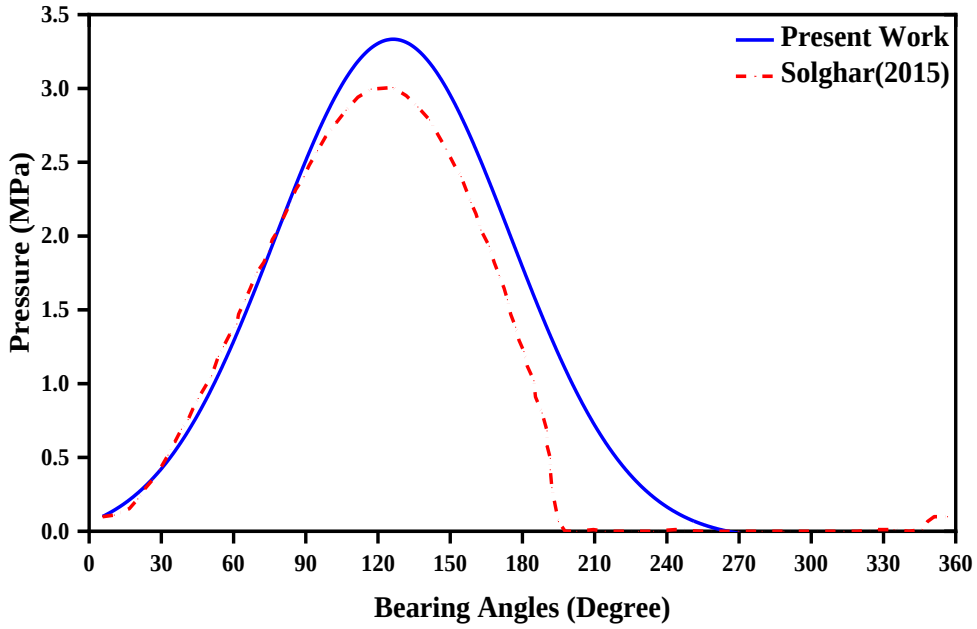

Figure(5.5a) Validation of the pressure distribution for a bearing lubricated with oil containing Al_2O_3 nanoparticles.

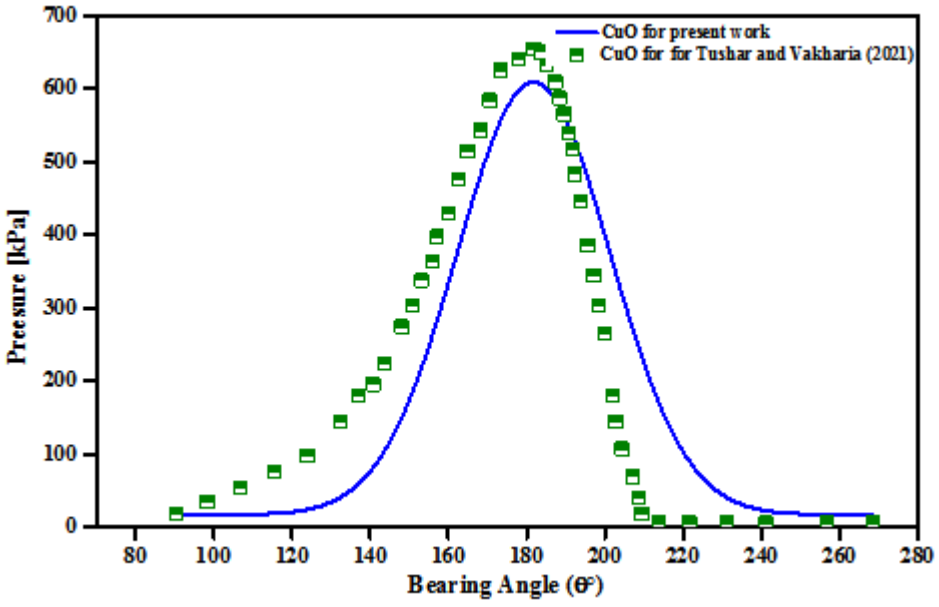

Figure(5.5b) Validation of the pressure distribution for a bearing lubricated with oil containing CuO nanoparticles.

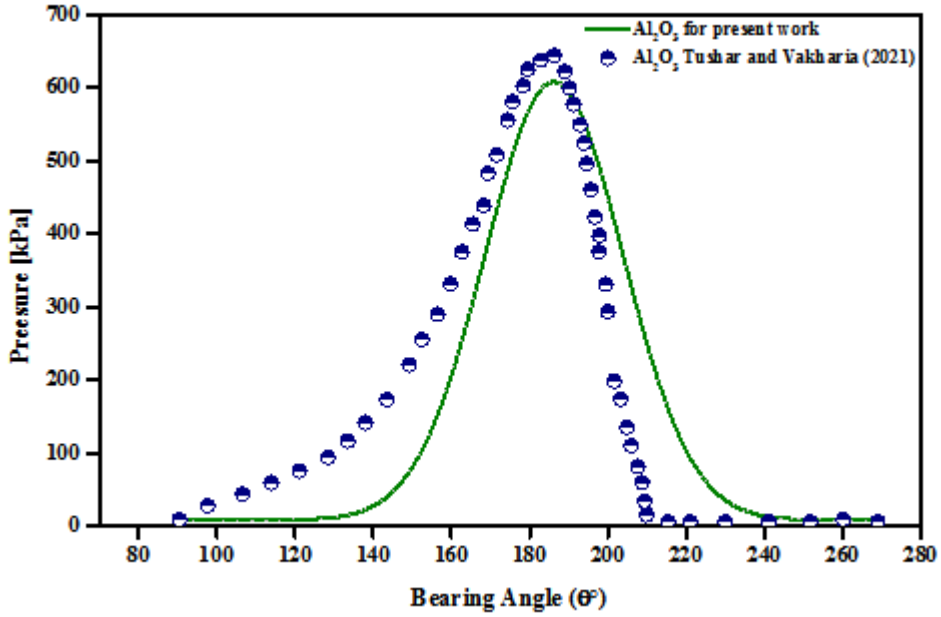

Figure(5.5c) Validation of the pressure distribution for a bearing lubricated with oil containing Al_2O_3 nanoparticles.

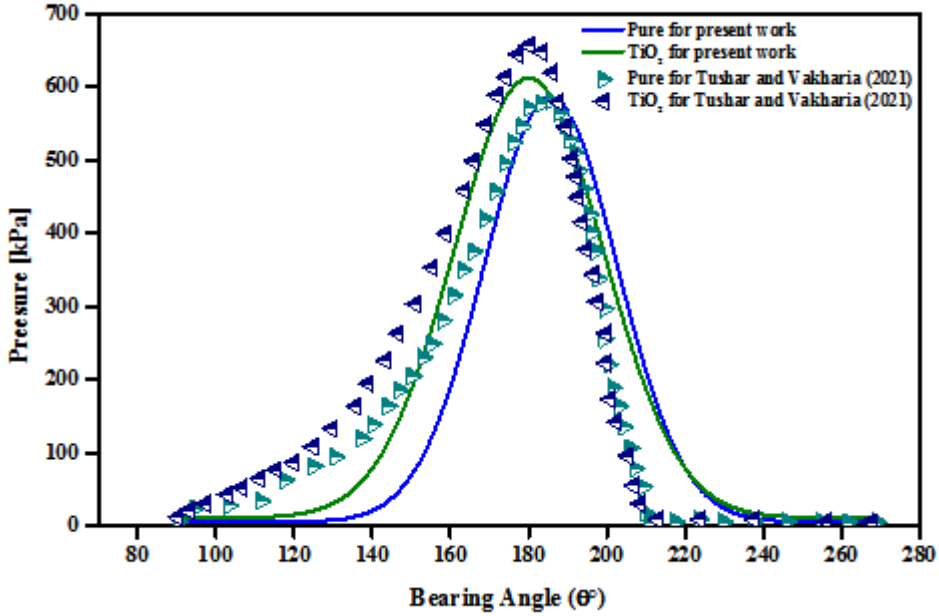

Figure(5.5d) Validation of the pressure distribution for a bearing lubricated with oil containing TiO_2 nanoparticles and base oil.

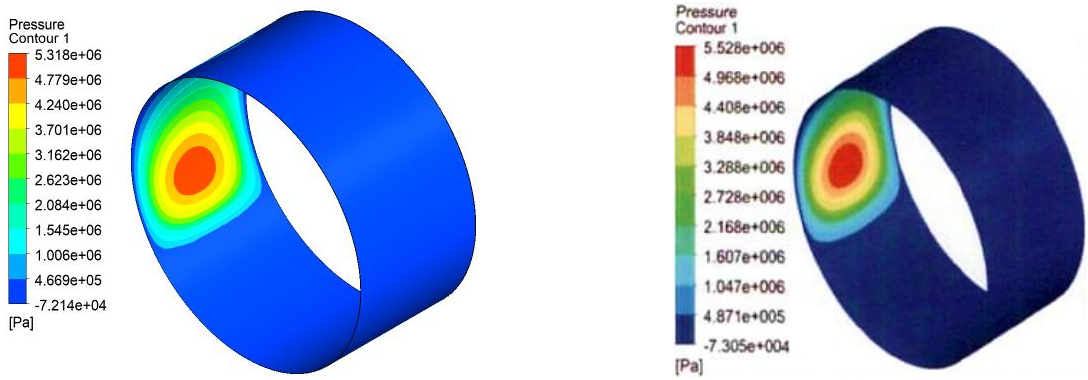

a. **Present work** b. **Dhande and Pande[54]**

Figure(5.6) Validation of pressure contours.

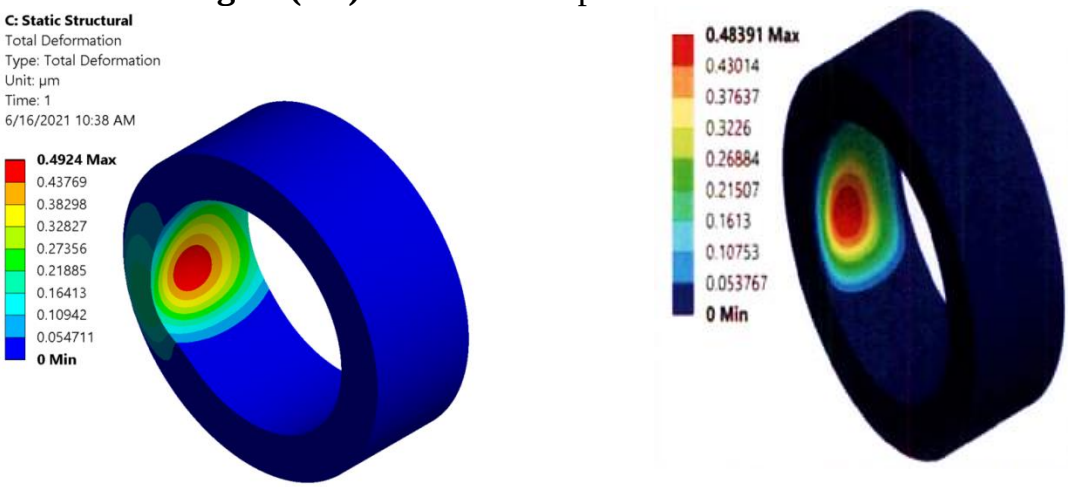

a. **Present work** b. **Dhande and Pande[54]**

Figure(5.7) Validation of deformation contours.

5.2. Effect of nanoparticles volume fraction

TEHD analysis was implemented for a journal bearing with geometrical and physical properties illustrated in the **table (4.1)** mentioned previously.

The effects of lubricating the bearing with nano lubricant that has different volume fractions of TiO_2, Al_2O_3 and CuO nanoparticles dispersed in the base oil on the bearing performance when it works at different

eccentricity ratios and journal speed of 3000rpm will be discussed in this article. The effect of using such lubricants on the pressure distribution of the bearing can be shown in **figures (5.8)**, **(5.9)**, and **(5.10)**. These figures represent the pressure distribution in the circumferential direction for a journal bearing working at an eccentricity ratio of 0.5 and journal speed of 3000rpm. These figures depict that the bearing oil film pressure enhances due to the existence of the nanoparticles dispersed in the base oil.

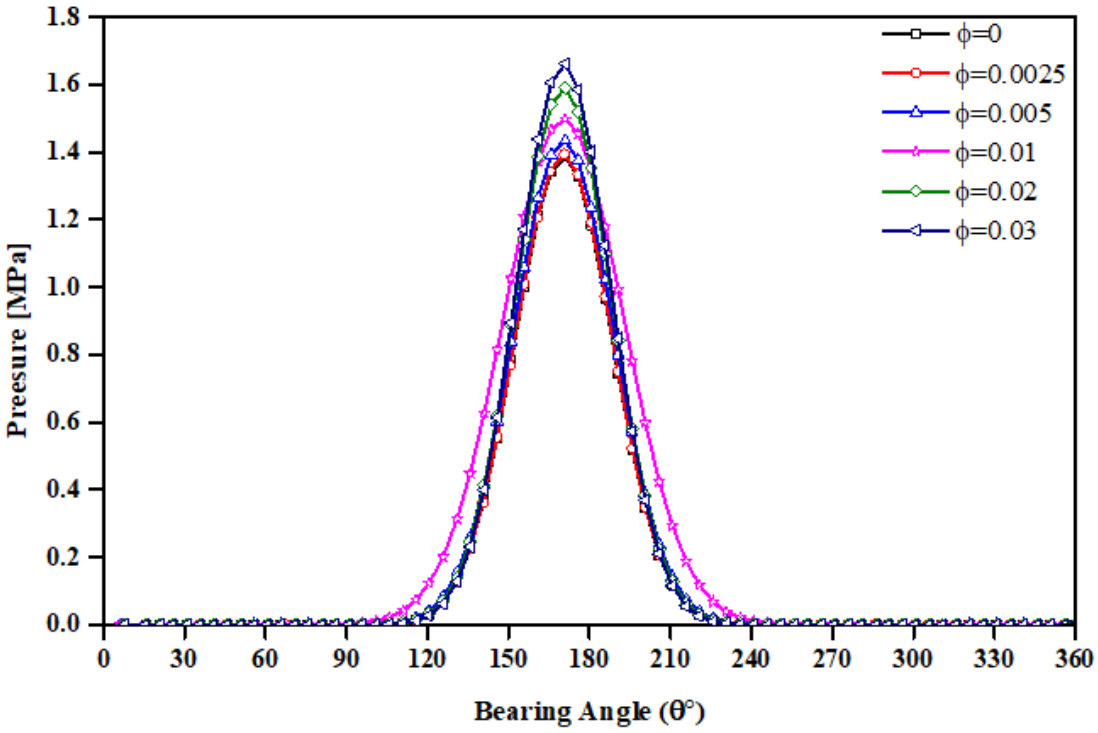

Figure(5.8) Effect of nanoparticles volume fraction of TiO_2 on the pressure distribution.

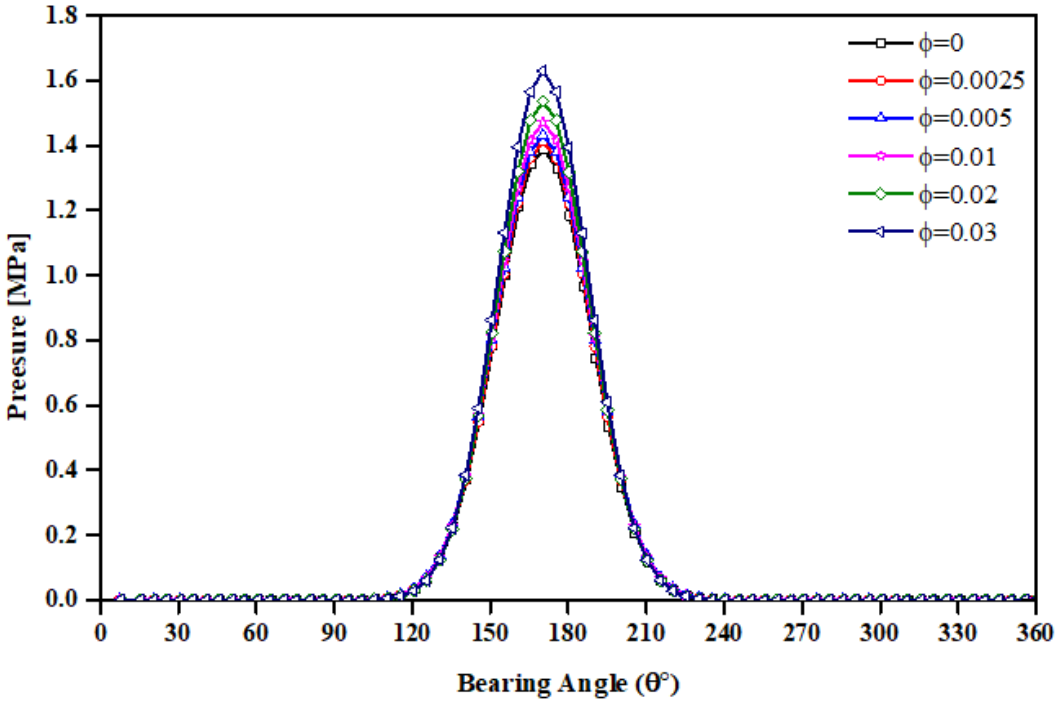

Figure(5.9) Effect of nanoparticles volume fraction of Al_2O_3 on the pressure distribution.

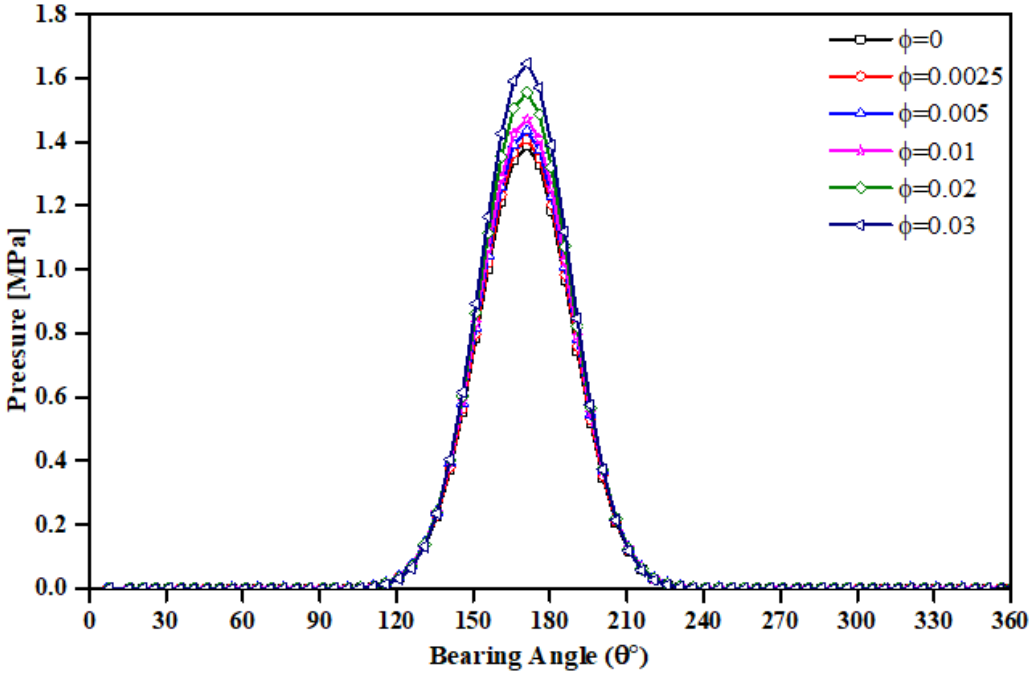

Figure(5.10) Effect of nanoparticles volume fraction of CuO on the pressure distribution.

However, the enhancement is more pronounced for the bearing lubricated with oil that has higher nanoparticle volume fractions. This can be attributed to the increase in oil viscosity due to the nanoparticle dispersion. **Figure (5.11)** shows that the bearing maxim pressure increases by 6% to 17.5% when it is lubricated with the base oil dispersed by 0.01 to 0.03 volume fraction of Al_2O_3 while it becomes 6% to 18.66% and 8.126% to 19.85% when the base oil dispersed with same volume fractions of CuO and TiO_2 respectively in comparison with that lubricated with pure oil. This **figure(5.11)** also obviously shows that the TiO_2 nanoparticles have the most pronounced effect on the maximum oil film pressure. This can be explained by referring to the viscosity measurements done by **Tushar et al. (2021)[29].** It was found that the oil dispersing with TiO_2–Nano-particles has the highest aggregate ratio$\left(\frac{a_a}{a} = 4\right)$ due to its surface effectiveness as a result of the very small size of such nanoparticles(20nm). The presence of these aggregates in the base oil works as an obstacle to the flow of lubricant and leads to an increase in Nano-lubricant viscosity and hence the oil film pressure.

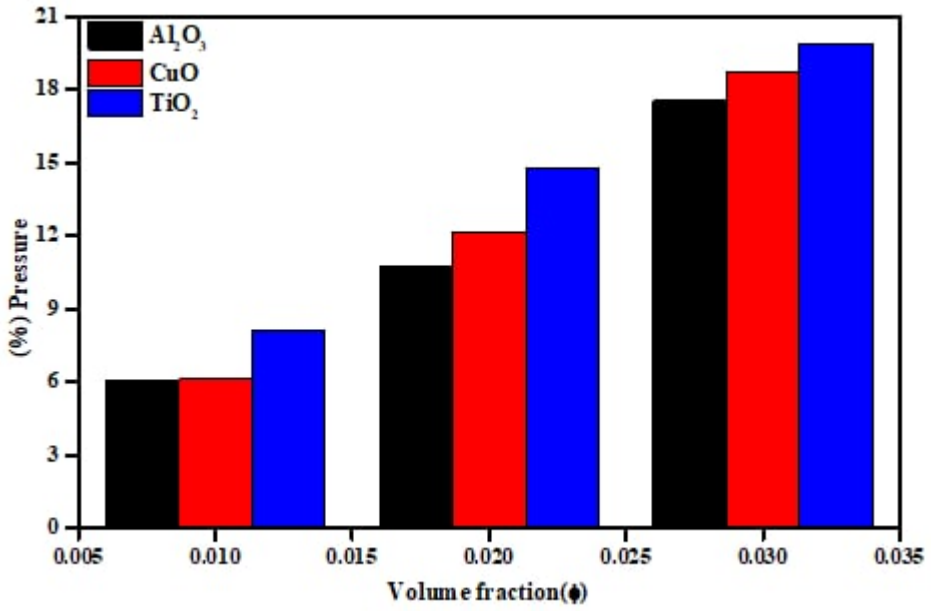

Figure(5.11) Percentage variation in maximum oil film pressure vs. nanoparticle volume fractions in comparison with the base oil.

Figure (5.12) displays the maximum oil film pressure when the bearing works at different eccentricity ratios and lubricated with TiO_2 Nano lubricant that have different volume fractions of nanoparticles. It can be observed from this figure that the maximum oil film pressure increases when the bearing works at higher eccentricity ratios. This can be assigned to the closeness of the journal and the bearing surfaces which causes a thinner oil film thickness which causes, higher oil film pressure. However, the increase in maximum oil film pressure becomes higher when the bearing lubricated with Nano lubricant has a higher volume fraction of dispersed nanoparticles due to the higher viscosity of such lubricants. This figure also clearly shows that the percentage increase in maximum oil film pressure becomes higher as the bearing works at a higher eccentricity ratio and when it is lubricated with Nano-lubricant with different Nano-particles volume fractions.

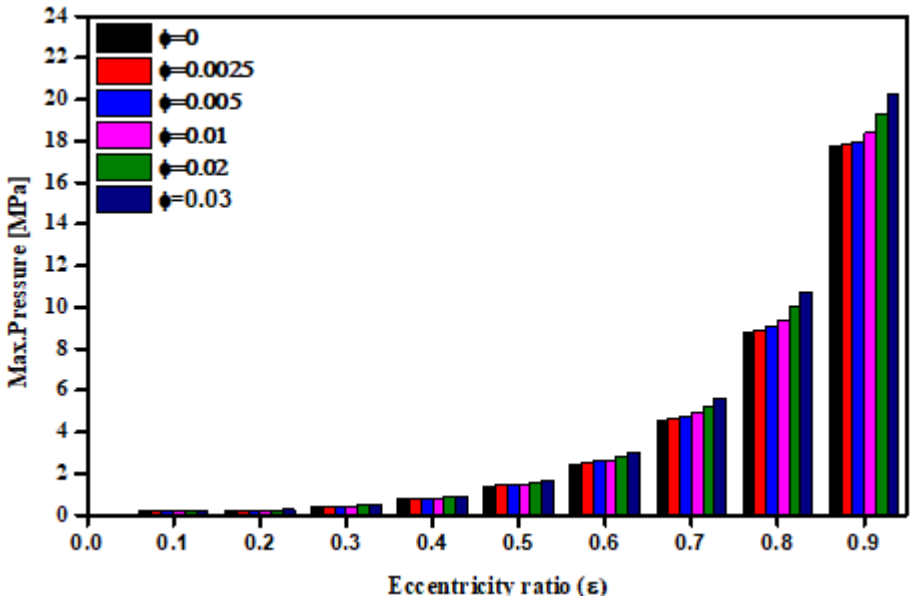

Figure(5.12) Max. pressure vs. eccentricity ratios for a bearing lubricated with TiO_2 Nano lubricant with different volume fractions at ε=0.5.

The maximum oil film pressure for a bearing working at eccentricity ratios of 0.5,0.7 and 0.8 lubricated with Nano lubricant that has a 3% volume fraction of TiO_2 nanoparticles are 1.8MPa, 5MPa, and 10MPa respectively. The effect of nanoparticles volume fraction dispersed in the base oil on the load carried by the bearing when it works at different eccentricity ratios can be shown in **figure (5.13)**.

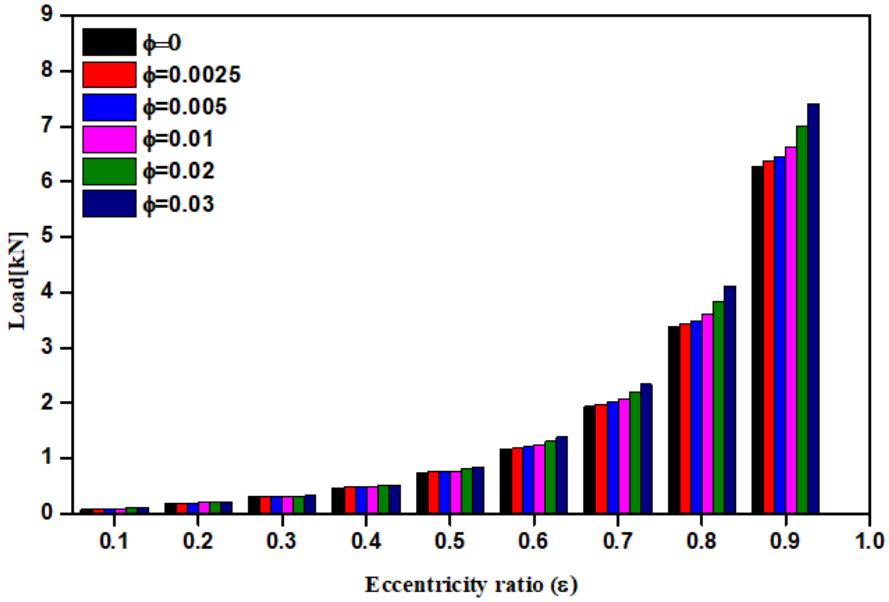

Figure(5.13) Bearing load vs. eccentricity ratios for a bearing lubricated with TiO_2 Nano lubricant with different volume fractions.

This figure depicts the enhancement of the load carried by the bearing lubricated withTiO_2 Nano-lubricant when it works at higher eccentricity ratio. The enhancement becomes more obvious when the bearing is lubricated with a Nano-lubricant that has a higher volume fraction of TiO_2 nanoparticles. This can be attributed to the higher oil film pressure generated when the bearing works under such circumstances as a result of the increase in viscosity of the Nano-lubricant due to the existence of the dispersed nanoparticles. **Figure (5.14)** shows that the load carried by the bearing works at an eccentricity ratio of 0.5 and journal speed 3000rpm increases by about 5% to 13.8% when lubricated with the base oil dispersed by 0.01 to 0.03 volume fraction of Al_2O_3 while it becomes about 4.8% to 14% and 5.2% to 14.3% when the base oil dispersed with same volume fractions of CuO and TiO_2 respectively in comparison with that of the pure oil. This can be credited to the increase in oil viscosity and hence the increase in oil film pressure for the bearing works under these conditions.

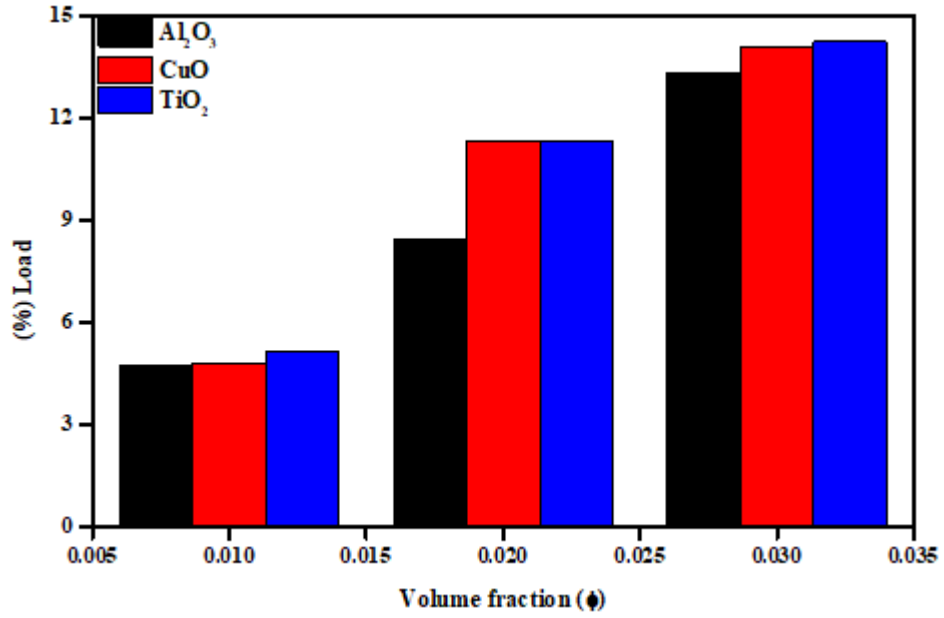

Figure(5.14) Percentage variation in bearing load vs. nanoparticle volume fractions in comparison with the base oil.

The variation of the maximum induced friction force on the journal surface when the bearing is lubricated with oil incorporated with different volume fractions of TiO_2 nanoparticles working at different eccentricity ratios and journal speed of 3000rpm is presented in **figure (5.15)**. It can be noticed that the maximum friction force increases as the bearing works at higher eccentricity ratios. The increase in maximum friction force becomes higher due to the higher dispersion of TiO_2 nanoparticles in the base oil. This can be clarified by the higher viscosity and shear rate for the bearing works under these conditions.

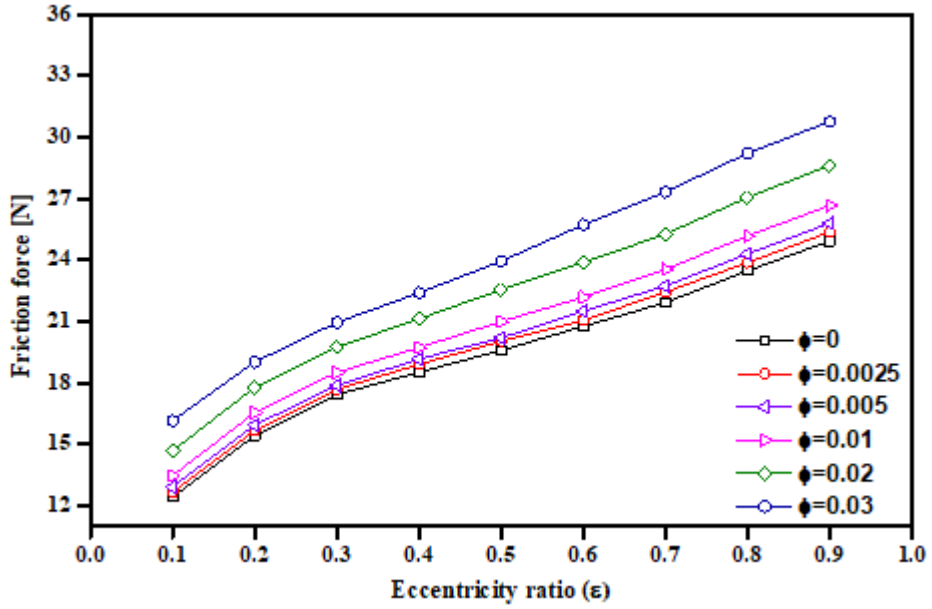

Figure(5.15) Maximum friction force vs. eccentricity ratio for a bearing lubricated with TiO_2nano-lubricant.

Figure (5.16) shows the relation between the percentage variation in induced friction force and the nanoparticles volume fractions of different materials for a bearing works at 0.5 eccentricity ratio and journal speed of 3000rpm. This figure shows that the induced friction force at the journal surface increases by about 5.7% to 18.4% when the bearing lubricated with the base oil dispersed by 0.01 to 0.03 volume fraction of Al_2O_3 while it becomes about 6.25% to 19.9% and 7.16% to 22.5% when the base oil dispersed with same volume fractions of CuO and TiO_2 respectively in comparison with that of the pure oil. This can be allocated to the higher Nano-lubricant viscosity for the bearing works under these conditions. It is well known that the induced friction force converted into heat causes an increase in the oil film temperature. The variation of the coefficient of friction when the bearing works at different eccentricity ratios can be shown in **figure (5.17)**. It can be shown from this figure that the coefficient of friction decreases as the bearing works at higher eccentricity ratios. This can be ascribed by the higher load carried by the bearing in comparison

with the induced friction force when the bearing works at such circumstances. It can be also noticed from this figure that the coefficient of friction increases.

As the bearing lubricated with Nano-lubricant with noticeable increase in the coefficient of friction was obtained when more TiO_2 nanoparticles were distributed in the base oil.

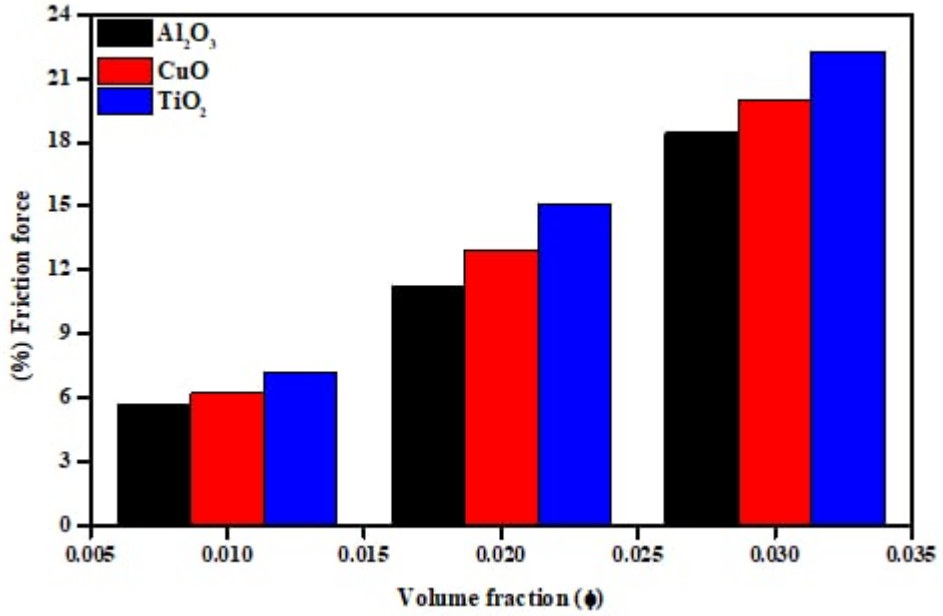

Figure(5.16) Percentage variation in bearing friction force vs. nanoparticle volume fractions in comparison with the base oil.

Figure (5.18) shows that the increase in the coefficient of friction when the bearing is lubricated with Nano-lubricant is negligible and does not exceed 7% in the worst conditions (highest volume fraction of nanoparticles).

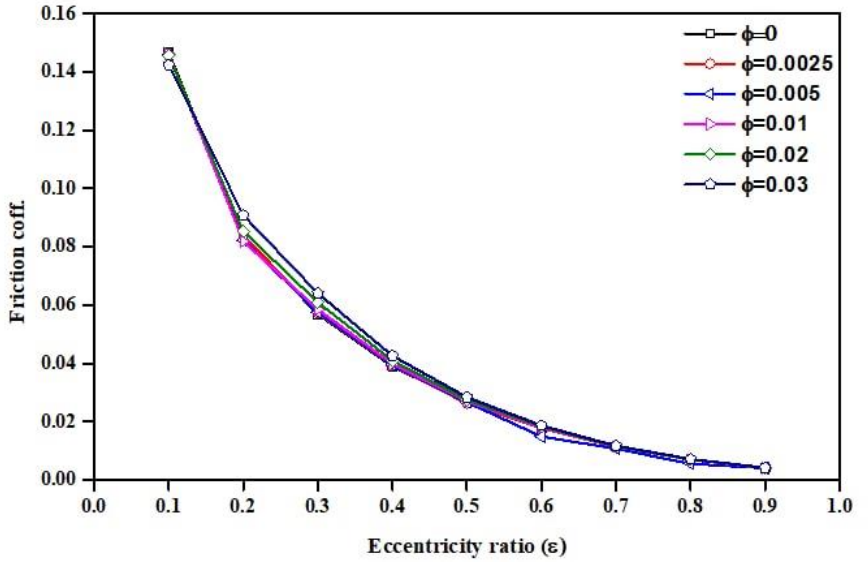

Figure(5.17) Variation of friction coefficient vs. eccentricity ratio with TiO_2nano-lubricant at ε=0.5.

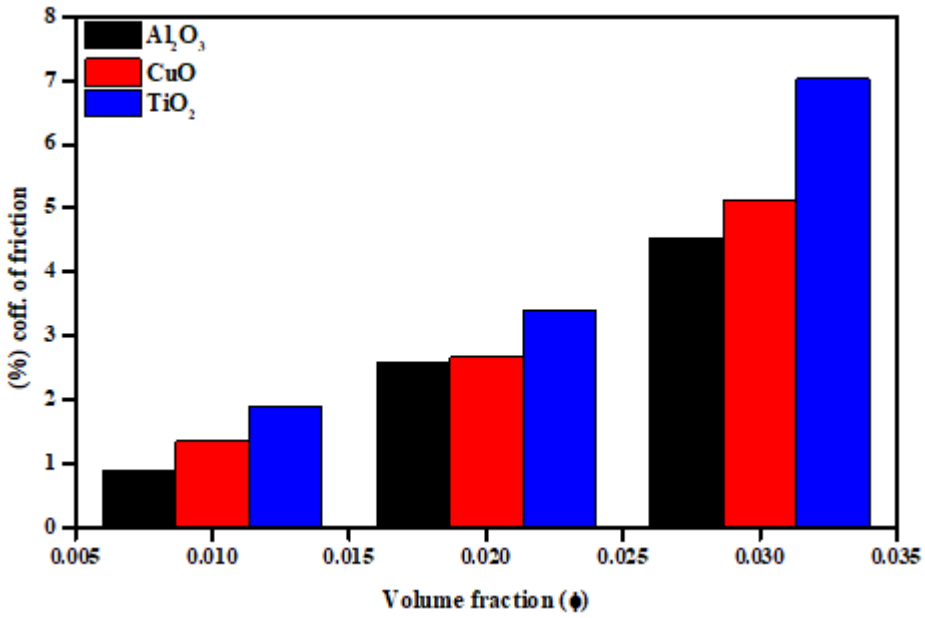

Figure(5.18) Percentage variation in bearing friction coefficient vs. nanoparticle volume fractions in comparison with the base oil.

The oil film temperature distribution for the bearing works at the same above circumstances can be shown in **figure (5.19)**. It can be considered from this figure that oil film temperature increases as the bearing are lubricated with TiO_2 Nano lubricant. The oil film temperature becomes

more pronounced for a higher particle concentration due to the higher viscous shear and induced friction force in this case. The variation of maximum oil film temperature for a bearing working at different eccentricity ratios lubricated with different volume fractions of TiO_2 Nano-lubricant can be shown in **figure (5.20)**. It can be regarded from this figure that a little increase in oil film temperature was sensed when the bearing was lubricated with TiO_2 Nano-lubricant that has a lower volume fraction of the nanoparticles (<0.01) i.e. the bearing behaves as if it is lubricated with pure oil. It can be also noticed from this figure that the bearing has a higher maximum oil film temperature when it works at a higher eccentricity ratio due to the high shear rate of the oil in this case. The maximum oil film temperature increases from 85^{o}C when the bearing works at an eccentricity ratio of 0.5 and is lubricated with TiO_2 Nano-lubricant that has 0.03 volume fraction of nanoparticles to 120^{o}C when the bearing works at eccentricity ratio of 0.9 lubricated with the same TiO_2 Nano-lubricant. The percentage variation in maximum oil film temperature when the bearing is lubricated with different Nano-lubricant dispersed with different volume fractions of TiO_2, Al_2O_3 and CuO Nano particles can be expressed in **figure (5.21)**. This figure indicated that there is a little increase in the maximum oil film temperature reaching about 3.3134% to 4.5% when the bearing is lubricated with base oil dispersed by 0.01 of different Nano materials. This percentage increases from 8.1% to 9.6% and 11.8% to 16.6% when the bearing is lubricated with different Nano-lubricant that has nanoparticles volume fractions of 0.02 and 0.03 respectively.

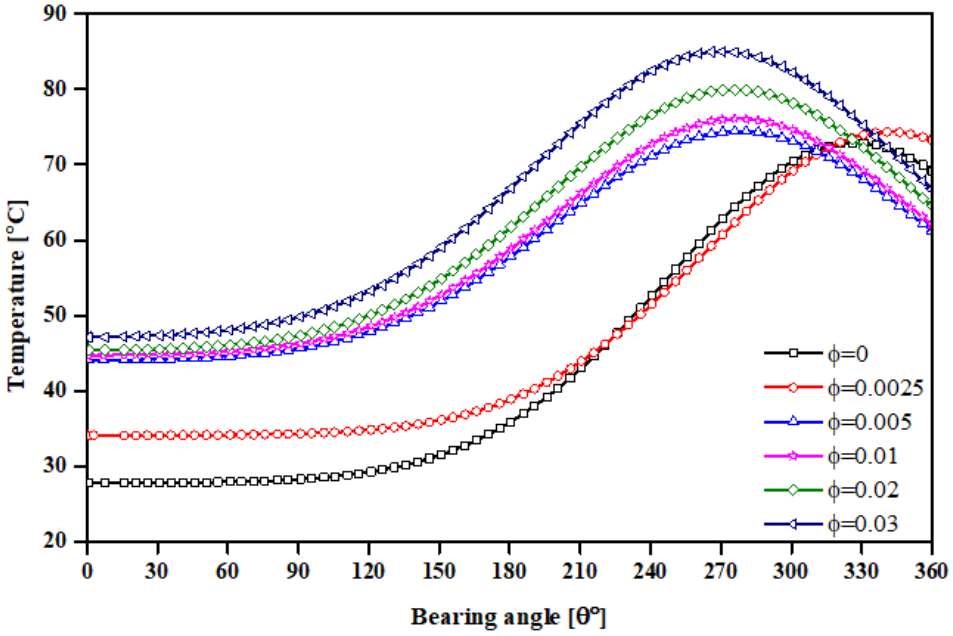

Figure(5.19) Temperature distribution in the circumferential direction for a bearing lubricated with TiO_2 nanoparticles with different particle concentrations.

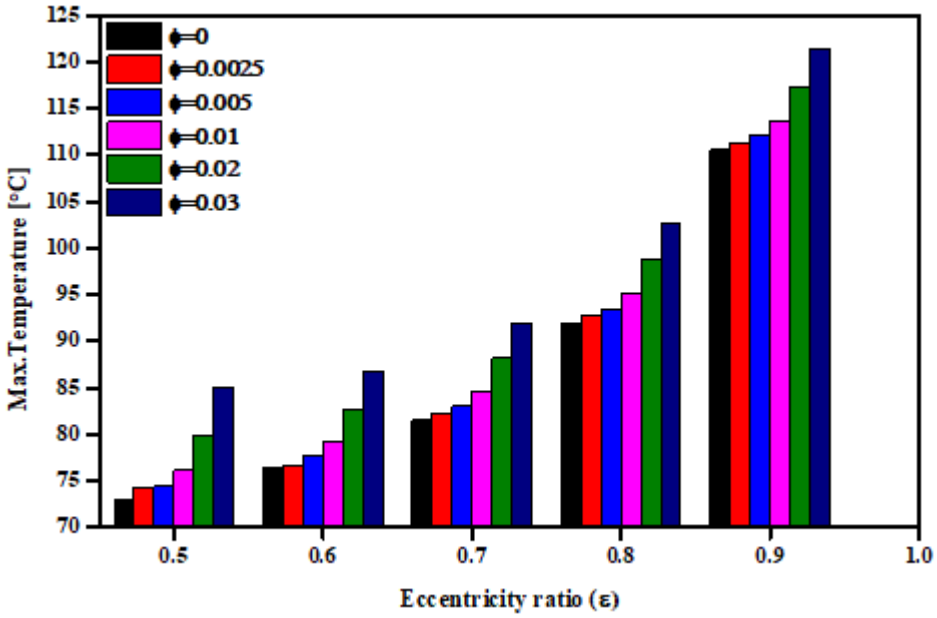

Figure(5.20) Oil film temperature vs. eccentricity ratios for a bearing lubricated with TiO_2 Nano lubricant with different volume fractions.

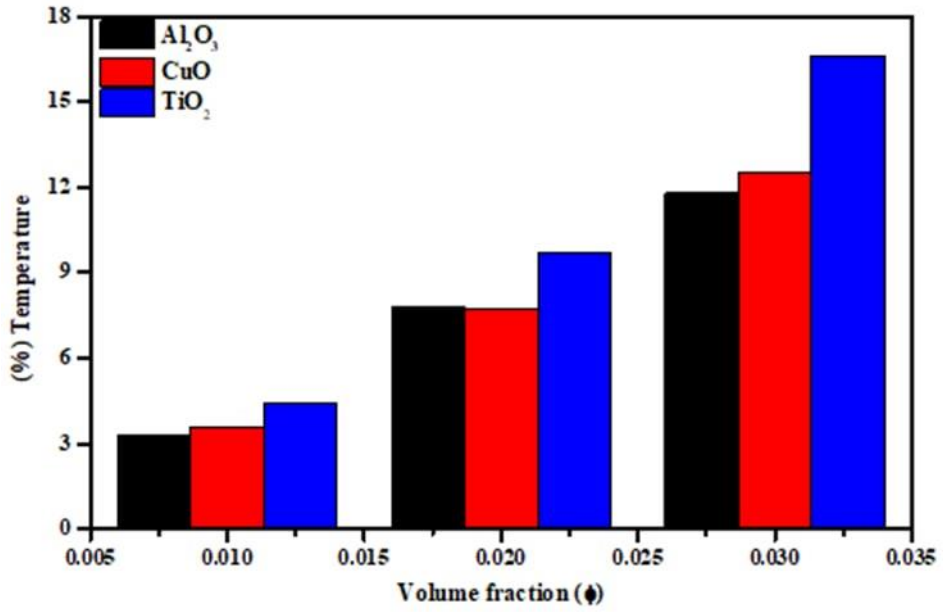

Figure(5.21) Percentage variation in oil film temperature vs. nanoparticle volume fractions in comparison with the base oil.

The variation of the attitude angle with eccentricity ratio of the journal bearing lubricated with TiO_2 Nano-lubricant and journal speed of 3000rpm can be considered in **figure (5.22)**. It is clear from this figure that the attitude angle decreases when the bearing works at higher eccentricity ratios. A marked decrease in attitude angle can be obtained when the bearing is lubricated with TiO_2 of a higher volume fraction of nanoparticles. The percentage variation of the journal bearing attitude angle when lubricated with different types of Nano-lubricants works at an eccentricity ratio of 0.5 with 3000 rpm can be shown in **figure (5.23)**. As can be seen from this figure the attitude angle of the bearing decreases by 11% to 30% when the bearing is lubricated with Al_2O_3 Nano-lubricant with 0.01 to 0.03 volume fraction of Al_2O_3 nanoparticles while it becomes about 12.5% to 33% and 15% to 37% when the base oil dispersed with same volume fractions of CuO and TiO_2 respectively in comparison with that of the pure oil.

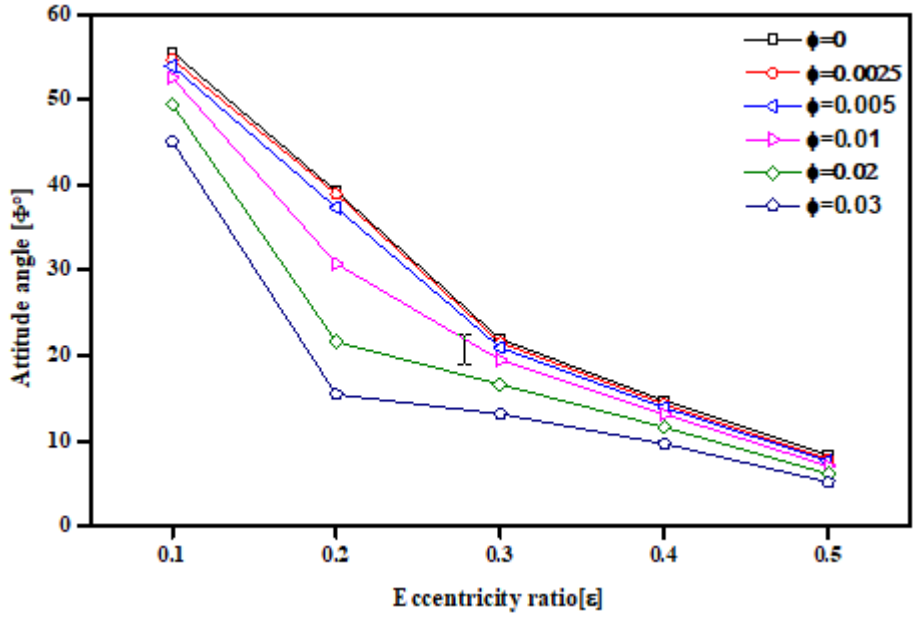

Figure(5.22) Attitude angle vs. eccentricity ratio for a bearing lubricated with TiO_2 of different volume fractions.

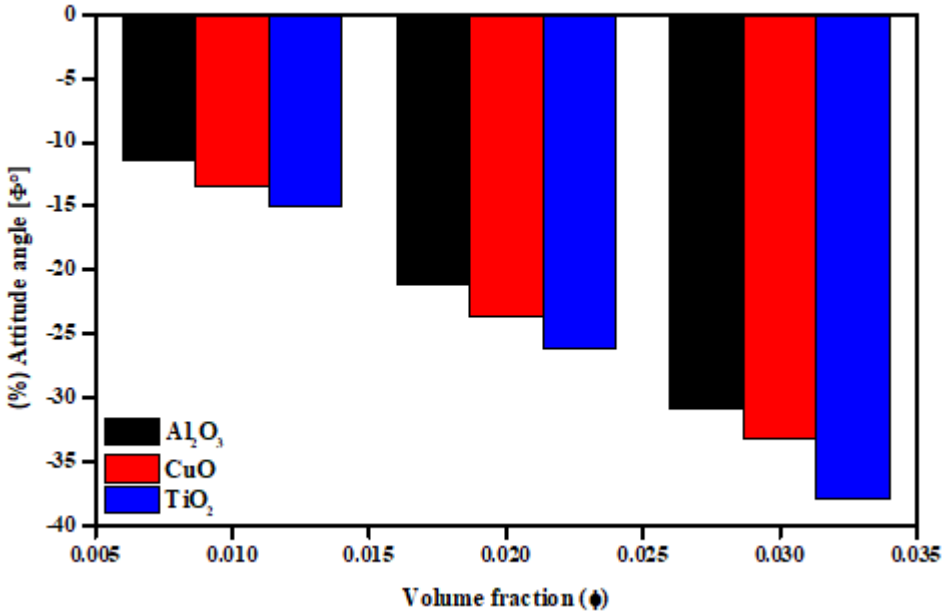

Figure(5.23) Percentage variation in bearing attitude angle vs. nanoparticle volume fractions in comparison with the base oil at ε=0.5 with 3000 rpm.

The variation of the side leakage flow from the ends of the bearing with the bearing eccentricity ratios when lubricated with TiO_2 Nano-lubricant that has different volume fractions of nanoparticles can be introduced as shown in **figure (5.24)**. The obtained results show that the

side leakage of the oil increases as the bearing works at a higher eccentricity ratio. This can be explained by the higher oil film pressure generated in this case. However, the leakage flow decreases when the bearing is lubricated with TiO_2 Nano-lubricant in comparison with that of pure oil. Moreover, the rate of decrease inside leakage flow becomes higher when a higher volume fraction of nanoparticles was dispersed in the base oil. This can be attributed to the lower velocity and hence the shear rate of the Nano-lubricant working under this circumstance.

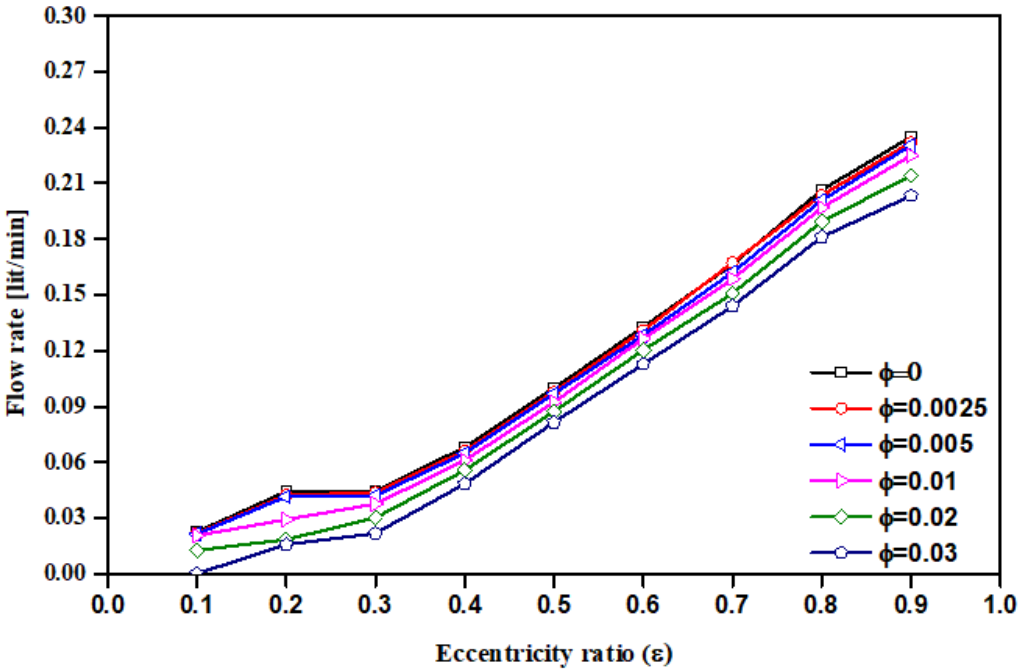

Figure(5.24) Side leakage of the oil for the journal bearing lubricated with TiO_2 Nano-lubricant with different volume fractions.

The percentage variations of the bearing side leakage flow rate when the bearing is lubricated with base oil dispersed with different volume fractions of nanoparticles and working at eccentricity ratio of 0.5 and journal speed of 3000rpm are presented in **figure (5.25)**. This figure depicts a higher percentage decrease in flow rate of the oil when the bearing is lubricated by Nano-lubricant with higher content of nanoparticles of different Nano materials. A maximum percentage decrease of 7.8% was

recorded when the bearing lubricated with 0.01volume fraction of TiO_2 Nano-lubricant while it becomes 18% when 0.03% volume fraction of TiO_2 nanoparticles was dispersed in the base oil.

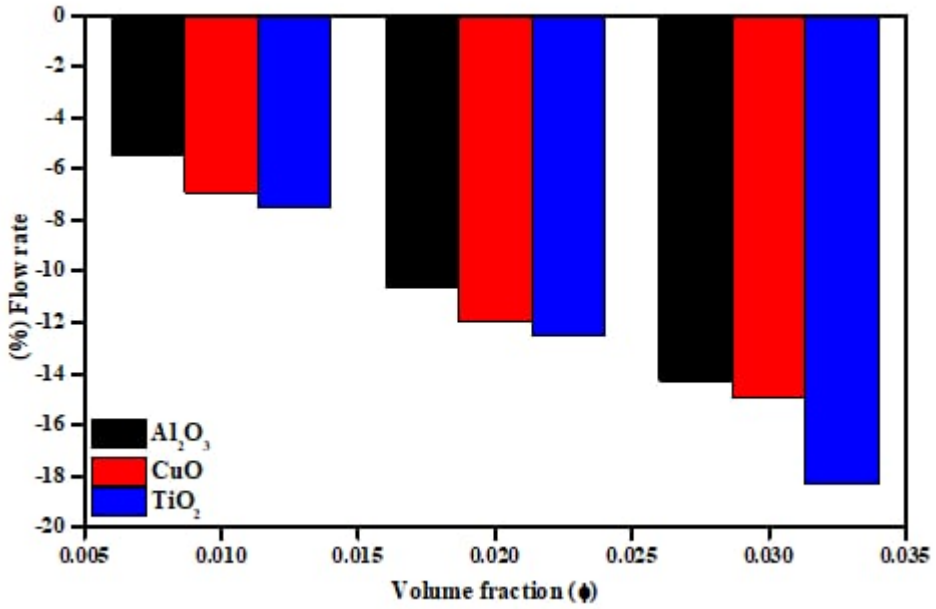

Figure(5.25) Percentage variation in bearing side leakage flow rate vs. nanoparticle volume fractions in comparison with the base oil.

Figure (5.26) shows the percentage variation of the maximum bearing deformation when it is lubricated with the base oil dispersed with different volume fractions of different nanoparticles. The bearing was simulated using a two-way FSI. It can be seen from this figure that the maximum bearing deformation increases when the bearing is lubricated with Nano-lubricant that has higher volume fractions of the nanoparticles. The higher oil film pressure builds up in bearing when it is lubricated with such lubricants is held responsible for this behavior. It has been previously shown that the oil film pressure increases when the volume fraction of the nanoparticles dispersed in lubricant increases. Also, as previously discussed that the oil dispersed with TiO_2 shows a tendency to generate a higher pressure hence, the bearing material deformation becomes higher when using TiO_2 Nano-lubricant. The percentage increase in bearing

deformation when lubricated with such Nano lubricant increases from about 5.4% when the bearing is lubricated with 0.01 TiO_2 to 18% when the volume fraction of such nanoparticles increases to 0.03 in comparison with that lubricated with pure oil.

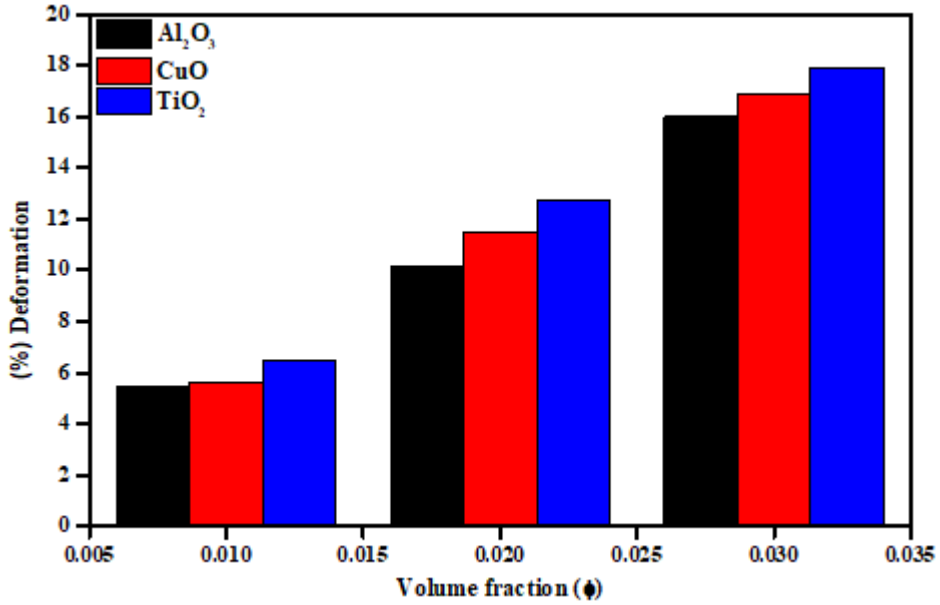

Figure(5.26) Percentage variation in bearing deformation vs. nanoparticle volume fractions in comparison with the base oil.

5.3. Effect of journal speed

The effects of journal speed on different performance characteristics of cylindrical journal bearing lubricated with Nano lubricant that has 0.03 volume fraction of dispersed TiO_2, Al_2O_3, and CuO nanoparticles work at different eccentricity ratios will be discussed in this article. **Figure (5.27)** shows the circumferential pressure distribution for a bearing working at an eccentricity ratio of 0.6 lubricated with Nano-lubricant produced by dispersion of 0.03 volume fraction of TiO_2 in the base oil. This figure displays that the oil film pressure increases with increasing journal speed and the maximum film pressure steadily increases with the journal speed. The maximum oil film pressure of 1.4MPa, 1.62MPa, and 1.8MPa were recorded for a bearing with journal speeds of 2000, 3000 and 4000 rpm

respectively. The maximum percentage increase in maximum oil film pressure was calculated and found to be 15.7% and 28.5% for the bearing works at 3000 and 4000rpm respectively in comparison with that operating at a journal speed of 2000rpm. The effect of lubricating the journal bearing with different Nano-lubricant that have 0.03 volume fraction of the nanoparticles and working at various journal speeds can be shown in **figure (5.28)**. This figure indicates that for the journal bearing lubricated with 0.03 TiO_2 Nano-lubricant the maximum pressure increases by 28% in comparison with that lubricated with pure oil and working at a journal speed of 2000rpm. This percentage becomes 22.4% and 20% when the bearing works at journal speeds 3000rpm and 4000rpm respectively in comparison with that lubricated with pure oil.

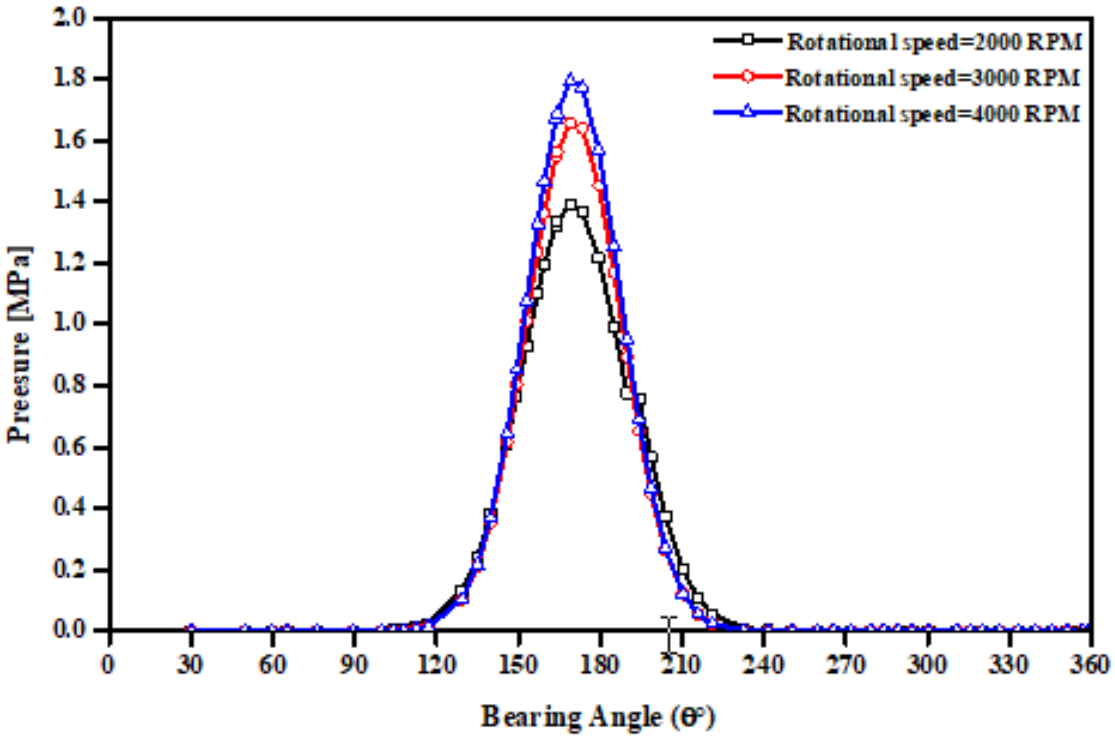

Figure(5.27) Effect of journal speed on the circumferential pressure distribution for a bearing lubricated with 0.03 volume fraction TiO_2 nano lubricant.

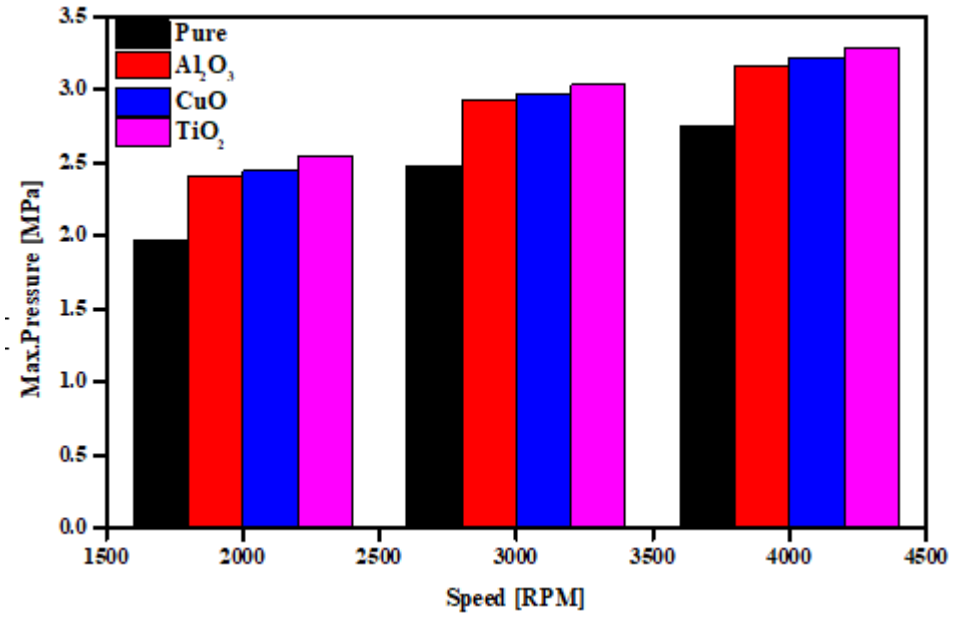

Figure(5.28) Variation of maximum pressure with journal speed for a journal bearing lubricated with different Nano lubricants.

The maximum oil film pressure is strongly affected by the eccentricity ratio of the bearing as presented in **figure (5.29)**. It can be noticed that the maximum pressure abruptly increased when the bearing works at higher eccentricity ratios since the maximum oil film pressures recorded in this case are 2.5MPa, 6MPa, 12MPa, and 22.5MPa for a bearing working at eccentricity ratios of 0.6, 0.7, 0.8 and 0.9 respectively. This can be accredited to the smaller gap between the journal and the bearing surfaces (film thickness) when the bearing works at higher eccentricity ratios. It is well known that the oil film pressure is very sensitive to the change in oil film thickness. **Figure (5.30)** illustrates the variation of the oil film temperature for the bearing lubricated with 0.03 volume fraction TiO_2 Nano-lubricant working at different journal speeds. This figure depicts that the oil film temperature increases as the journal speed increases. It can be noticed from this figure that the maximum oil film temperature increases from 74°C when the journal speed is 2000rpm to 84°C and 95°C when the journal speed is 3000rpm and 4000rpm respectively. This is can be

attributed to the increase of the oil film shear rate at higher journal speed and hence increasing the viscous shear and the temperature of the oil film.

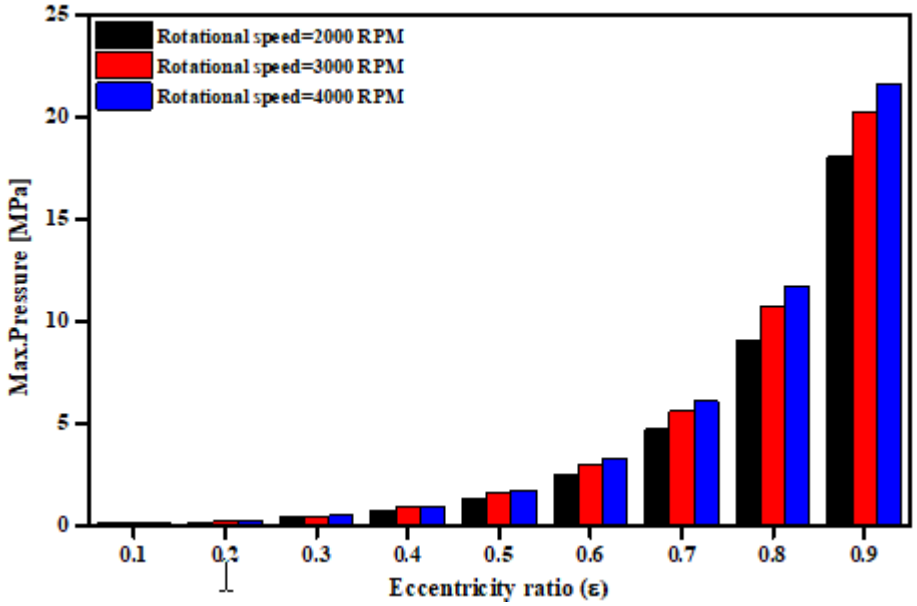

Figure(5.29) Maximum oil film pressure vs. eccentricity ratio for a bearing with different journal speeds with fraction TiO_2 nano lubricant.

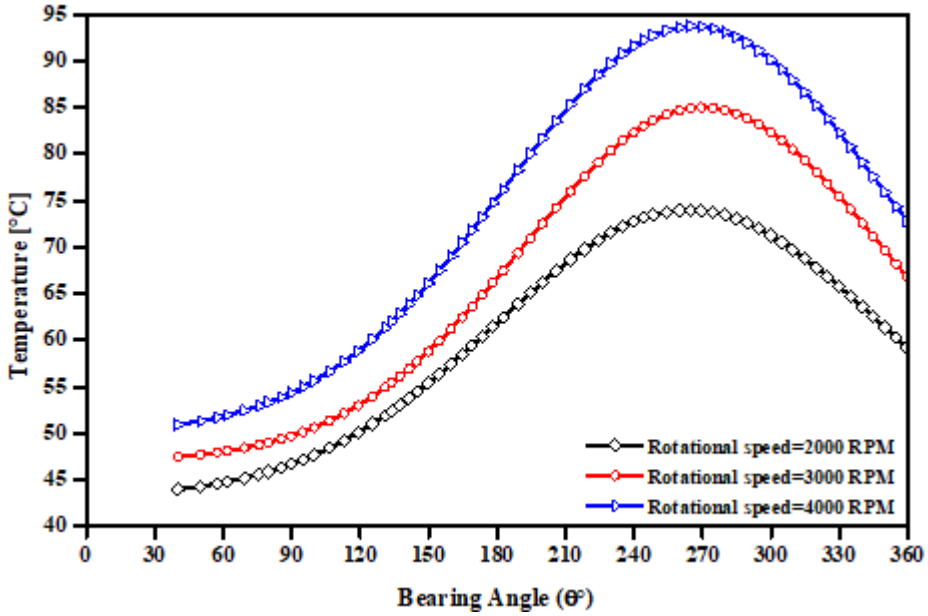

Figure(5.30) Variation of circumferential temperature distribution with journal rotational speed.

The variation of the maximum bearing oil film temperature with journal speed when lubricated with different Nano-lubricant is illustrated in

figure (5.31). The data presented in this figure show that dispersing different nanoparticles with the base oil slightly affect the maximum oil film temperature for a given journal rotational speed.

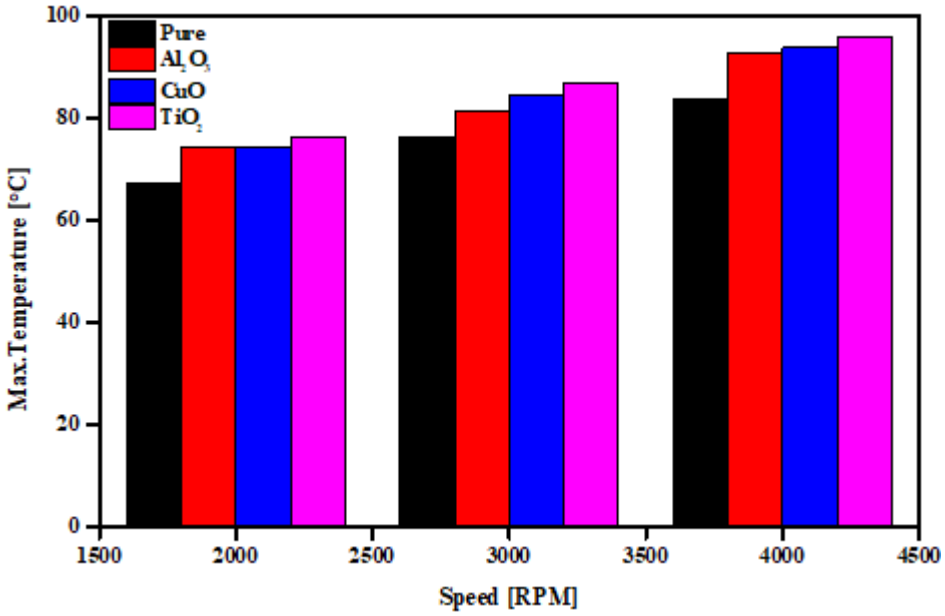

Figure(5.31) Variation of maximum oil film temperature with journal speed using different Nano-lubricant.

The variation in maximum deformation of the journal bearing works at an eccentricity ratio of 0.6 and different journal speeds lubricated with different Nano-lubricants with 0.03 volume fraction of the nanoparticles can be shown in **figure (5.32)**.

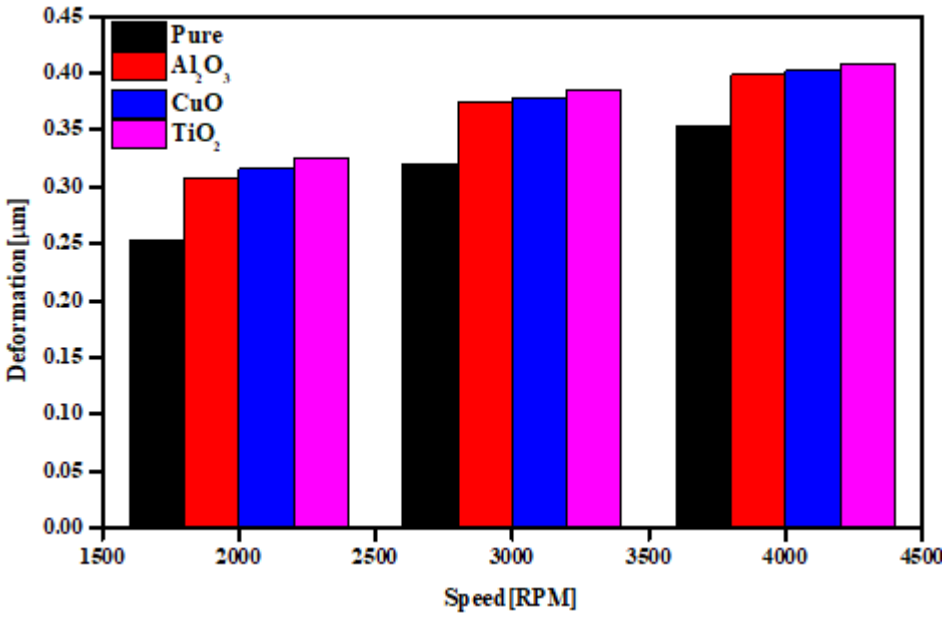

Figure(5.32) Variation of maximum deformation of the journal bearing lubricated with different Nano-lubricant.

This figure depicts that the maximum deformation of the bearing shell material increases with increasing the journal speed in comparison with that of pure oil. This can be explained by the increase of the oil film pressure when the bearing works at a higher journal speed. This figure also illustrated that the type of nanoparticles dispersed in the base oil has a slight effect on the bearing deformation. The variation of the induced friction force with the journal speed when the bearing is lubricated by oil dispersed with different types of nanoparticles can be shown in **figure (5.33)**. It is clearly shown from this figure that the induced friction increases by about 25% when it is lubricated with Nano-lubricant that has 0.03 volume fraction of the nanoparticles and when the journal speeds are 2000, 3000 and 4000rpm respectively in comparison with that lubricated with pure oil. The percentage increase in induced friction force becomes 40% when the bearing is lubricated with Nano-lubricant that has 0.03 volume fraction of TiO_2 and the journal speed increases from 2000rpm to 4000rpm. This can be accredited to the increase of both the viscous

shearing due to the increase of lubricant viscosity and the shearing rate due to the increase in the journal speed.

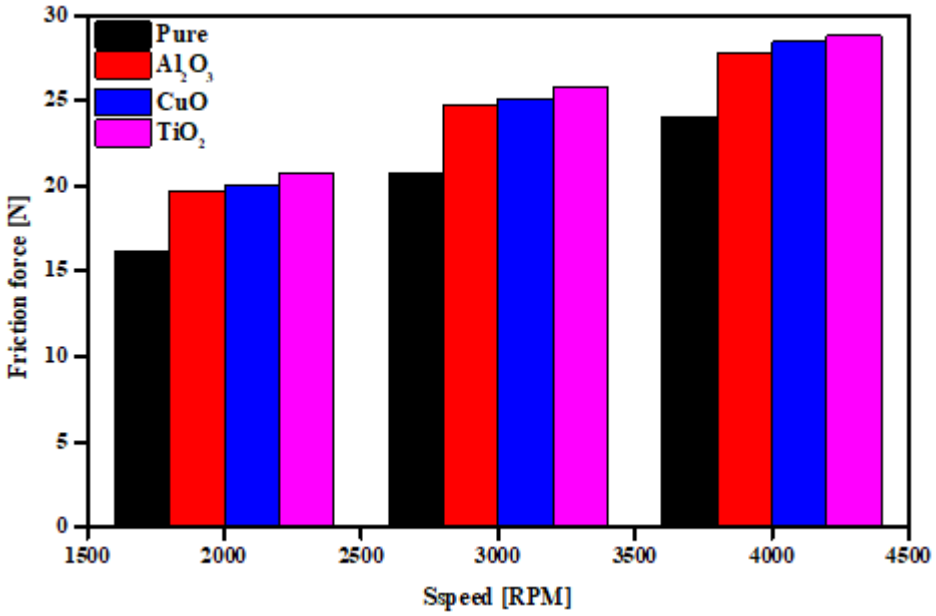

Figure(5.33) Variation of friction force with the journal speed when the bearing lubricated with different Nano-lubricant.

Figure (5.34) shows the variation of friction force of the journal bearing lubricated with TiO_2 Nano-lubricant with 0.03 volume fraction of the nanoparticles works at different eccentricity ratios and journal speed. The induced friction force increases when the bearing works at high journal speed and eccentricity ratios. This can be assigned to the higher oil film shear rate when the journal and bearing surfaces become closer to each other when the bearing works at higher eccentricity ratios and when the bearing works at higher speeds. However, it can be noticed from this figure that the friction force of 16N becomes 34N when the bearing works at an eccentricity ratio of 0.9 rather than 0.1 and a journal speed of 4000rpm.

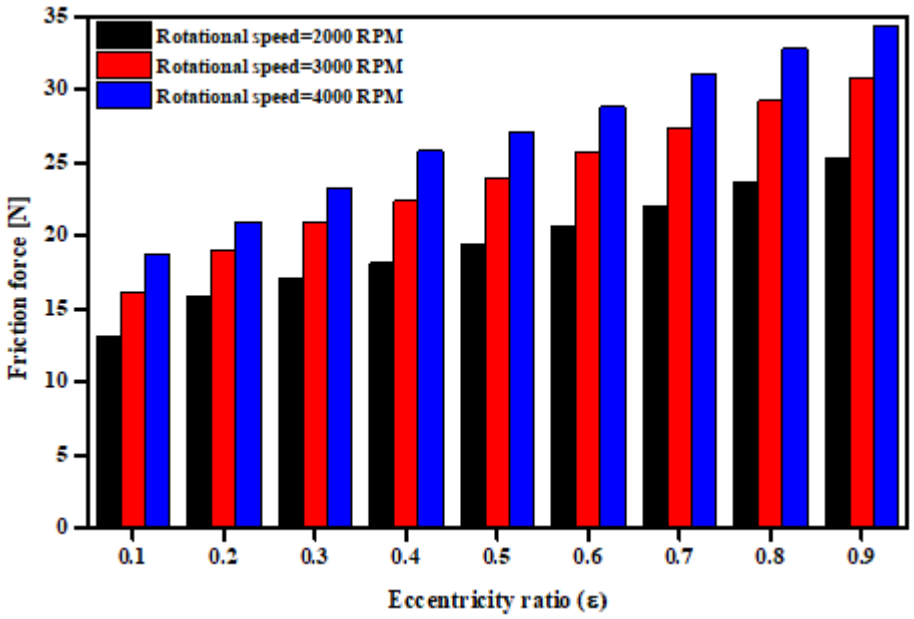

Figure(5.34) Variation of friction force with the eccentricity ratios of the journal bearing lubricated with TiO_2 Nano-lubricant.

The variation of side leakage flow rate with the journal speed for the bearing working at an eccentricity ratio of 0.6 and lubricated with different Nano-lubricants can be shown in **figure (5.35)**. This figure illustrates that the oil side leakage decreases when the bearing is lubricated with Nano-lubricant that has a 0.03 volume fraction of the nanoparticles due to the increase of the oil viscosity while it increases when the bearing works at higher journal speed due to the increase in pressure gradient in the axial direction. However, the rate of increase inside leakage flow becomes lower when the bearing is lubricated with different Nano lubricants in comparison with that lubricating with pure oil. **Figure (5.36)** indicates the variation of the attitude angle when the bearing works at different eccentricity ratios and journal rotational speed. This figure shows that the attitude angle decreases as the bearing works at a higher speed. More decrease in attitude angle was noticed when the bearing works at higher eccentricity ratios. This can be explained by knowing that the journal displaced vertically

downward only and the fluid film generating a responding force with a higher horizontal component (F_x).

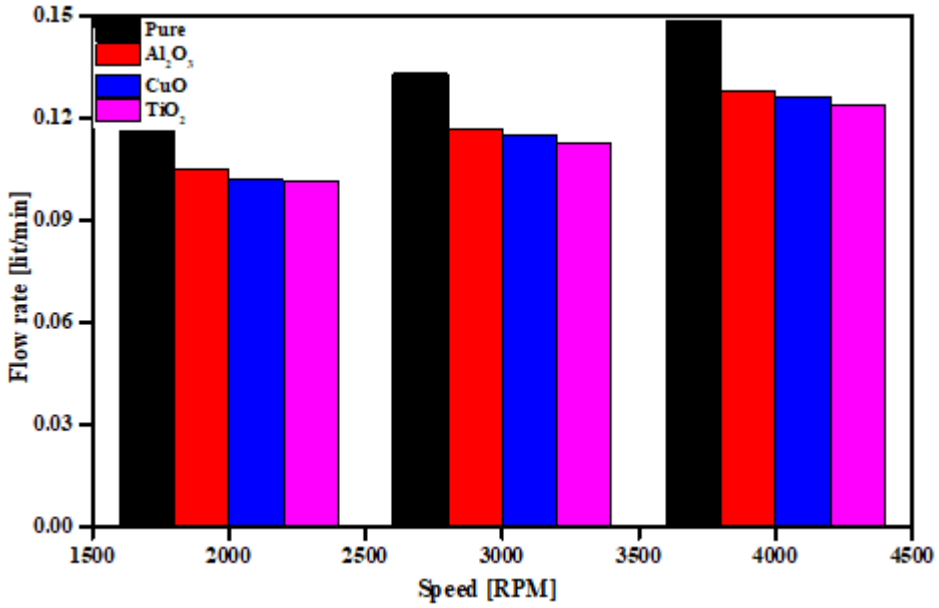

Figure(5.35) Variation of the side leakage flow rate with the journal speed for a bearing lubricated with different Nano-lubricant.

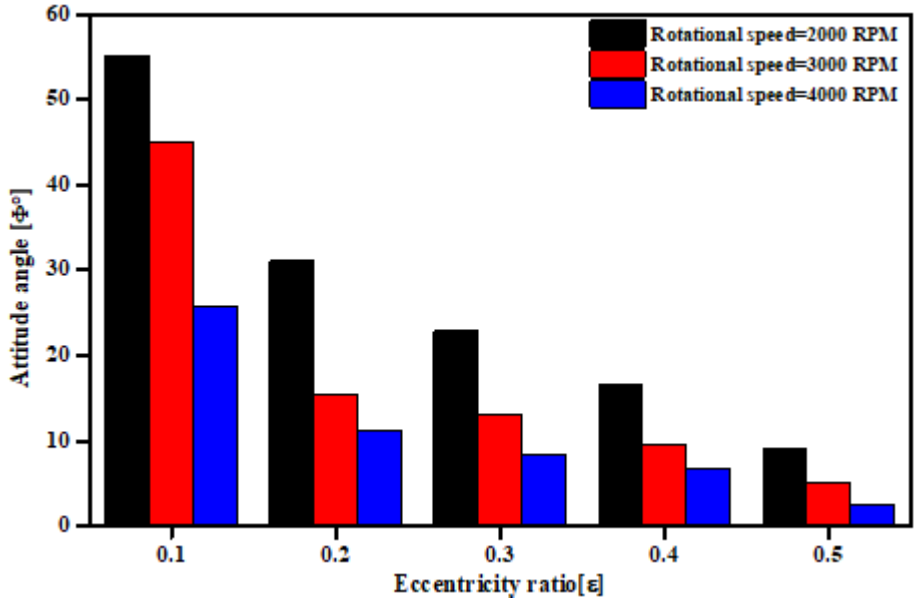

Figure(5.36) Variation of the attitude angle with the eccentricity ratios for a bearing working at different journal speeds.

5.4. Effect of cavitation

In most works related to the field of hydrodynamic lubrication, the negative pressure generated in this zone is neglected and taken to be equal to zero. In the present work, the cavitation effect on the oil film pressure and temperature distributions when the bearing is lubricated with Nano lubricant has been studied. **Figure (5.37)** illustrates the effect of considering the cavitation on the pressure distribution of a journal bearing lubricated with Nano-lubricants with different volume fractions of TiO_2 nanoparticles working at an eccentricity ratio of 0.5.

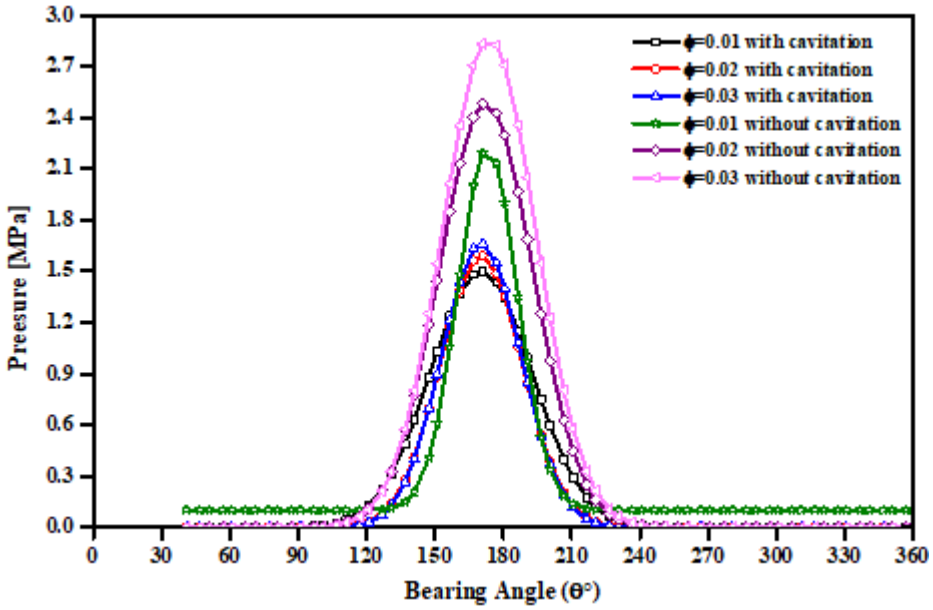

Figure(5.37) Cavitation effect on the pressure distribution.

This figure depicts that the maximum oil film pressure drops when considering the cavitation effect. This can be attributed to the decrease in oil film density and viscosity for the two-phase (liquid-gas) lubricant which was affect the viscous term of the Navier Stocks equations. However, the oil film pressure increases when the oil-lubricated bearing is dispersed with higher volume fractions of TiO_2 nanoparticles. It can also be seen from this figure that the effective zone of the bearing increases when using a higher volume fraction of the nanoparticles. This indicates that the decrease in oil

film pressure due to the cavitation can be substituted by using the Nano-lubricants with a small volume fraction of nanoparticles dispersed in the base oil.

Table (5.1) Shows the maximum oil film pressure decrease obtained when considering the cavitation effect with TiO_2 Nano-lubricant.

Volume Fraction%	P_{max} (MPa) Without cavitation	P_{max} (MPa) With cavitation	% Decrease in P_{max}
0.01	2.22	1.52	31.5
0.02	2.49	1.61	35.3
0.03	2.86	1.67	41.6

The data explored in this **table(5.1)** shows that the oil film pressure decreases by 31.5%, 35.3%, and 41.6% when the cavitation effect was considered. This leads to the conclusion that the cavitation effect should not be neglected since it affects the overall performance characteristics of the bearing.

The numerical results presented in **figure (5.38)** show the combined effect of journal speed and cavitation on the oil film pressure. It can be observed that the oil film pressure decreases when the cavitation was considered to evaluate the pressure distribution of a journal bearing working at an eccentricity ratio of 0.5 and lubricated with 0.03 volume fraction of TiO_2 Nano-lubricant working at different journal speeds. This can be explained by increasing the cavitation area as the rotational speed increases from 2000 to 4000 rpm due to the higher pressure drops in this case as can be shown in **figure (5.39 a, b, c)**. This figure shows that the

cavitation area gradually increases as the rotational speed increases. However, the oil film pressure generated is still higher when the bearing works at a higher journal speed.

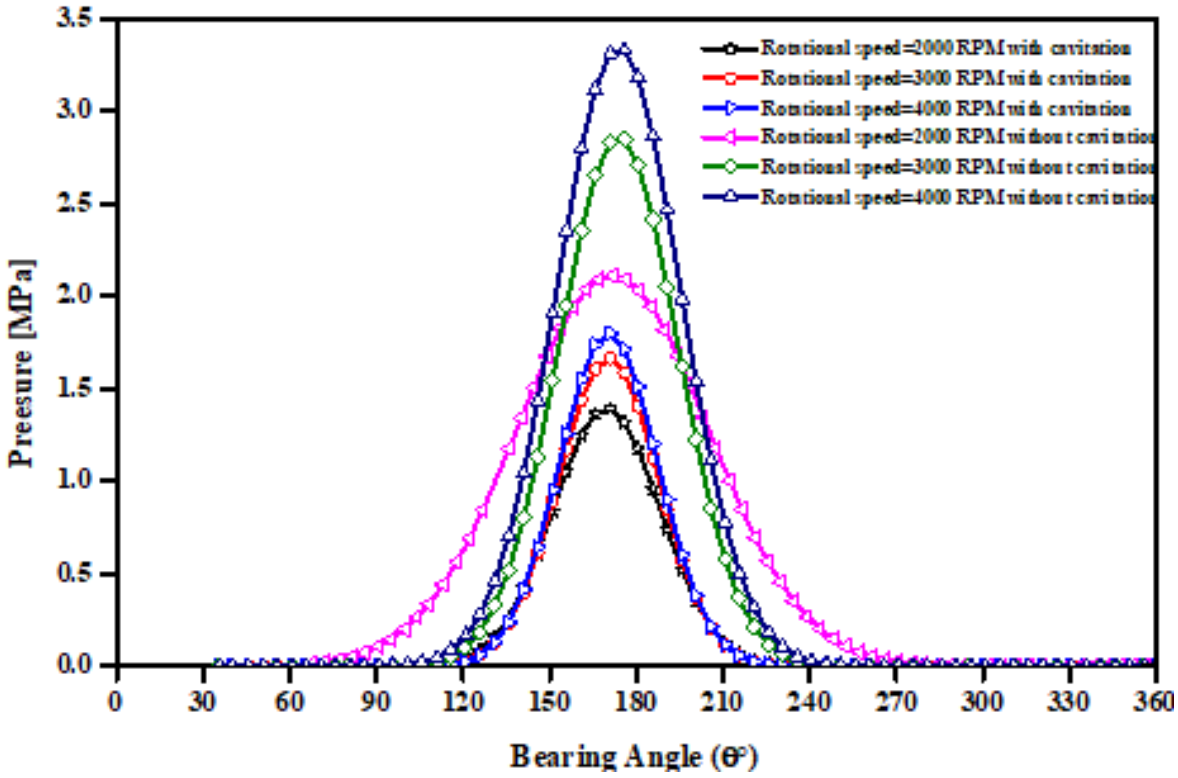

Figure(5.38) Effect of journal speed on the circumferential pressure distribution with and without cavitation effect.

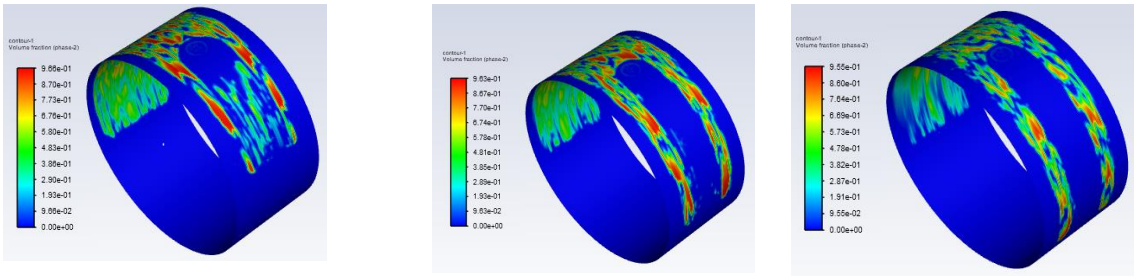

a: N=2000rpm b: N=3000rpm c: N=4000rpm

Figure(5.39) Rotational speed effect on the volume fraction of cavitation.

However, the oil film pressure increases when the bearing works at higher journal speeds. This can be explained by the vertical downward movement of the journal which decreases the oil film thickness and increases the oil film pressure.**[59]**

The maximum decrease in oil film pressure due to the combined effect of the cavitation and journal speed effect was considered as illustrated in **table (5.2)**.

Table(5.2) Percentage decrease in maximum oil film pressure when considering the cavitation effect with volume fraction 3%.

Speed (rpm)	P_{max}(without cavitation) (MPa)	P_{max}(with cavitation) (MPa)	%Decrease
2000	2.1	1.45	30.9
3000	2.9	1.65	43.1
4000	3.45	1.75	49.2

Figure (5.40) shows the effect of cavitation on the oil film temperature distribution when the bearing works at an eccentricity ratio of 0.5 and is lubricated with TiO_2 Nano-lubricant that has different volume fractions of nanoparticles. This figure clearly shows that the maximum oil

film temperature decreases with the percentages shown in **table (5.3)** when the cavitation effect was taken into consideration. This can be attributed to the lower oil viscosity and density due to the existence of air bubbles with the Nano-lubricant which makes the lubricant behave as a multi-phase flow.

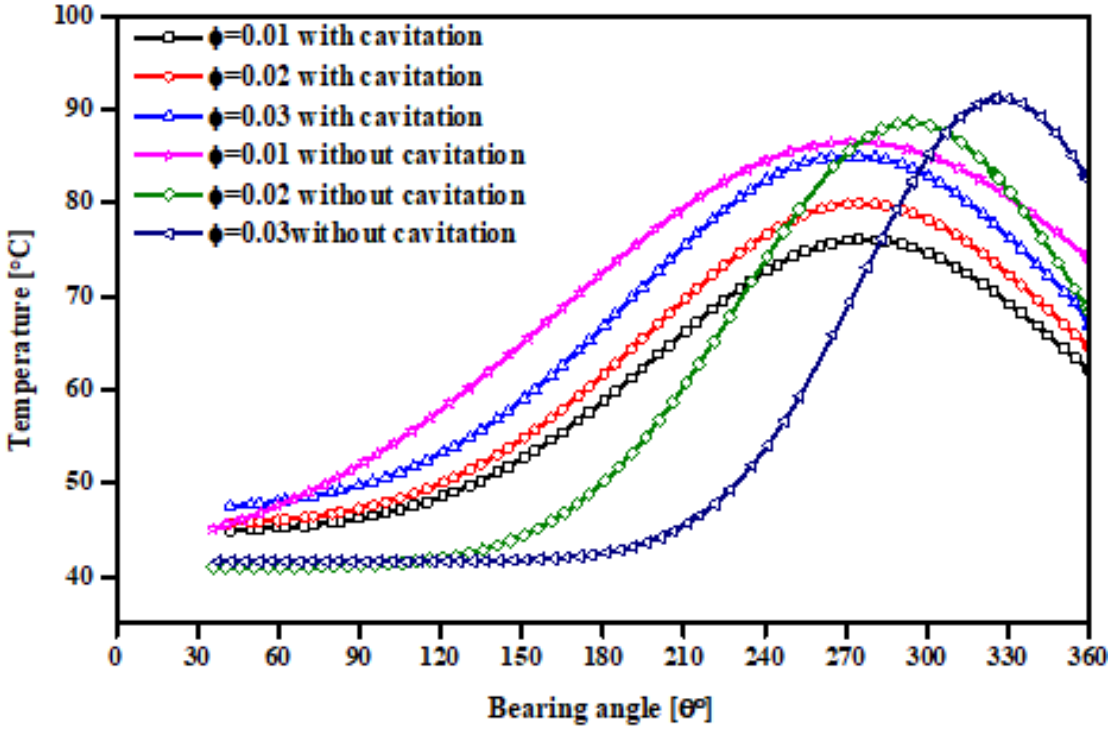

Figure(5.40) Effect of cavitation on the oil film temperature distribution.

Table(5.3) Percentage decrease in maximum oil film temperature when considering the cavitation effect.

Volume Fraction	**T_{max} (without cavitation)**	**T_{max} (with cavitation)**	**% Decrease**
0.01	85	75	11.7
0.02	87	79	9.1
0.03	90	83	7.7

It can be also be noticed from this figure that the oil film temperature becomes more uniform and the maximum oil film temperature moves towered the bearing inlet.

5.5. Effect of elastic deformation

Elastohydrodynamic analysis of a journal bearing was performed by solving the hydrodynamic forces by using (CFD) analysis, then the forces were transferred to the structural analysis and vice versa using fluid-structure interaction (FSI) approach. The combined effects of thermal and elastic deformation (FSI solution) on the oil film pressure of a journal bearing lubricated with 0.03 volume fraction TiO_2 Nano-lubricant working at an eccentricity ratio of 0.5 can be observed from **figure (5.41)**. In this figure, the behavior of the oil film pressure for journal bearings with considering the elastic and rigid shell has been presented by comparing the results of TEHD solution with that obtained from the THD solution. It was observed from this figure that the oil film pressure decreases when the elastic deformation of the bearing liner has been considered in comparison with the rigid bearing. The active area of the bearing increases and the cavitation area decreases when neglecting the elastic deformation of the bearing liner which indicates a higher load-carrying capacity in this case. This leads to the main conclusion that the elastic deformation of the bearing material effectively affects the generated oil film pressure and hence the main bearing parameters and cannot be neglected by the designers to get reasonable results. The decrease in oil film pressure when considering the elastic deformation of the bearing material can be explained by the increase of the oil film thickness and the sensitivity of the oil film pressure to the inverse of the oil film thickness.

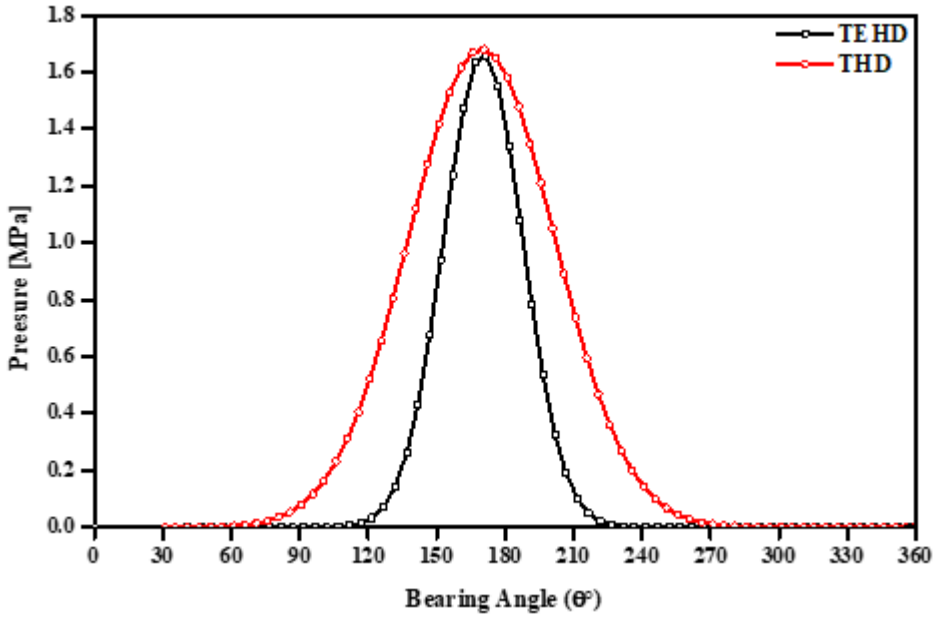

Figure(5.41) Effect of THD and TEHD solution on the pressure distribution of 0.03 volume fraction TiO2 Nano-lubricated journal bearing at $\boldsymbol{\varepsilon = 0.5}$.

The oil film temperature distribution obtained from TEHD and THD solutions is presented in **figure (5.42)**. This figure reveals that considering the bearing elastic deformation leads to a lower generated oil film temperature. This figure remarks that the maximum oil film temperature obtained from TEHD solution is slightly lower than that obtained by using THD solution. However, the oil film temperature obtained when considering the elastic deformation of the bearing material is decreased by about 25% in comparison with that obtained for a rigid bearing. This can be justified by the greater gap between the journal and the bearing due to the elastic deformation which reduces the lubricant shearing rate and hence the induced friction force. Also, the location of the maximum oil film temperature was moved towered the outlet by about 60^{o} when considering the bearing elastic deformation in comparison to that of rigid bearing.

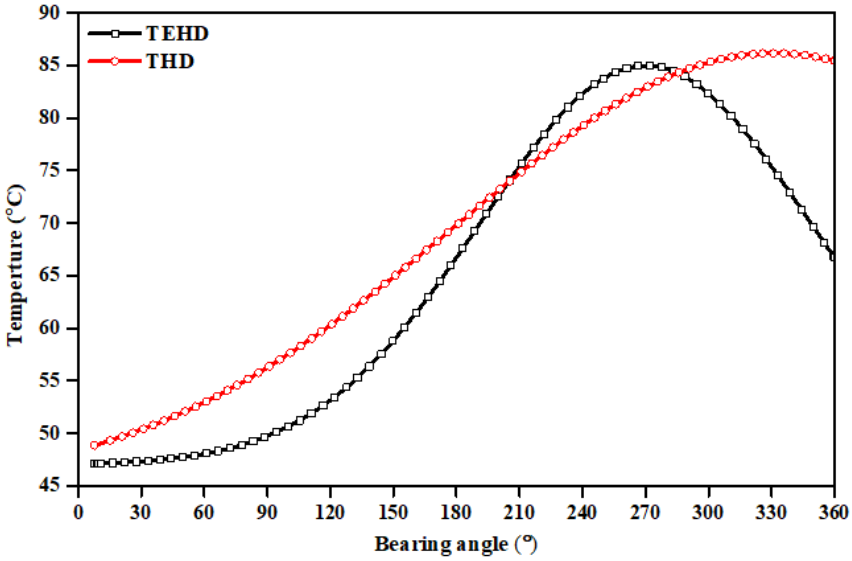

Figure(5.42) Effect of THD and TEHD solution on the temperature distribution of 0.03 volume fraction TiO_2 Nano-lubricated journal bearing $\boldsymbol{\varepsilon = 0.5}$.

The load carried by the bearing studied in the present work working at different eccentricity ratios when using THED and THD solutions can be shown in **figure (5.43)**. This figure reveals that the load carried by the bearing increases when the bearing works at higher eccentricity ratios and it became lower when the elastic deformation of the bearing shell was taken into consideration. This can be explained by the lower oil film pressure obtained in this case.

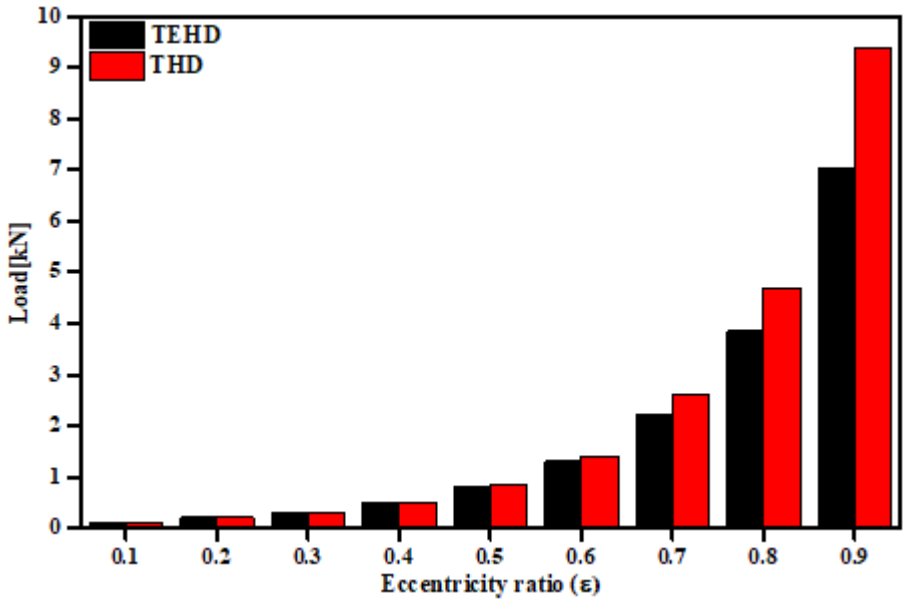

Figure(5.43) Load carrying capacity vs. eccentricity ratio for both TEHD and THD solutions.

5.6. Journal center equilibrium position

The equilibrium position of the journal center can be found where there is a force balance between the vertical component (Y component) of the hydrodynamic load and the externally applied load on the bearing with the horizontal component of the load (X component) is equal to zero. So, the problem of optimizing targets to get zero X-imbalance and Y-load equal to the externally applied load giving the correct equilibrium position. For this purpose, the approach used by **Dhande [39]** in determining the equilibrium position of the journal center was followed in the present work. Elastohydrodynamics means that the hydrodynamic forces are computed in the fluid domain using the CFD approach while the elastic deformations are computed at the structural domain**[39]**. The computed fluid forces are transferred to the structural domain and vice versa. The design exploration can be obtained via three stages, namely, the design of experiments (DOE), Response Surface analysis (RSA), and optimization. The response surface for a bearing lubricated with pure oil and journal speed of 3000rpm shown

in **figure (5.44)** was generated using the DOE data presented in **table (5.4)**. The data presented in this table was obtained by guessing the upper and lower bound of the bearing eccentricities and attitude angles within which the solution was expected. An optimal space-filling design algorithm was used to get the design points and a matrix of experiments is generated. The design points are used to build the response surface which performs the relationship between the eccentricity, attitude angle, and output parameters such as fluid reaction forces.

Table(5.4) Design point as a result of the design of experiments for a bearing lubricated with pure oil.

Table of Outline A2: Design Points of Design of Experiments

	A	B	C	D	E	F	G	H	I	J	K
1	Name	Update Order	P1 - length (mm)	P2 - angle (degree)	P3 - Mesh Max	P6 - fy-op	P7 - fx-op	P8 - load-op	P9 - Total Deformation Maximum (um)	P10 - X-origin (m)	P11 - Y-origin (m)
2	1 DP 7	7	0.023056	31.667	33.37	-592.36	-318.11	672.37	0.056612	-1.2104E-05	-1.9623E-05
3	2 DP 9	9	0.028611	40.556	42.038	-1054.4	-200.46	1073.3	0.10327	-1.8603E-05	-2.1738E-05
4	3 DP 3	3	0.011944	53.889	30.291	-206.03	-87.296	223.77	0.013049	-9.6496E-06	-7.0395E-06
5	4 DP 6	6	0.020278	49.444	32.077	-478.46	-91.207	487.08	0.038459	-1.5407E-05	-1.3184E-05
6	5 DP 2	2	0.0091667	27.222	27.585	-78.669	-159.57	177.91	0.0089609	-4.1932E-06	-8.1514E-06
7	6 DP 4	4	0.014722	36.111	28.389	-254.15	-113.6	278.38	0.020002	-8.6766E-06	-1.1894E-05
8	7 DP 5	5	0.0175	62.778	34.03	-360.53	8.3764	360.63	0.026277	-1.5562E-05	-8.0052E-06
9	8 DP 8	8	0.025833	58.333	37.205	-785	61.385	787.4	0.070622	-2.1987E-05	-1.3562E-05
10	9 DP 1	1	0.0063889	45	29.357	-69.929	-93.576	116.82	0.0061454	-4.5176E-06	-4.5176E-06

The relation between the X-component of the bearing force, the bearing eccentricity, and the attitude angle is clearly shown in **figure (5.44)**.

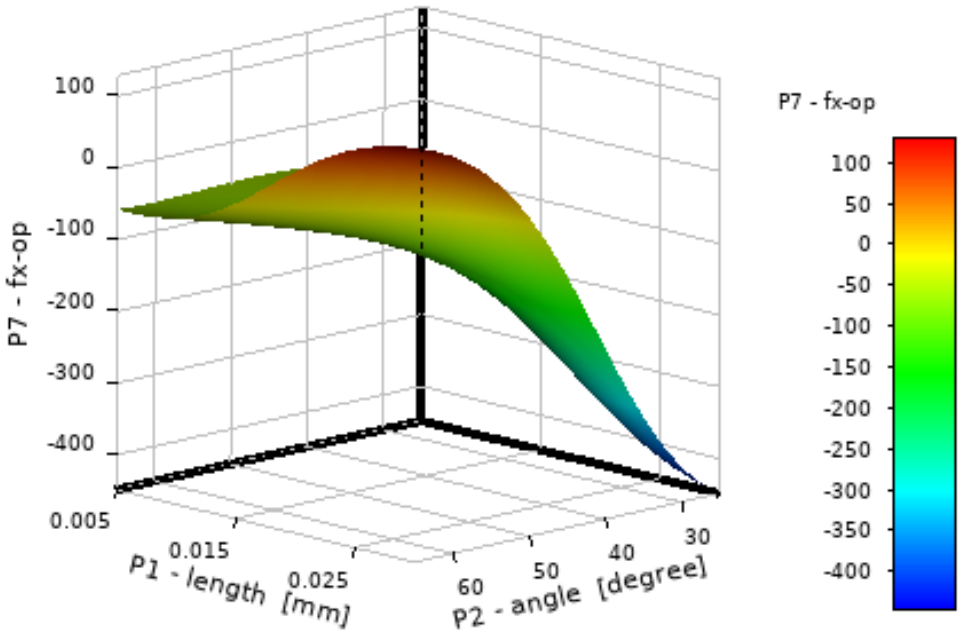

Figure(5.44) X-load component versus bearing eccentricity and attitude angle.

Figure(5.45) shows the Y-component of the load against the bearing eccentricity and attitude angle.

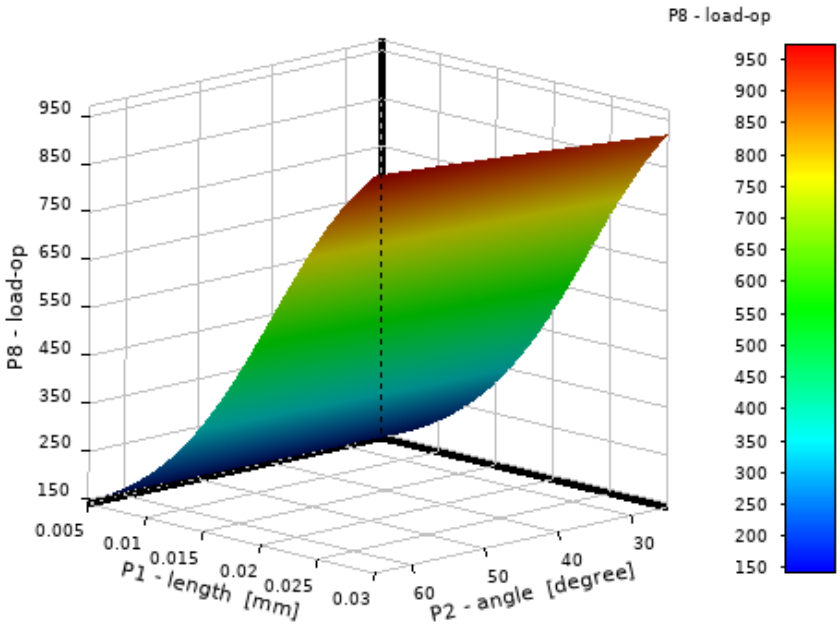

Figure(5.45) Y-load component versus bearing eccentricity and attitude angle.

The optimization constraint and the optimum results obtained for the journal center of a bearing lubricated with pure oil are presented in **tables (5.5)** and **(5.6)**. The goodness of fit shown in **figure (5.46)** confirms how well the surface fit is close to the data points.

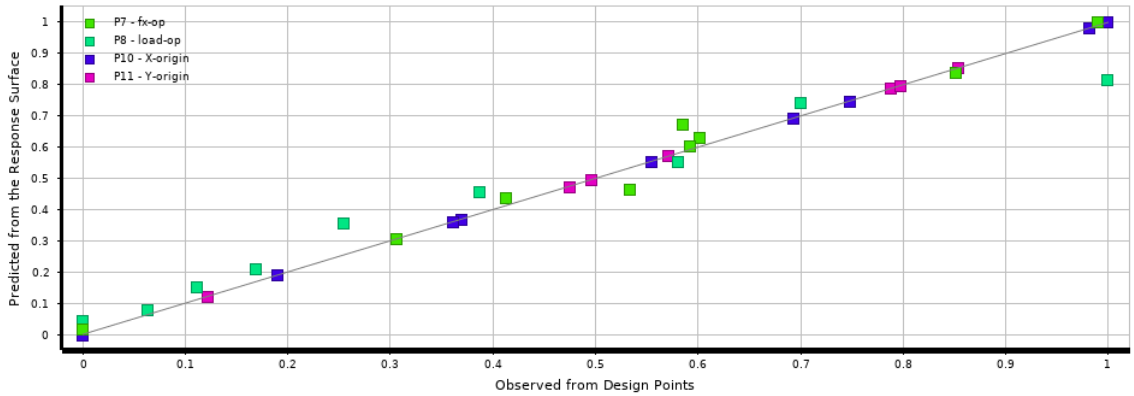

Figure(5.46) Goodness of fit.

Table(5.5) Optimization constraint.

Table of Schematic E4: Optimization

	A	B	C	D	E	F	G
1	Name	Parameter	Objective		Constraint		
2			Type	Target	Type	Lower Bound	Upper Bound
3	Seek P8 = 970	P8 - load-op	Seek Target	970	No Constraint		
4	Seek P7 = 0	P7 - fx-op	Seek Target	0	No Constraint		

Table(5.6) Optimum solution for the journal centre.

Candidate Points

	Candidate Point 1	Candidate Point 2	Candidate Point 3
P1 - length (mm)	0.029875	0.029905	0.029875
P2 - angle (degree)	51.165	52.804	55.171
P7 - fx-op	12.708	35.72	63.456
P8 - load-op	952.43	955.27	957.35

Table of Schematic E4: Optimization , Candidate Points

	A	B	C	D	E	F	G	H	I	J
1	Reference	Name	P1 - length (mm)	P2 - angle (degree)	P3 - Mesh Max	P6 - fy-op	P7 - fx-op		P8 - load-op	
2							Parameter Value	Variation from Reference	Parameter Value	Variation from Reference
3		Candidate Point 1	0.029875	51.165	38.195	-1044.9	12.708	-79.97%	952.43	-0.51%
4		Candidate Point 2	0.029905	52.804	38.281	-1039.4	35.72	-43.71%	955.27	-0.22%
5	◉	Candidate Point 3	0.029875	55.171	38.384	-1026.3	63.456	0.00%	957.35	0.00%

The procedure of the optimization adopted in the present work leads to the best possible solution called candidate points as can be shown from the **table(5.6)** based on the constraints presented in **table (5.5)**. If the guessed values are not closer to the required solution a refined point from the response surface can be used to get the required solution. The complete solution is repeated with the optimal design point to get the optimal bearing performance. The above procedure was used with the bearing lubricated with Nano lubricant that has different types of dispersed nanoparticles, manly, TiO_2, Al_2O_3 and CuO with volume fraction of 0.03 of the nanoparticles. The results obtained can be shown in **tables (5.7)** to **(5.9)** as follows:

1. For a bearing lubricated with TiO_2 Nano-lubricant:

The results of the optimum journal center and the load carried by the bearing when it lubricated with Nano-lubricant that has 0.03 volume fraction of TiO_2 nanoparticles can be shown in **table (5.7)**.

Table(5.7) Optimum journal centre for a bearing lubricated with 0.03 TiO_2 Nano-lubricant.

Candidate Points			
	Candidate Point 1	Candidate Point 2	Candidate Point 3
P1 - length (mm)	0.029929	0.029892	0.02995
P2 - angle (degree)	55.664	57.532	58.915
P7 - fx-op	0.0065809	22.815	38.849
P8 - load-op	1120.6	1122.7	1127.5

Table of Schematic E4: Optimization , Candidate Points

	A	B	C	D	E	F	G	H	I	J
1	Reference	Name	P1 - length (mm)	P2 - angle (degree)	P3 - Mesh Max	P6 - fy-op	P7 - fx-op		P8 - load-op	
2							Parameter Value	Variation from Reference	Parameter Value	Variation from Reference
3		Candidate Point 1	0.029929	55.664	38.411	-1184.2	0.0065809	-99.98%	1120.6	-0.61%
4		Candidate Point 2	0.029892	57.532	38.48	-1171.1	22.815	-41.27%	1122.7	-0.42%
5		Candidate Point 3	0.02995	58.915	38.536	-1166.7	38.849	0.00%	1127.5	0.00%

2. Bearing lubricated with Al_2O_3 Nano-lubricant:

The results of the optimum journal center and the load carried by the bearing when it lubricated with Nano-lubricant that has 0.03 volume fraction of Al_2O_3 nanoparticles can be shown in **table (5.8)**.

Table(5.8) Optimum journal centre for a bearing lubricated with 0.03 Al_2O_3 Nano-lubricant.

Candidate Points

	Candidate Point 1	Candidate Point 2	Candidate Point 3
P1 - length (mm)	0.029999	0.029995	0.029999
P2 - angle (degree)	62.387	62.744	63.152
P7 - fx-op	-0.01982	2.9494	6.2579
P8 - load-op	1111.1	1111.6	1112.5

Table of Schematic E4: Optimization , Candidate Points

	A	B	C	D	E	F	G	H	I	J
1	Reference	Name	P1 - length (mm)	P2 - angle (degree)	P3 - Mesh Max	P6 - fy-op	P7 - fx-op		P8 - load-op	
2							Parameter Value	Variation from Reference	Parameter Value	Variation from Reference
3	○	Candidate Point 1	0.029999	62.387	38.65	-1112.9	-0.01982	-100.32%	1111.1	-0.13%
4	○	Candidate Point 2	0.029995	62.744	38.66	-1110	2.9494	-52.87%	1111.6	-0.08%
5	◉	Candidate Point 3	0.029999	63.152	38.672	-1107.3	6.2579	0.00%	1112.5	0.00%

3. Bearing lubricated with CuO Nano-lubricant:

The results of the optimum journal center and the load carried by the bearing when it lubricated with Nano-lubricant that has 0.03 volume fraction of CuO nanoparticles can be shown in **table (5.9)**.

Table (5.9) Optimum journal centre for a bearing lubricated with 0.03 CuO Nano-lubricant.

Candidate Points

	Candidate Point 1	Candidate Point 2	Candidate Point 3
P1 - length (mm)	0.029875	0.029875	0.027724
P2 - angle (degree)	60.653	59.885	58.786
P7 - fx-op	3.1457	-4.1309	1.5316
P8 - load-op	1126	1124.4	1035.4

Table of Schematic E4: Optimization , Candidate Points

	A	B	C	D	E	F	G	H	I	J
1	Reference	Name	P1 - length (mm)	P2 - angle (degree)	P3 - Mesh Max	P6 - fy-op	P7 - fx-op		P8 - load-op	
2							Parameter Value	Variation from Reference	Parameter Value	Variation from Reference
3	○	Candidate Point 1	0.029875	60.653	38.587	-1175.4	3.1457	105.39%	1126	8.75%
4	○	Candidate Point 2	0.029875	59.885	38.562	-1179.7	-4.1309	-369.72%	1124.4	8.60%
5	◉	Candidate Point 3	0.027724	58.786	38.283	-1034.8	1.5316	0.00%	1035.4	0.00%

Chapter Six

Conclusions

and

Recommendations

An extensive TEHD numerical study of a Nano-lubricated journal bearing is performed in the present work using the CFD FSI technique. The main factors affecting the performance of such bearing such as particle concentration, nanoparticles type, journal speed, elastic deformation, and cavitation are investigated. A suitable optimization technique is implemented to define the equilibrium position of the journal center. Maximum pressure, maximum temperature, load carried by the bearing, flow rate, and the bearing material deformation are the main studied parameters. The results obtained lead to the following concluding remarks:

1. The increase of the nanoparticles volume fraction up to 3% proved to be beneficial in enhancing the load carried by the bearing and decreasing the side leakage flow especially when it works under a high eccentricity ratio at the expense of a slightly higher friction force.
2. Generally, using Nano-lubricant with different particles and volume fractions alters the negative effect of the bearing elastic deformation. The bearing load-carrying capacity becomes higher by 5.2% to 14.3% when the bearing is lubricated with different Nano-lubricant in comparison with the base oil.

3. The journal center equilibrium position is obtained by using the efficient response surface optimization technique.
4. Using TiO_2 nanoparticles with the base oil show higher pressure and load-carrying capacity than that of Al_2O_3 and CuO.
5. In comparison to the base oil, several cases of different Nano lubricants demonstrate an increase in maximum pressure ranging from 6% to 19.85%.
6. The maximum oil film temperature of the bearing was increased by about 3.3134% to 16.6% when lubricated with a nano-lubricant that has a higher volume fraction of nanoparticles.
7. The deformation of the bearing material increases when the bearing works at a higher eccentricity ratio (ε) and rotational speed (N) by about 5.4% to 18%.

6.1. Recommendations:

The following points can be studied as future works:

1. Comparative study for the EHL performance of journal bearing lubricated with Bio-Based Nano-lubricants and synthetic lubricants.
2. CFD analysis of static and dynamic performance of Bio-based Nano lubricated journal bearing in turbulent flow regime considering elastic and variable viscosity effects.
3. Thermo-hydrodynamic performance of journal bearing lubricated with PTFE and MoS_2 Nano-lubricants considering cavitation effect.
4. CFD analysis of thermo-elasto-hydrodynamic lubrication of multi-lobe journal bearings.

References

References

1. Hili, M.A., Bouaziz, S., Maatar, M., Fakhfakh, T. and Haddar, M., 2010. Hydrodynamic and elastohydrodynamic studies of a cylindrical journal bearing. Journal of hydrodynamics, 22(2), pp.155-163.
2. Sun, J., Deng, M., Fu, Y. and Gui, C., 2010. Thermohydrodynamic lubrication analysis of misaligned plain journal bearing with rough surface.
3. He, Z.P., Zhang, J.H., Xie, W.S., Li, Z.Y. and Zhang, G.C., 2012. Misalignment analysis of journal bearing influenced by asymmetric deflection, based on a simple stepped shaft model. Journal of Zhejiang University SCIENCE A, 13(9), pp.647-664.
4. Brito, F.P., Miranda, A.S., Claro, J.C.P. and Fillon, M., 2012. Experimental comparison of the performance of a journal bearing with a single and a twin axial groove configuration. Tribology International, 54, pp.1-8.
5. Zhang, Z.S., Yang, Y.M., Dai, X.D. and Xie, Y.B., 2013. Effects of thermal boundary conditions on plain journal bearing thermohydrodynamic lubrication. Tribology Transactions, 56(5), pp.759-770.
6. Brito, F.P., Miranda, A.S., Claro, J.C.P., Teixeira, J.C., Costa, L. and Fillon, M., 2014. The role of lubricant feeding conditions on the performance improvement and friction reduction of journal bearings. Tribology International, 72, pp.65-82.
7. Akbarzadeh, P., Mikaeeli, S.Z. and Rahimiyan, M., 2018. Multiobjective optimization of thermohydrodynamic journal bearing using MOPSO algorithm. Proceedings of the Institution of Mechanical Engineers, Part J: Journal of Engineering Tribology, 232(6), pp.657-671.
8. Lambha, S.K., Kumar, V. and Verma, R., 2019, July. Elastohydrodynamic analysis of couple stress lubricated cylindrical journal bearing. In Journal of Physics: Conference Series (Vol. 1240, No. 1, p. 012165). IOP Publishing.
9. Li, B., Sun, J., Zhu, S., Fu, Y., Zhao, X., Wang, H., Teng, Q., Ren, Y., Li, Y. and Zhu, G., 2019. Thermohydrodynamic lubrication analysis of misaligned journal bearing considering the axial movement of journal. Tribology International, 135, pp.397-407.

10. Chetti, B. and Zouggar, H., 2019. Steady-state performance of a circular journal bearing lubricated with a non-Newtonian fluid considering the elastic deformation of the liner. Proceedings of the Institution of Mechanical Engineers, Part J: Journal of Engineering Tribology, 233(9), pp.1389-1396.

11. Sekhar, P.S., Sajja, V.S., Murthy, V.R.K. and Parthiban, S., 2019. A semi analytical approach in thermal analysis of Hydrodynamic lubrication of journal bearing. Materials Today: Proceedings, 19, pp.2650-2653.

12. Liu, C., Zhao, B., Li, W. and Lu, X., 2019. Effects of bushing profiles on the elastohydrodynamic lubrication performance of the journal bearing under steady operating conditions. Mechanics & Industry, 20(2), p.207.

13. Zhang, Y., Guoding, C.H.E.N. and Lin, W.A.N.G., 2019. Thermoelastohydrodynamic analysis of misaligned bearings with texture on journal surface under high-speed and heavy-load conditions. Chinese Journal of Aeronautics, 32(5), pp.1331-1342.

14. Shenoy, B.S., Binu, K.G., Pai, R., Rao, D.S. and Pai, R.S., 2012. Effect of nanoparticles additives on the performance of an externally adjustable fluid film bearing. Tribology International, 45(1), pp.38-42.

15. Binu, K.G., Shenoy, B.S., Rao, D.S. and Pai, R., 2014. A variable viscosity approach for the evaluation of load carrying capacity of oil lubricated journal bearing with TiO_2 nanoparticles as lubricant additives. Procedia materials science, 6, pp.1051-1067.

16. Binu, K.G., Shenoy, B.S., Rao, D.S. and Pai, R., 2014. Static characteristics of a fluid film bearing with TiO_2 based nanolubricant using the modified Krieger–Dougherty viscosity model and couple stress model. Tribology International, 75, pp.69-79.

17. Nicoletti, R., 2014. The importance of the heat capacity of lubricants with nanoparticles in the static behavior of journal bearings. Journal of tribology, 136(4), p.044502.

18. Babu, K.S., Nair, K.P. and Rajendrakumar, P.K., 2014. Computational analysis of journal bearing operating under lubricant containing Al_2O_3 and ZnO nanoparticles. International Journal of Engineering, Science and Technology, 6(1), pp.34-42.

19. Gunnuang, W., Aiumpornsin, C. and Mongkolwongrojn, M., 2015. Effect of nanoparticle additives on journal bearing lubricated with

non-Newtonian Carreau fluid. In Applied Mechanics and Materials (Vol. 751, pp. 137-142). Trans Tech Publications Ltd.

20. Solghar, A.A., 2015. Investigation of nanoparticle additive impacts on thermohydrodynamic characteristics of journal bearings. Proceedings of the Institution of Mechanical Engineers, Part J: Journal of Engineering Tribology, 229(10), pp.1176-1186.

21. Suryawanshi, S.R. and Pattiwar, J.T., 2018. Effect of TiO_2 Nanoparticles Blended with Lubricating Oil on the Tribological Performance of the Journal Bearing. Tribology in Industry, 40(3).

22. Abdollahzadeh Jamalabadi, M.Y., Alamian, R., Yan, W.M., Li, L.K., Leveneur, S. and Safdari Shadloo, M., 2019. Effects of nanoparticle enhanced lubricant films in thermal design of plain journal bearings at high Reynolds numbers. Symmetry, 11(11), p.1353.

23. Khan, P., Dhanola, A. and Garg, H.C., 2020. Elasto-hydrodynamic analysis of journal bearing operating with nanolubricants. Proceedings of the Institution of Mechanical Engineers, Part J: Journal of Engineering Tribology, 235(5), pp.963-974.

24. Ramaganesh, R., Baskar, S., Sriram, G., Arumugam, S. and Ramachandran, M., 2020. Finite element analysis of a journal bearing lubricated with nano lubricants. FME Transactions, 48(2), pp.476-481.

25. Dhanola, A. and Garg, H.C., 2020. Thermohydrodynamic (THD) Analysis of Journal Bearing Operating with Bio-based Nanolubricants. Arabian Journal for Science and Engineering, 45(11), pp.9127-9144.

26. Dang, R.K., Chauhan, A. and Dhami, S.S., 2020. Static thermal performance evaluation of elliptical journal bearings with nanolubricants. Proceedings of the Institution of Mechanical Engineers, Part J: Journal of Engineering Tribology, 235(8), pp.1627-1640.

27. Bui, T.A., Le, D., Pham, V.H., Nguyen, T. and Bui, N.T., 2020. A study of Al_2O_3 nanoparticle effect on lubricant to hydrodynamic journal bearing. International Journal of Mechanical and Production, ISSN (P): 2249–6890; ISSN (E): 2249–8001

28. Singh, A., Verma, N., Chaurasia, A. and Kumar, A., 2020, March. Effect of TiO_2 additive volume fraction in lubricant oil on the performance of hydrodynamic journal bearing. In IOP Conference Series: Materials Science and Engineering (Vol. 802, No. 1, p. 012005). IOP Publishing.

29. Tushar P. Gundarneeya, D. P. Vakharia., 2021 "*Performance Analysis of Journal Bearing with Nanolubricants* , Doctoral dissertation, Gujarat technological university Ahmedabad.

30. Dang, R.K., Dhami, S.S., Goyal, D. and Chauhan, A., 2021. Effect of TiO_2 and CuO Based Nanolubricants on the Static Thermal Performance of Circular Journal Bearings. *Tribology in Industry*, *43*(3), p.420.

31. Liu, H., Xu, H., Ellison, P.J. and Jin, Z., 2010. Application of computational fluid dynamics and fluid–structure interaction method to the lubrication study of a rotor–bearing system. Tribology Letters, 38(3), pp.325-336.

32. Li, Q., Yu, G., Liu, S. and Zheng, S., 2012. Application of computational fluid dynamics and fluid structure interaction techniques for calculating the 3D transient flow of journal bearings coupled with rotor systems. Chinese Journal of Mechanical Engineering, 25(5), pp.926-932.

33. Bendaoud, N., Mehala, K., Youcefi, A. and Fillon, M., 2012. An experimental and numerical investigation in elastohydrodynamic behaviour of a plain cylindrical journal bearing heavily loaded. Proceedings of the Institution of Mechanical Engineers, Part J: Journal of Engineering Tribology, 226(10), pp.809-818.

34. Chasalevris, A. and Sfyris, D., 2013. Evaluation of the finite journal bearing characteristics, using the exact analytical solution of the Reynolds equation. Tribology International, 57, pp.216-234.

35. Lin, Q., Wei, Z., Wang, N. and Chen, W., 2013. Analysis on the lubrication performances of journal bearing system using computational fluid dynamics and fluid–structure interaction considering thermal influence and cavitation. Tribology International, 64, pp.8-15.

36. Singla, A., Kumar, A., Bala, S., Singh, P. and Chauhan, A., 2014, March. Thermo-hydrodynamic analysis on temperature profile of circular journal bearing using computational fluid dynamics. In 2014 Recent Advances in Engineering and Computational Sciences (RAECS) (pp. 1-6). IEEE.

37. Czaban, A., 2015. CFD analysis of hydrodynamic pressure distribution in non-Newtonian oil in journal bearing lubrication gap. In Solid State Phenomena (Vol. 220, pp. 37-42). Trans Tech Publications Ltd.

38. Dhande, D.Y. and Pande, D.W., 2016, September. Numerical analysis of multiphase flow in hydrodynamic journal bearing using CFD coupled Fluid Structure interaction with cavitation. In 2016 International Conference on Automatic Control and Dynamic Optimization Techniques (ICACDOT) (pp. 964-971). IEEE.

39. Dhande, D.Y. and Pande, D.W., 2017. A two-way FSI analysis of multiphase flow in hydrodynamic journal bearing with cavitation. Journal of the Brazilian Society of Mechanical Sciences and Engineering, 39(9), pp.3399-3412.

40. Dhande, D.Y. and Pande, D.W., 2018. Multiphase flow analysis of hydrodynamic journal bearing using CFD coupled fluid structure interaction considering cavitation. Journal of King Saud University-Engineering Sciences, 30(4), pp.345-354.

41. Dhande, D.Y., Lanjewar, G.H. and Pande, D.W., 2019. Implementation of CFD–FSI technique coupled with response surface optimization method for analysis of three-lobe hydrodynamic journal bearing. Journal of the Institution of Engineers (India): Series C, 100(6), pp.955-966.

42. Chen, Y., Sun, Y., He, Q. and Feng, J., 2019. Elastohydrodynamic behavior analysis of journal bearing using fluid–structure interaction considering cavitation. Arabian Journal for Science and Engineering, 44(2), pp.1305-1320.

43. Chen, Y., Feng, J., Sun, Y., Peng, X., Dai, Q. and Yu, C., 2019. Effect of groove shape on the hydrodynamic lubrication of journal bearing considering cavitation. Engineering Computations.

44. Kyrkou, M.E. and Nikolakopoulos, P.G., 2020. Simulation of thermo-hydrodynamic behavior of journal bearings, lubricating with commercial oils of different performance. Simulation Modelling Practice and Theory, 104, p.102128.

45. Rasep, Z., Yazid, M.N.A.W.M. and Samion, S., 2021. A study of cavitation effect in a journal bearing using CFD: A case study of engine oil, palm oil and water. Jurnal Tribologi, 28, pp.48-62.

46. Versteeg, H.K. and Malalasekera, W., 1995. An introduction to computational fluid dynamics: the finite volume method. longman Group Ltd, First edition, Pearson education.

47. Zwart,P., Gerber, A. and Belamri, T., 2004.A two-phase flow model for predicting cavitation dynamics. Fifth international conference multiphase flow. Yokohama, Japan, May 30–June 3.

48. Krieger, I.M. and Dougherty, T.J., 1959. A mechanism for non-Newtonian flow in suspensions of rigid spheres. Transactions of the Society of Rheology, 3(1), pp.137-152.

49. Kole, M. and Dey, T.K., 2011. Effect of aggregation on the viscosity of copper oxide–gear oil nanofluids. International Journal of Thermal Sciences, 50(9), pp.1741-1747.

50. Mishra, P. C., Mukherjee, S., Nayak, S. K., and Panda, A., 2014. A brief review on viscosity of nanofluids. International nano letters, 4(4), 109-120.

51. Chen, H., Ding, Y., and Tan, C. ,2007. Rheological behaviour of nanofluids. *New journal of physics*, *9*(10), 367.

52. Khonsari, M.M. and Booser, E.R., 2017. Applied tribology: bearing design and lubrication. John Wiley & Sons.

53. Logan, D.L., 2016. A first course in the finite element method. Cengage Learning.

54. Dhande, Dinesh Yashwant.,2017, Analysis of hydrodynamic journal bearing with elastic bushing, Doctoral dissertation, department of mechanical engineering college of engineering, pune.

55. Fluent, A.N.S.Y.S., 2015. Release 16.0, Theory Guide; ANSYS. Inc.: Canonsburg, PA, USA.

56. Li, Q., Zhang, S., Wang, Y., Xu, W.W. and Wang, Z., 2019. Investigations of the three-dimensional temperature field of journal bearings considering conjugate heat transfer and cavitation. Industrial Lubrication and Tribology.

57. Bompos, D.A. and Nikolakopoulos, P.G., 2016. Tribological design of a multistep journal bearing. Simulation Modelling Practice and Theory, 68, pp.18-32.

58. Ferron, J., J. Frene, and R. Boncompain.,1983. A study of the thermohydrodynamic performance of a plain journal bearing comparison between theory and experiments.422-428.

59. He, M., Cloud, C.H., Byrne, J.M. and Vázquez, J.A., 2016. Fundamentals of fluid film journal bearing operation and modeling. In Asia Turbomachinery & Pump Symposium. 2016 Proceedings.. Turbomachinery Laboratories, Texas A&M Engineering Experiment Station.

60. Harnoy, A., (2002). Bearing design in machinery: engineering tribology and lubrication. CRC press., published in the Taylor & Francis e-Library.

61. Poole Jr, C. P., and Owens, F. J., 2003. Introduction to nanotechnology. John Wiley & Sons.

APPENDIXES

Appendix (A):User Defined Function (UDF) for temperature dependent viscosity.

The program developed in C language in order to input temperature dependant viscosity is presented in this section as below:

```
#include "udf.h"
#define BETA 0.032
#define PHIM 0.605
#define ETA -2.5
#define PHI 0.01
#define D 1.8
#define ao 4.0
#define Tin 299.9
#define muin 0.0788
DEFINE_PROPERTY(cell_viscosity, cell, thread)
{
real mu_lam;
real PHIA;
```

```
real temp=C_T(cell, thread);

PHIA=PHI*pow(ao,3-D);

mu_lam=pow((1-(PHIA/PHIM)),ETA*PHIM)*muin*exp(-
BETA*(temp-Tin));

return mu_lam;
}
```

Appendix (B): Published research

Article citation info: 1
Kadhim ZH, Ahmed SY, Abass BA. CFD analysis of nano-lubricated journal bearing considering variable viscosity and elastic deformation effects. Diagnostyka 2022;23(1): 2022101. https://doi.org/10.29354/diag/145034

DIAGNOSTYKA, 2022, Vol. 23, No. 1

e-ISSN 2449-5220
DOI: 10.29354/diag/145034

CFD ANALYSIS OF NANO-LUBRICATED JOURNAL BEARING CONSIDERING VARIABLE VISCOSITY AND ELASTIC DEFORMATION EFFECTS

Zainab H. KADHIM, Saba Y. AHMED, Basim A. ABASS

University of Babylon, College of Engineering, Mechanical Engineering Department, Babylon, Iraq
zainab.kebash@student.uobabylon.edu.iq.com

Abstract

The main objective of the present work is to study the behavior of Nano-lubricated journal bearing considering elasticity and variable viscosity effects. A mathematical model for a journal bearing is employed using three-dimensional computational fluid dynamics. The study is implemented for a journal bearing with laminar flow and smooth surfaces lubricated with pure oil as well as lubricants containing different concentrations of Al_2O_3 Nano-particles. The dependence of the oil viscosity on the temperature is considered by using the modified Krieger Dougherty model. Pressure, temperature and elastic deformation in addition to the bearing load-carrying capacity of the bearing working under different eccentricity ratios (0.1-0.6) have been studied. The mathematical model is confirmed by comparing the results of the pressure and temperature distributions obtained in the current work with those obtained by Ferron et al.(1983) for a bearing lubricated with pure oil. Also, the pressure obtained for the Nano-lubricated bearing of the present work is validated with that obtained by Solighar (2015). The results are found in good agreement with a maximum deviation not exceeding 5%. The obtained results show that the oil film pressure increases by about 17.9% with a slight decrease in oil film temperature and friction coefficient.

Keywords: hydrodynamic journal bearings, computational fluid dynamics, thermo-hydrodynamic lubrication, nano-lubricant, elastic deformation.

1. INTRODUCTION

The safe and smooth operation of rotating machines is limited by the reliability of the bearings. Hydrodynamic bearings are extensively used due to their simplicity, improved damping properties, high precision and high loads. It can be used in marine propellers, turbo and electric generators and IC Engines. The increasing journal bearing operating speeds leads to a higher range of temperature distribution that adversely impact the viscosity of the lubricant and the performance of the bearing. Different works have been implemented considering the thermal performance of various types of hydrodynamic bearings. The effect of bearing misalignment on thermo-hydrodynamic performance of journal bearing was extensively studied by [1-3]. Numerical results indicated that the influence of journal axial motion on the performance of the bearing is maximum when the thermal effect is taken into account. Thermal performance of journal bearings with various number of axial grooves has been investigated by [4-6].It was found that the bearing with twin axial grooves deteriorate when the bearing working under high loads in comparison with the single groove one. The combined effect of oil film temperature and the elastic deformation on its performance characteristics of the journal bearing was extensively studied by many workers [7-8]. The obtained results show an increase in maximum oil film pressure and load carrying capacity with sharp increase in oil film temperature due to journal misalignment when considering the elastic deformation of the bearing. The oil containing dispersed nano particles shows a higher viscosity in comparison with the base oil and hence influences the oil film temperature and the overall bearing performance. Different types of nano particles were used as an additives to the base oil such as TiO_2 [10-11], Si,SiO_2, Al, Al_2O_3,Cu, and CuO[12], Al_2O_3 and ZnO[13], Al_2O_3 [14-15]. Different viscosity models were used to include the effect of the dispersed nano particles on the viscosity of the base lubricant. Krieger Dougherty is found to be the most accurate viscosity model used in such works. As the bearing is lubricated with nano lubricant, the load caried by the bearing increases.
Few studies dealt with the combined impact of nano lubrication and thermal effects on journal bearing performance. In all of the work previously mentioned, the energy equation was solved simultaneously with the classical Reynolds equation. However, extensive work has been implemented using fluid structure interaction with computational

CFD Analysis of Thermohydrodynamic Behavior of Nanolubricated Journal Bearings Considering Cavitation Effect

Saba.Y. Ahmed [1], Basim A. Abass[2*], Zainab H. Kadhim[3]

[1] University of Babylon/College of Engineering/Mechanical Eng. Dept.
eng.saba.yasoob@uobabylon.edu.iq
[2] University of Babylon/College of Engineering/Mechanical Eng. Dept.
eng.basim.ajeel@uobabylon.edu.iq
[3] University of Babylon/College of Engineering/Mechanical Eng. Dept
zainab.kebash@student.uobabylon.edu.iq
**corresponding author*

Abstract

The present work displays an extensive numerical analysis for the thermo-hydrodynamic (THD) behavior in finite length journal bearings lubricated with different types of Nano-lubricants considering cavitation effect. The effects of nanoparticle concentrations, cavitation and temperature rise on the performance parameters of such bearings have been explored. The bearing is simulated using Computational Fluid Dynamic (CFD) approach. The effect of using different types of Nano-lubricants with different volume fractions of TiO_2 and Al_2O_3 nanoparticles dispersed in Veedol Avalon ISO Viscosity grade 46 oil has been demonstrated. Modified Krieger-Dougherty equation has been implemented with the thermal viscosity model to to evaluate the oil effective viscosity. The obtained results show that concerning the TiO_2 nanoparticles, results in a higher oil film pressure and load carrying capacity in comparison with Al_2O_3. The bearing equilibrium position was obtained by using Response Surface analysis (RSA) with optimal space-filling design technique. The numerical model was validated by comparing the results obtained in the present work with that obtained by Feron et al.. The results were found to be in a good confermation. The attained results show that the maximum pressure grows by 21% when the bearing lubricated with Nano-lubricant.

Keywords: Hydrodynamic journal bearings, computational fluid dynamics, thermohydro-dynamic lubrication, Nano-lubricant, cavitation effect, optimization.

1.Introduction

Journal bearing is the most commonly hydrodynamic bearing used to support the rotating shafts in industrial machine due its simplicity and low cost. It is mainly used to support the external applied load due to the generated pressure in its oil film. This type of bearings suffers from instability when it works at high speeds. The oil film temperature increases due to the viscous shearing of the oil film resulting in a decrease in the oil viscosity which negatively affects the performance of the bearing. Also, the oil film pressure drops at the divergent part of the bearing and when it becomes below than the saturation pressure the dissolved air bubbles released leading

Dear author,

In order for your paper to be published, please consider the comments of our technical board.

Equations are not written in Math type, according to the Instructions for authors. Please rewrite all equations in Math type. Figure 1 quality is pretty low, so please provide a figure of better quality. The same goes for Fig. 2.
Table 3 is not a table, but an image. Please make it in a form of a table.

Use the version of your paper attached to this e-mail for making corrections and send us the improved version **as soon as possible**, and until **December 30th** at the latest.

Kindest regards,

Editorial Board of the Journal of the Serbian Society for Computational Mechanics
6 Sestre Janjic Street
34000 Kragujevac, Serbia
E-mail: sscm@kg.ac.rs

Title	Journal of the Serbian Society for Computational Mechanics
Abbreviation	J. Serb. Soc. Comput. Mech.
Publication Type	Journal
Subject Area, Categories, Scope	Computational Mechanics (Q3)
h-index	9
Overall Rank/Ranking	17700
SCImago Journal Rank (SJR)	0.229
Impact Score	1.44
Publisher	The Serbian Society for Computational Mechanics (SSCM)
Country	Serbia
ISSN	18206530

الخلاصة

تم دراسة تحليل CFD ثلاثي الأبعاد وظواهر التدفق متعدد المراحل لمحمل المجلة الهيدروديناميكية مع التجويف المتكامل. تم إجراء عمليات المحاكاة مع الأخذ في الاعتبار تشوهات المحامل الواقعية عن طريق تفاعلات بنية السوائل ثنائية الاتجاه (FSI) جنبًا إلى جنب مع التجويف باستخدام برنامج ANSYS Workbench. تُستخدم وحدة تحسين التصميم لتوليد الحل الأمثل لزاوية الموقف والغرابة للجمع بين سرعة التشغيل والحمل. يتم فحص المحامل مع التجويف وبدونه. ينخفض الحمل الذي يحمله هذا النوع من المحامل ينخفض بشكل كبير عن طريق زيادة درجة حرارة طبقه الزيت الناتج عن التأثير الحراري نتيجة القص اللزج لطبقة الزيت بالإضافة إلى المادة التي تحمل التشوه المرن. لقد وجد أنه يمكن تحسين أداء الزيت الأساسي عن طريق تشتيت كمية صغيرة من جزيئات النانو المختلفة بأجزاء حجم مختلفة. تم فحص أن كل حمل مدعوم على هذا المحمل تم تعزيزه أثناء استخدام هذا النوع من زيوت التشحيم. يتم استخدام أنواع مختلفة من جزيئات النانو مثل اوكسيد التيتانيوم واوكسيد الالمنيوم واوكسيد النحاس TiO_2 و Al_2O_3 و CuO والجسيمات النانوية كمواد مشتتة مع الزيت الأساسي لتعزيز خصائصها الفيزيائية وبالتالي الأداء الثابت للمحمل. تعتبر بيانات خصائص التشغيل لهذا المحمل مهمة جدًا لمصمم المحمل وأرباب العمل للتخلص من درجة حرارة طبقة الزيت المرتفعة التي تسبب فشل المحمل. في العمل الحالي، تم تصميم محمل عادي المشحم بمواد تشحيم مختلفة من النانو بشكل رقمي مع الأخذ في الاعتبار تأثيرات درجة حرارة طبقه الزيت والتشوه المرن لمادة المحمل. علاوة على ذلك، يمكن أن يحدث التجويف في المنطقة المتباعدة من المحمل مما يؤدي إلى تلف المكونات وفشلها ويحد من الحمل الأقصى المطبق. ومن ثم، فإن تأثير التجويف على أداء المحمل يجب أن يؤخذ في الاعتبار لتصميم موثوق. تم تنفيذ معادلة Krieger-Dougherty المعدلة مع نموذج اللزوجة الحرارية من أجل النظر في اختلاف لزوجة زيت التشحيم النانوي مع درجة حرارة طبقة الزيت ولتقييم لزوجته الفعالة. تم استخدام ديناميكية الموائع الحسابية (CFD) لنمذجة طبقات السائل للمحمل بينما تم استخدام تفاعل بنية السوائل (FSI) لنمذجة التشوه المرن في مادة المحمل. تم نقل التشوه المرن إلى طبقة السائل والعكس باستخدام تقنية FSI ثنائية الاتجاه في برنامج ANSYS FLUENT. تم تحديد موضع التوازن لمركز العمود بسبب ظروف التشغيل المريحة باستخدام تقنية التحسين المناسبة. تم تنفيذ دراسة التحقق للتأكد من صحة النموذج العددي من خلال مقارنة نتائج الحالات المختلفة (THD، TEHD، THD مع تزييت النانو) التي تم تحقيقها في هذه العملية التي تم البدء

بها مع مثل هذه المستلمة عبر مشغلين مختلفين عدديًا أيضًا تجريبيًا. تضمن نهايات التحقق هذه تنفيذ النموذج العددي بثقة. على الرغم من تنفيذ عدد كبير من الأعمال عدديًا لدراسة خصائص المحمل العادي المشحم بالزيت النقي، إلا أنه تم تنفيذ القليل من الأعمال الواقعية بالنظر إلى التأثيرات المجمعة للظروف المذكورة سابقًا لدراسة أداء elato-hydro-dynamic لمثل هذه المحامل عند التشحيم باستخدام زيوت التشحيم النانوية باستخدام CFD وFSI ثنائي الاتجاه. تم فحص أداء المحمل في أجزاء مختلفة من حجم الجسيمات من الجسيمات النانوية وسرعات المجلة ونسب الانحراف المختلفة. توضح النتائج التي تم الحصول عليها في العمل الحالي أن الحد الأقصى لضغط غشاء الزيت يزداد بنسبة 6٪ إلى حوالي 20٪ عند التشحيم بمواد تشحيم مختلفة من النانو مقارنةً بالزيت النقي، حيث يصبح الحمل الذي يحمله المحمل حوالي 14.3٪. تنخفض زاوية اتجاه المحمل بنسبة 11٪ إلى 37٪ مع حساب زيادة قوة الاحتكاك بنسبة 16٪ وزيادة تشوه المحمل عند تشحيمه بمزيت التشحيم النانو هذا حوالي 18٪ عندما يتم تشحيم المحمل بـ TiO2 عند الحجم يزداد جزء من هذه الجسيمات النانوية إلى 0.03 مقارنةً بالجزء المشحم بالزيت النقي.

جمهورية العراق
وزارة التعليم العالي والبحث العلمي
جامعة بابل / كلية الهندسة
قسم الهندسة الميكانيكية

تحليل الأداء الهيدروديناميكي المرن الحراري للمحامل المقعدية المزيتة بزيوت حاوية على جسيمات متناهية في الصغر باستخدام ديناميك الموائع الحسابية

رسالة
مقدمة إلى جامعة بابل / كلية الهندسة وهي جزء من متطلبات نيل شهادة الماجستير في الهندسة/ الهندسة الميكانيكية/ميكانيك تطبيقي

أعدت من قبل
زينب حافظ كاظم كبيش

بأشراف
أ.د.باسم عجيل عباس
أ.د. صبا يعسوب احمد

1442 هـ
2021 م